

Contents

Preface	iii
Acknowledgments	xiii
Executive Summary	xv
Chapter 1	
Introduction to the 1994 Entrapment Zone Study	1
Motivation for the Study	1
Background	3
Conceptual Model of Concentration Maxima	4
Entrapment Zone as Habitat	6
Study Objectives	6
Sample Design	7
Conditions During Cruises	8
References Cited	11
Chapter 2	
Results from the Hydrodynamic Element of the 1994 Entrapment Zone study in Suisun Bay	13
Abstract	13
Introduction	13
Historical Perspective	16
Definitions	17
Timescales	18
Existing Conceptual Model of Entrapment in the Northern Reach of San Francisco Bay	19
Gravitational Circulation	19
Principal Findings	19
Gravitational Circulation	21
Delta Acoustic Doppler Current Profiler Data	28
Revised Conceptual Model of Entrapment	33
Revised Conceptual Model of Gravitational Circulation	33
Horizontal Richardson Scale	35
Overturning or Straining Timescale	35
Alternative Entrapment Mechanisms	43
Vertical Migration	43
Stokes Drift	47
Management Implications	50
Acknowledgments	51
References	51
Glossary	54
Appendix. Fundamentals of Baroclinic and Barotropic Flows	57
Numerical Modeling Implications	61
Net Tilt Scaling	61

Chapter 3	Microbial Production in the San Francisco Bay Entrapment Zone	63
	Abstract	63
	Introduction	63
	Materials and Methods	65
	Chlorophyll and Particulate Organic C and N	66
	Bacterial Biomass, Production and Size Fractionation	66
	Results	67
	Discussion	73
	Conclusions	76
	Management Implications	77
	Directions for Future Studies	77
	Acknowledgments	78
	Literature Cited	78
Chapter 4	Tidally Oriented Vertical Migration and Position Maintenance of Zooplankton in Northern San Francisco Bay	83
	Abstract	83
	Introduction	84
	Data Analysis Methods	85
	Methods for 1994 Field Studies	87
	Results of Data Analysis	90
	Results of 1994 Field Studies	94
	Discussion	104
	References Cited	108
Chapter 5	Vertical Migration and Retention of Native and Exotic Larval Fishes within the Entrapment Zone of a Tidally Dominant Estuary	111
	Abstract	111
	Introduction	112
	Background	112
	Methods	114
	Results	114
	Discussion	129
	Implications	131
	Literature Cited	132

Tables

Chapter 1

1	Conditions During Sampling and Samples Taken	9
---	--	---

Chapter 3

1	Locations of Stations Occupied During the Entrapment Zone Study	65
2	Thymidine Metabolism Index for Populations of Bacteria from the San Francisco Estuary, April 28, 1994	73

Chapter 4

1	Sampling Stations Included in Analysis of Channel Zooplankton Data	86
2	Frequency of Occurrence of Peaks in Abundance versus Distance Up the Axis of the Estuary Meeting the Criteria for Each Variable	86
3	Robust Regression Statistics for Peak Positions versus X_2 and Median Width of the Peaks	93
4	Statistics for Differences Between Position of Peaks and X_2	93
5	Regression Statistics for Analyses of Covariance of Log Abundance of Macrozooplankton at 1 Meter Depth versus Tidal Velocity and Day vs Night	93
6	Regression Statistics for Weighted Regressions of Mean Depth of Center Mass of Copepods versus Tidal Velocity	97
7	Coefficients with Standard Errors and Significance for Response Surface Model for Macrozooplankton, Used to Estimate Flux	101
8	Coefficients with Standard Errors and Significance for Response Surface Model for Copepods, Used to Estimate Flux	102
9	Coefficients with Standard Errors and Significance for Response Surface Model for Optical Backscatter Voltage, Used to Estimate Flux	103

Chapter 5

1	Total Catch of Larval and Juvenile Fishes Collected During Depth-Specific Sampling	115
2	Chi-Square Statistics from Comparisons of Proportion of Fish Caught in Surface, Middle, and Bottom Samples between Day and Night and between Ebb and Flood Tides for Longfin Smelt, Striped Bass, and Yellowfin Goby	123

Figures

Executive Summary

1	Distribution of Zooplankton with Respect to Salinity Before and After 1987	xvi
2	Study Area	xiii
3	Tidally Filtered Velocity Along the Axis of the Channel at Chipps Island	xix
4	Bacterial Activity and Abundance Associated with Particles as a Percent of Total Bacterial Activity or Abundance, Plotted Against Salinity	xx
5	Abundance of <i>Neomysis mercedis</i> at 1-Meter Depth as a Function of Tidal Velocity and Day versus Night	xxi
6	Depth of Center of Mass of <i>Eurytemora affinis</i> Population as a Function of Tidal Velocity, for Adults, by Day Only	xxi
7	Proportion of Longfin Smelt Larvae in Depth Bins on Ebb and Flood Tides for Cruises A and B	xxi
8	Flux of Zooplankton Along the Estuary	xxii

Chapter 1

1	Schematic Longitudinal Section of the Estuary Showing Isohalines and Conceptual Models of Interaction between Behavior of Particles and Longitudinal Movement	5
2	Freshwater Outflow Calculated in the DWR DAYFLOW Program for March-May 1994	8
3	Cruise A, April 18-19, 1994	10
4	Cruise B, April 26-27, 1994	10
5	Cruise C, May 17-18, 1994	10
6	Cruise A Salinity Profiles on Ebb and Flood Tides at Stations 1, 3, and 6	10
7	Cruise B Salinity Profiles on Ebb and Flood Tides at Stations 1, 3, and 6	10
8	Cruise C Salinity Profiles on Ebb and Flood Tides at Stations 1, 3, and 6	10
9	Cruise A Optical Backscatter Voltage on Ebb and Flood Tides at Stations 1, 3, and 6	11
10	Cruise B Optical Backscatter Voltage on Ebb and Flood Tides at Stations 1, 3, and 6	11
11	Cruise C Optical Backscatter Voltage on Ebb and Flood Tides at Stations 1, 3, and 6	11

Chapter 2

1	Conceptual model of the entrapment and null zones	14
2	Approximate 1994 entrapment zone study <i>in situ</i> instrument positions, north San Francisco Bay	15
3	Conceptual model of the tidal and residual currents in the north bay	20
4	Delta outflow estimates (DAYFLOW), October 1, 1993, to July 1, 1994	22
5	X2 computed from an ARIMA model that predicts X2 from log delta outflow and yesterday's X2	22

6	Stick plots of residual currents at station CNCRD, April 4 through June 21, 1994	23
7	Stick plots of residual currents at station MAL, April 14 through June 20, 1994	24
8	Stick plots of residual currents at station MRTNZ, April 21 through June 22, 1994	25
9	Stick plots of residual currents at station CAR, April 23 through May 30, 1992	26
10	Stick plots of residual currents at station CONC, April 28 through May 29, 1992	27
11	Stick plots of residual currents at station MK8, April 14 through June 20, 1994	29
12	Stick plots of residual currents at station ANTCH, April 14 through June 20, 1994	30
13	Time series plot of near-bed and near-surface salinity at Antioch	31
14	Time series plot of near-bed salinity on the Sacramento River at channel marker 8	31
15	Delta outflow (DAYFLOW), atmospheric pressure, and wind speed at channel marker 27 in Suisun Bay	32
16	Horizontal Richardson number: a ratio of two timescales	34
17	Overturning time scale estimated using the root-mean-squared near-surface current and depths from acoustic Doppler current profiler data as a function of estuarine position	36
18	Conceptual model of gravitational circulation in the north bay based on the overturning timescale	37
19	Overturning time scale and current speed during spring current maximums, root-mean-squared current, and neap current minimums	38
20	Time series plots of delta outflow (DAYFLOW), Mallard Island low-pass-filtered salinity, and the basinwide horizontal low-pass-filtered, near-bed gradient dS/dx for 1992, 1993, and 1994	39
21	Time series plots of salinity and the basinwide horizontal salinity gradient, dS/dx , Mallard Island	40
22	Time series plots of the salinities at Martinez and Mallard Island	40
23	Time series plots of the low-pass-filtered along-channel component of the surface current squared, the local horizontal salinity gradient in Suisun Cutoff as computed by conductivity/temperature instruments deployed 1.5 kilometers apart along the axis of Suisun Cutoff, and the salinity in Suisun Cutoff	42
24	Horizontal salinity gradient data versus tidally-filtered salinity conducted at Suisun Cutoff during autumn 1994 and spring 1995	43
25	Time series plots of the near-bed and near-surface salinities; the near-bed and near-surface, along-channel speed; and the flood/ebb normalized shear at Mallard Island	46
26	Time series plots of the depth-averaged, along-channel current; the vertical shear; and the tidally averaged vertical shear at Mallard Island	47
27	Time series of depth of Mallard Island and the low-pass-filtered, depth-averaged, along-channel speed and the Stokes drift velocity	48
28	Normalized sea level and depth-averaged velocity at Mallard Island	49
29	Phase lag assuming a semidiurnal tidal period of 12.42 hours between sea level and the currents at Mallard Island	
30	Phase lag, assuming a semidiurnal tidal period of 12.42 hours, between sea level and the currents at Mallard Island	50
31	Example of the pressure distributions on a gate that separates two fluids of different densities	59

32	Example of the net pressure distributions on a gate that separates two fluids of different densities and different water levels	61
----	---	----

Chapter 3

1	Chlorophyll Concentrations in the Study Area, April 19, April 28, and May 17, 1994	68
2	Spatial Variation in Water Temperature, Chlorophyll Concentration, and Salinity and L-Leucine Incorporation Rate and Cell-Specific L-Leucine Incorporation Rte on April 28, 1994	68
3	Concentration of Particulate Organic Carbon, Particulate Organic Nitrogen, and the C:N Ratio of Particulate Matter on April 19, 1994	69
4	Concentration of Particulate Organic Carbon, Particulate Organic Nitrogen, and the C:N Ratio of Particulate Matter on April 28, 1994	69
5	Concentration of Phytoplankton and Bacterioplankton Biomass to Particulate Organic Carbon in Samples from the Study Area on April 19 and April 28	70
6	Abundance of Bacteria in Samples from Suisun Bay and the Sacramento-San Joaquin Delta on April 19, April 28, and May 17	70
7	L-Leucine Incorporation Rtes in Samples from Suisun Bay and the Sacramento-San Joaquin Delta on April 19, April 28, and May 17	71
8	Cell-Specific L-Leucine Incorporation Rates in Samples from Suisun Bay and the Sacramento-San Joaquin Delta on April 19, April 28, and May 17	71
9	Attenuation Coefficients for Photosynthetically Active Radiation Measured in Suisun Bay and the Sacramento-San Joaquin Delta on April 19 and April 28	72
10	Percentage of the Bacteria Population Associated with Particles in Samples from Suisun Bay and the Sacramento-San Joaquin Delta on April 19, April 28, and May 17	72
11	Percentage of Total Leucine Incorporation Associated with Particles in Samples from Suisun Bay and the Sacramento-San Joaquin Delta on April 19, April 28, and May 17	72

Chapter 4

1	Relationship to Salinity of Selected Variables from Single Surveys	90
2	Salinity at Peaks of Concentration or Abundance Plotted Against X ₂	91
3	Position of Peaks in River Kilometer versus X ₂ on Date at the Midpoint of Each Survey	92
4	Abundance of Zooplankton in Spring 1994 versus Salinity from Routine Monitoring Surveys and Entrapment Zone Cruises	94
5	Population Ratios, by Cruise and Station	95
6	Abundance of Macrozooplankton at 1-Meter Depth by Day and Night versus Water Column Mean Tidal Velocity	96
7	Mean Depth, as Percent of Water Column Taken from Surface to the Deepest Sample, versus Water Column Mean Tidal Velocity for Three Copepod Species	97
8	Mean Depth of Center of Mass and Water Column Mean Values for Chlorophyll and Optical Backscatter Voltage	98

9	Image Plots of Acoustic Backscatter Intensity versus Depth and Time for Four Stations during Cruise B	99
10	Calculated Longitudinal Flux of Macrozooplankton per Unit Cross-Sectional Area .	101
11	Calculated Longitudinal Flux of Total Copepods per Unit Cross-Sectional Area . .	102
12	Calculated Longitudinal Flux of Particulate Matter per Unit Cross-Sectional Area Estimated from Optical Backscatter Voltage	103

Chapter 5

1	Abundance of Prickly Sculpin, Shimofuri Goby, Yellowfin Goby, Longfin Smelt, and Striped Bass	116
2	Vertical Partitioning of Larval Abundance in Surface, Middle, and Bottom Samples for Prickly Sculpin, Longfin Smelt, and Striped Bass Larvae . .	117
3	Vertical Partitioning of Abundance According to Larval Size in Surface, Middle, and Bottom Samples for Striped Bass, Yellowfin Goby, and Longfin Smelt Larvae Along All Cruises	118
4	Vertical Partitioning of Delta Smelt Catch for Each Sampling Cruise with Larval Size Range	118
5	Vertical Distribution of Percentage of Longfin Smelt Caught on Ebb and Flood Tides During Day and Night for Cruises A and B	119
6	Vertical Distribution of Percentage of Striped Bass and Yellowfin Goby Caught on Ebb and Flood Tides During Day and Night for Cruises A and B	120
7	Vertical Distribution of Percentage of Striped Bass and Yellowfin Goby Caught on Ebb and Flood Tides During Day and Night for Cruise C	121
8	Vertical Distribution of Percentage of Longfin Smelt, Striped Bass and Yellowfin Goby Caught During Day and Night for Cruises A and B	122
9	Vertical Distribution of Percentage of Striped Bass and Yellowfin Goby Caught During Day and Night for Cruise C	123
10	Vertical Distribution of Percentage of Longfin Smelt, Striped Bass and Yellowfin Goby Caught During Ebb and Flood Tides for Cruises A and B	124
11	Vertical Distribution of Percentage of Striped Bass and Yellowfin Goby Caught During Ebb and Flood Tides for Cruise C	125
12	Percentage of Total Abundance of Yellowfin Goby Caught in Surface and Bottom Samples in Relation to Vertically Averaged Tidal Speed for Each Tow During Cruise C	126
13	Percentage of Total Abundance of Striped Bass Caught in Surface and Bottom Samples in Relation to Vertically Averaged Tidal Speed for Each Tow During Cruise C	127
14	Percentage of Total Abundance of Striped Bass Larvae Caught in Surface Samples in Relation to Vertically Averaged Tidal Speed for Each Tow During Cruise C	128

Acknowledgments

Funding for this study was provided by the Interagency Ecological Program (DWR Contract B-59634 to San Francisco State University and internal IEP funding). We thank Randy Brown and Jim Arthur for their support and encouragement in all phases of this study, and Harlan Proctor and Steve Hayes for organizing vessel and logistical support. We are grateful to Sam Luoma and members of the Science Advisory Group for their thorough review of this report. Guidance and encouragement from Steve Monismith, Jeffrey Koseff (Stanford University), Ralph Cheng (USGS), and Peter Smith (USGS) were essential in the design and execution of the hydrodynamic element of the study. We thank Lloyd Brenn, Eric Santos, and Dave Morgan for their long hours as crew of the research vessels. We also thank Doug Ball, Hank Gebhard, and Mike Simpson for their help in making things work. Finally, we thank the following people for their help during the cruises: Jim Arthur, Doug Ball, John Baker, Pam Casselman, Steve Hayes, Liz Howard, Heather Peterson, Mike Simpson, Ted Sommer, and Kitty Triboli. The field study described in Chapter 2 required the help of a number of people, including Jim Burau, Rick Oltmann (USGS), Rick Adorador (USGS), Scott Posey (USGS),

Peggy Lehman

done

EXECUTIVE SUMMARY

The entrapment zone has long been considered an important region of the San Francisco estuary. It has been the subject of several previous studies, and its location has been suggested as an index of condition of the estuarine ecosystem. A close correlate of this location, X_2^1 , is now used as a management objective on the basis that X_2 is correlated with the abundance or survival of several estuarine-dependent species. X_2 is a crude tool to use for this purpose, but it can be refined only through improved understanding of the various mechanisms underlying these correlations. These mechanisms probably differ among species, but for species resident in and near the entrapment zone, the correlation with X_2 may be due to variations in intensity of trapping mechanisms with position of the entrapment zone. Therefore, it is worthwhile to investigate these trapping mechanisms, the nature of the entrapment zone as habitat, and the responses of the entrapment zone to changes in X_2 or outflow from the Sacramento-San Joaquin Delta.

Studies of the entrapment zone of the San Francisco estuary have been conducted in springs of 1994, 1995, and 1996. These studies have been funded by the Interagency Ecological Program and conducted by scientists from IEP member agencies, the Romberg Tiburon Center for Environmental Studies, Bodega Marine Laboratory, and the University of California at Santa Cruz. This report presents results from 1994, a low-flow year. Subsequent reports will describe results from 1995 and 1996 and highlight differences among years.

This report is organized in chapters that comprise more-or-less independent papers, with an introductory chapter for the entire study. This Executive Summary presents highlights of the overall study plan and summarizes the major findings.

Background

Studies of entrapment processes in the San Francisco estuary began with the work of Peterson and Arthur and Ball. Those studies, together with related work from other estuaries, provided a conceptual model of the function of the entrapment zone. Briefly, that model describes the entrapment zone as a region near the null zone, the landward limit of gravitational circulation or tidally averaged two-layer flow, where particles are trapped

2*

The distance up the axis of the estuary from the Golden Gate to the point where salinity is 2 psu (practical salinity units) 1 meter off the bottom.

through the interaction of their sinking and the net landward bottom current. This model was extended by Cloern and others to include the growth of phytoplankton: net growth occurs over shoals in Suisun Bay, while net respiration occurs in channels, and the proximity of the entrainment zone to shoals enhances accumulation of biomass in the channels.

The circulation of Suisun Bay is now known to be more complex than this simple model would suggest, and tidal processes are much more important than previously believed. In 1994 (as in subsequent years), landward flow at the bottom occurred in the southern channel of Suisun Bay only for very brief periods during neap tides under a variety of freshwater flow conditions. Ebb/flood asymmetries in the vertical structure of tidal velocity are less pronounced than previously believed because of strong vertical mixing. Thus, the entrainment zone can be characterized as a dynamic and variable physical environment. Yet, maxima in turbidity and in abundance peaks of zooplankton and larval fish persist under most conditions of tide and freshwater inflow. How do these maxima persist, and what are the implications for population regulation in the estuary? Revisions in the conceptual model of the physics of the entrainment zone seem to demand parallel revisions for biology. We wish to understand how and why organisms are retained, and to what extent this retention mitigates the effect of losses from the populations to advection and dispersion away from the population centers. Furthermore, there is a need to improve understanding of the biological and chemical characteristics of the entrainment zone to try to understand what advantage organisms might gain by concentrating there. The entrainment zone differs from landward regions in having a higher salinity and often increased turbidity; it also differs in the chemical and biotic composition of particles, which may improve the quality of particles as food for higher trophic levels.

Inhabitants of the entrainment zone include phytoplankton, bacteria, microzooplankton, several copepods, two species of mysid, amphipods, and some

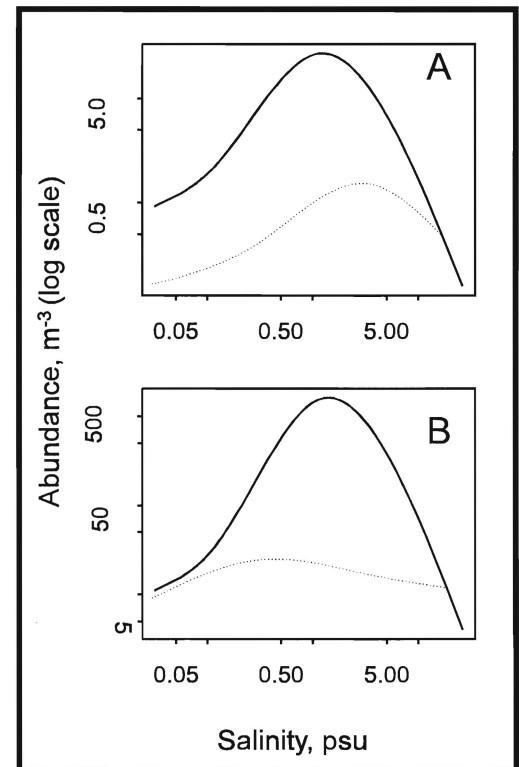


Figure 1
DISTRIBUTION OF ZOOPLANKTON
WITH RESPECT TO SALINITY
BEFORE AND AFTER 1987

Lines are natural spline curves fit to data from the

larval fish including longfin smelt, striped bass, and yellowfin gobies. Since the spread of the clam *Potamocorbula amurensis* in 1987, maxima in phytoplankton biomass have largely disappeared, and maxima in abundance of many of the entrapment zone species have shifted landward to a lower salinity (Figure 1). The results presented here should be interpreted with respect to the current, not the former, distributional patterns.

The general question being addressed by the Entrapment Zone Project Work Team is:

By what mechanisms do particles and organisms aggregate in and near the entrapment zone, and what is the advantage for organisms in doing so?

Objectives of the 1994 study were:

- To determine the relationship between vertical and longitudinal positions of common entrapment zone species and the velocity field under various conditions of tide and outflow.
- To determine the significance of particle-associated bacteria as potential sources of food for entrapment zone species and their dependence on organic matter delivered by streamflow.
- To obtain information on small-scale spatial (particularly vertical) distribution of larval fish and zooplankton.

Study Design

The sampling program had three major elements: continuous monitoring at fixed stations, intensive sampling on three cruises of R/V *San Carlos*, and spatially detailed sampling on three cruises from R/V *Questuary* and R/V *Polaris*. In addition, substantial theoretical work was done on the physical basis for gravitational circulation and on the interaction between variability in velocity and vertical distributions of organisms and particles to produce observed maxima.

Continuous monitoring data were collected with ADCPs (acoustic doppler current profilers) placed at the edge of the main shipping channel at four locations in Suisun Bay and the western delta (Figure 2). In addition, CTDs recorded conductivity, temperature, depth, and optical backscatter at these and several other locations. Data used to interpret biological sampling were taken from the Mallard Slough ADCP, which was close to the center of the sampled area.

Intensive sampling was done on two neap tides and one spring tide in April and May from R/V *San Carlos*. We attempted to sample in a Lagrangian mode, *ie*, by following water masses rather than by sampling at fixed stations, to prevent aliasing of tidal and salinity effects. Stations were fixed in salinity rather than in space: we sampled at 1, 3, and 6 mS/cm surface specific conductance (roughly 0.5, 1.6, and 3.3 psu salinity) to

approximate the entrainment zone and nearby locations landward and seaward of it.

We used paired 60-cm-diameter, 500- μ m-mesh Bongo nets to sample for larval fish and larger zooplankton such as *Neomysis*. These nets, which are capable of being opened and closed at depth, were used to sample near the bottom, at mid-depth, and at the surface to determine the vertical distribution of organisms. We used a high-volume pump sampler to sample for smaller zooplankton (mainly copepods) and phytoplankton at the same depths as the net, plus intermediate depths as time on station permitted.

The study design represented two improvements over similar previous efforts. First, the number and volume of samples taken was unprecedented in this estuary. Second, ancillary data provided a much more comprehensive view of the physical habitat than was available in previous studies. We used a GPS receiver to record precise locations of samples, a Seabird CTD to obtain vertical profiles of temperature, salinity, and optical backscatter (OBS, related to concentration of fine particles), and a shipboard-mounted, downward-looking acoustic doppler current profiler. The ADCP gave us instantaneous measurements of velocity profiles that were invaluable in timing our samples to the turn of the tide and backscatter intensity profiles that gave some information on the vertical distributions of organisms of about 1-mm size.

Samples for bacterial abundance and production were taken from R/V *Questuary* on a transect of stations up the main channel of the bay through the entrainment zone by day. Because the spatial and temporal scale for this part of the project differed from that focusing on larger organisms, there was no need to sample concurrently. We determined bacterial biomass and production separately for particle-bound and free-living bacteria. Natural particulate matter was gently filtered to separate the two fractions. Biomass was estimated from counts of bacterial cells in each fraction, and production was determined by the rate of incorporation of radioactively labeled leucine. We also determined whether particle-bound bacteria were digesting organic matter differently from free-living bacteria.

Results and Discussion

Contrary to the historical model of the entrainment zone, gravitational circulation was rare in Suisun Bay in 1994, with net currents throughout the water column directed seaward (Figure 3). The only exception to this

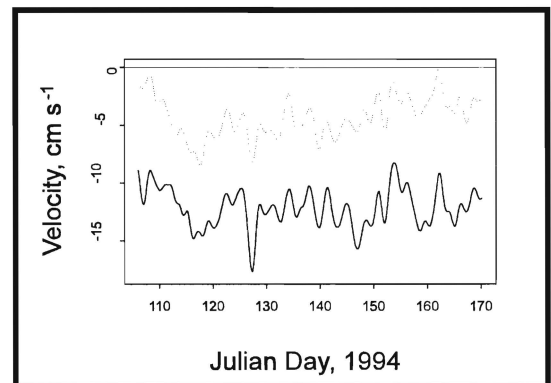


Figure 3
TIDALLY FILTERED VELOCITY ALONG THE
AXIS OF THE CHANNEL AT CHIPPS ISLAND

From the fixed
acoustic doppler

was in brief bursts of landward bottom currents that occurred around some of the slack tides. These do not appear sufficient to overcome the net seaward transport of the entire water column that is the more common condition.

A revised conceptual model of gravitational circulation illustrates the effect of shallow water. Gravitational circulation may develop depending on the relative magnitudes of two opposing factors: the longitudinal density gradient and vertical shear in the tidal velocity profiles. The longitudinal density gradient, with higher-density water seaward and lower-density water landward, provides the pressure gradient that produces gravitational circulation. Without tides, this circulation would proceed as in the previous conceptual model. The effect of tidal shear is to produce turbulence that breaks down stratification, greatly reducing the magnitude of two-layer bi-directional gravitational flow. This tidal shear increases as the ratio of the tidal current speed to depth. Thus, gravitational circulation is most likely to happen in deep water with a large horizontal density gradient and weak tidal currents. The “horizontal Richardson number”, which is the ratio of density to shear forces, is lowest for central Suisun Bay, accounting for infrequent gravitational circulation there.

Bacterial biomass in the entrapment zone was comparable to other stations, and bacterial production was actually higher landward. The proportion of bacteria production attached to particles was high, particularly in and seaward from the entrapment zone (Figure 4). This means that the dynamics of particle movement in the entrapment zone should affect the movement of bacterial biomass. The bacteria attached to particles appeared to differ in their metabolic activities from the free-living bacteria, suggesting a different role in metabolizing organic matter. Association with particles may facilitate the transfer of bacterial production to higher trophic levels through direct grazing by zooplankton or benthos on relatively large, bacteria-rich detrital particles. We believe this may be important: although bacterial production is low compared to other estuaries, primary production is relatively lower, such that the ratio of bacterial to primary production is high compared with other estuaries.

We observed variability in the growth of bacteria in water from different regions of the delta, particularly during low flows of 1994. Water from the San Joaquin side appeared to support more rapid growth than Sacramento

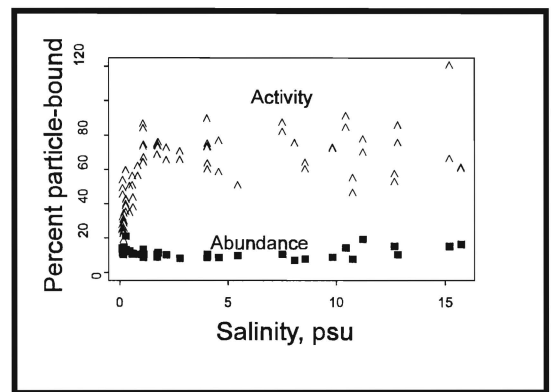


Figure 4
BACTERIAL ACTIVITY AND ABUNDANCE
ASSOCIATED WITH PARTICLES AS A
PERCENT OF TOTAL BACTERIAL ACTIVITY
OR ABUNDANCE,
PLOTTED AGAINST SALINITY

River water, suggesting that it contained more labile organic matter. Natural or project-caused variation in the delivery of this water could be responsible for some of the observed variation in growth rate of bacteria in the entrapment zone.

Phytoplankton data indicate some variability among samples, with slightly higher chlorophyll concentration near the bottom. Longitudinal gradients were large: chlorophyll decreased sharply from the 3-mS/cm station to the 6-mS/cm station, and taxonomic composition changed with station. This distribution of chlorophyll is different from that observed in years before the arrival of the clam *Potamocorbula amurensis*, when chlorophyll maxima were common in the entrapment zone.

Net zooplankton included the mysids *Neomysis mercedis* and *Acanthomysis* sp. and amphipods as a group. All three taxa migrated vertically on diel and tidal patterns: all were more abundant at the surface by night and on the flood than by day and on the ebb (Figure 5). The increase in surface abundance was due partly to migration off the bottom, and partly to redistribution within the water column.

Smaller zooplankton migrated tidally but to a lesser extent (Figure 6) and without a substantial diurnal component of migration. This contrasts with results from many other estuaries, where *Eurytemora affinis* and *Pseudodiaptomus* species remain on the bottom by day and rise into the water column at night. The difference could be due to the low light levels at depth in the entrapment zone in the San Francisco estuary, which would

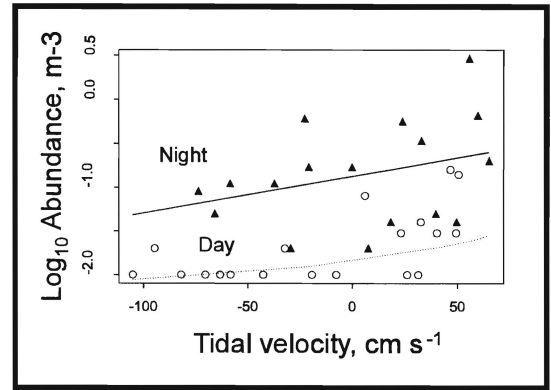


Figure 5
ABUNDANCE OF *NEOMYSIS MERCEDIS* AT 1-METER DEPTH AS A FUNCTION OF TIDAL VELOCITY AND DAY VERSUS NIGHT

Positive is flood tide.

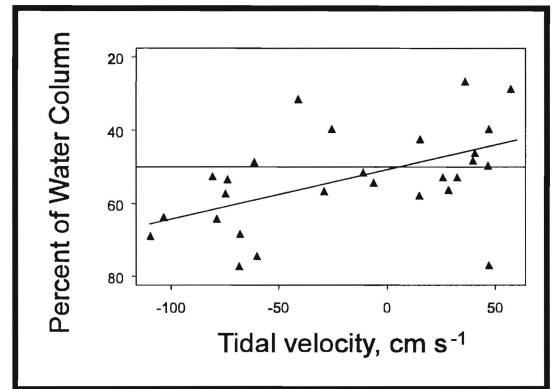


Figure 6
DEPTH OF CENTER OF MASS OF *EURYTEMORA AFFINIS* POPULATION AS A FUNCTION OF TIDAL VELOCITY, FOR ADULTS, BY DAY ONLY

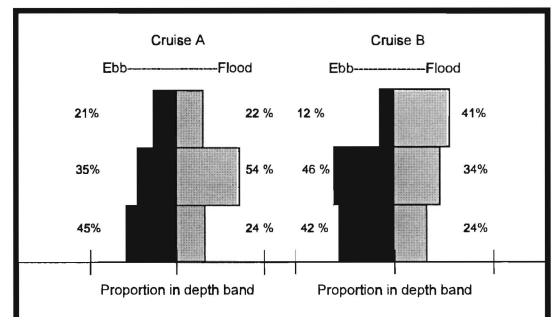


Figure 7
PROPORTION OF LONGFIN SMELT LARVAE IN DEPTH BINS ON EBB AND FLOOD TIDES FOR CRUISES A AND B

reduce vulnerability to visual predation.

Three of the five most abundant species of larval fish in our samples (striped bass, longfin smelt, and yellowfin goby) consistently migrated vertically, occurring near the surface on flood tides and near the bottom on ebb tides (Figure 7). Striped bass larvae appeared to change vertical position at or near slack tides. The degree and onset of vertical migration was presumably influenced by air-bladder development and affinity for the entrapment zone habitat. Prickly sculpin and shimofuri goby larvae consistently occurred near the surface and disappeared from our samples in the late larval stage. These species may move laterally in the late larval stage before settling in shoal/slough habitats.

We examined shipboard ADCP data on the vertical distribution of sound-scattering particles in the water. During the cruises it became apparent from their vertical movements that scattering layers were composed of organisms: layers were seen to move up and down in the water column in apparent response to sunlight. The relationship between sound scattering and organism abundance was significant but not strong, probably because we did not sample at the same depths as the layers of scatterers, and also because we did not determine biomass of organisms in the net samples. Backscatter intensity varied dielily and with tidal velocity as for the net-caught zooplankton.

The tidal variation in vertical distribution of all species (including amphipods as a “species”) resident in or slightly landward of the entrapment zone is probably due to active migration rather than some passive mechanism. A passive mechanism would have applied also to phytoplankton and nonliving particles, but vertical distribution of chlorophyll did not vary with tidal currents. Suspended particle concentration (measured as OBS voltage) increased in the water column on the flood relative to the ebb, but its vertical distribution did not vary tidally, consistent with re-

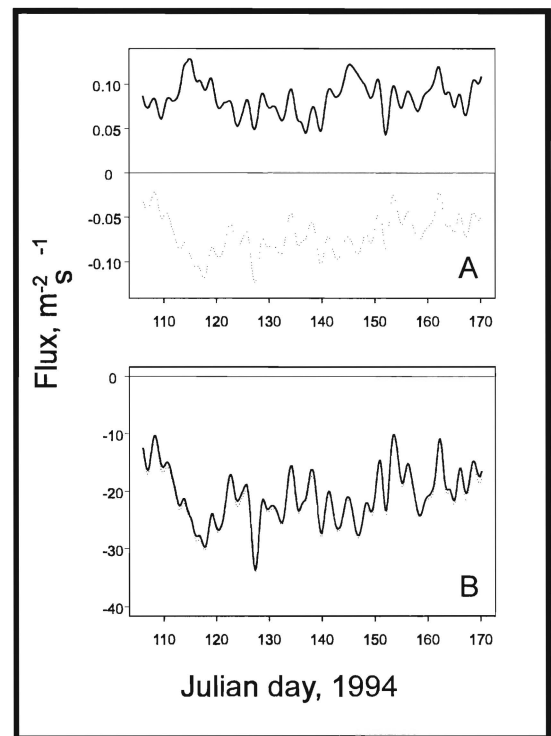


Figure 8
FLUX OF ZOOPLANKTON ALONG THE ESTUARY

Calculated from response surfaces to the depth distributions and ADCP velocity data from

suspension of particles off the bottom due to greater bottom shear on the flood.

For total net-caught zooplankton, total copepods, and suspended particles, we calculated net flux along the axis of the estuary due to currents alone and due to the interaction of oscillating tidal currents with the observed time-dependent vertical distributions. Net fluxes due to residual currents were always seaward because of the net flow due primarily to freshwater input. The flux of net-caught zooplankton was reversed by the interaction of their tidal migration off the bottom and tidal currents, so that they moved landward at all three stations (Figure 8A). Copepods, however, migrated only within the water column, and apparently did not go to the bottom as did the larger net-caught zooplankton. With the observed tidal velocity profiles, this pattern was insufficient to reverse, or even to substantially reduce, their seaward transport (Figure 8B).

This last result was surprising, since the longitudinal distributions of copepods and larger zooplankton were historically quite similar (Figure 1). There are several possible ways to reconcile this result with the observation of persistent maxima in copepod abundance, all of which need to be tested in future studies.

Summary of Key Findings

- Gravitational circulation occurs when the longitudinal density gradient is large relative to the effects of tidally produced vertical shear, which breaks down the stratification necessary for gravitational circulation to occur.
- Gravitational circulation was uncommon in Suisun Bay in late spring of 1994 because of the shallow depth and large tidal currents resulting in intense vertical mixing.
- A large fraction of the activity and biomass of bacteria in the entrapment zone is associated with particles, rather than free-living bacteria.
- Particle-associated bacteria may be metabolically distinct from free-living bacteria and may provide an important pathway for organic carbon to be incorporated into larger organisms.
- Tidal vertical migration is apparently a universal behavior of entrapment zone and near-entrapment zone resident species of zooplankton and larval fish; some species also migrated dielly.
- The migratory pattern did not vary appreciably with distance landward or seaward of the entrapment zone, although abundance varied considerably.
- Migratory patterns of zooplankton did not change among cruises during the studies, but those of larval fish changed as the fish developed.

- Migratory patterns of net-caught zooplankton were sufficient to reverse net seaward movement.
- Migratory patterns of copepods were insufficient to reverse net seaward movement, suggesting an alternative explanation for their longitudinal distributions.

Significance of These Results to the Interagency Ecological Program

Our results provide new insights into the biological implications of circulation patterns in Suisun Bay. These insights may be applicable to many macrotidal estuaries. For example, although tidally oriented vertical migration in estuaries has been observed before, it has never been observed in such a variety of organisms as seen in our study.

Our results also have several implications for management of the estuary:

- Substantial changes in bathymetry, such as by dredging landward of the Benicia bridge, could have a profound effect on gravitational circulation, with unknown effects on the biota.
- Organism behavior appears to exert an overriding influence on longitudinal movement, at least for larger zooplankton and probably larval fish. Conceptual and simulation models of the movements of such organisms cannot describe these organisms as passive particles.
- Despite similar longitudinal distributions, the mechanism for concentration of large zooplankton and copepods appears to differ, which may help to explain why the former respond in abundance much more strongly to variation in X_2 .
- The entrapment zone differs from other parts of the estuary in the feeding environment for small organisms: bacteria should be more available to zooplankton grazers in the entrapment zone than elsewhere in the estuary. This provides further evidence that bacteria are a key component of the food web of this part of the estuary.
- Increasing organic matter input to the entrapment zone through maintaining or stimulating organic production in the freshwater delta may be more effective at stimulating secondary production in the entrapment zone than simply increasing the total flux of organic matter by increasing flow.

Chapter 1

Introduction to the 1994 Entrapment Zone Study

Wim Kimmerer
Romberg Tiburon Center
San Francisco State University
PO Box 855
Tiburon, CA 94920

Entrapment of particles in the low-salinity region was one of the first topics of focused, multidisciplinary studies in the San Francisco estuary (Peterson *et al* 1975; Arthur and Ball 1979). Theoretical and experimental investigations in this region have resulted in an increasing level of understanding and an increasing appreciation of the complexity of this area (Cloern *et al* 1983; Kimmerer 1992). The earlier studies were based on a conceptual model of the hydrodynamics of the estuary that focused mainly on net (*ie*, tidally averaged) flows. Recent revisions of concepts about how

tidal and net flows interact has forced a re-examination of the physical environment and, therefore, also the mechanisms by which particles and organisms are concentrated in the low-salinity region of the estuary.

This section provides an overall introduction to the study, including the general theory and the aspects of sample design common to two or more parts of the study. Subsequent chapters provide a more specific context for the results described, as well as details of the methods.

Motivation for the Study

Our study of the entrapment zone is motivated by management interest, scientific curiosity, and technological development.

The 1994 agreement among agencies and stakeholders to provide additional protection to the ecosystem of San Francisco Bay relied heavily on a salinity standard. This standard establishes objectives for the position of X₂, the distance up the axis of the estuary from the Golden Gate to the point where salinity is 2 psu (practical salinity units) at 1 meter off the bottom. X₂ is correlated with delta outflow and also with the abundance or survival of several estuarine-dependent species (Jassby *et al* 1995). These "Fish-X₂" relationships provided the rationale for setting a standard

based on salinity. X₂ is a crude tool to use for managing the estuary, but it can be refined only through improved understanding of the various mechanisms underlying these correlations.

The implicit assumption underlying the X₂ standard and the CALFED process is that shallow low-salinity habitat is essential to the estuarine ecosystem, and that providing more of it will be beneficial. The central position of this assumption in current and proposed management scenarios indicates a major change in beliefs about how the ecosystem responds to flow. Where once the prevailing view of flow effects had to do with transport and flushing, the present view recognizes the limited

effect of freshwater flow on current velocities in the tidal estuary and posits that the position of a given salinity range, rather than flow *per se*, has the greatest influence on the ecosystem.

This belief has not been tested. Yet, great differences in management of the estuarine ecosystem are implied by these alternative views of its function. If habitat is indeed limiting, then constructing more habitat in the delta should offer a similar benefit to providing more flow. On the other hand, if populations are influenced directly by flow or exports, then changing the flow and export regime would be more effective than creating habitat.

Given that the cost of alternative actions could reach billions of dollars, it seems essential to understand as well as possible how freshwater flow influences the ecosystem. The mechanisms by which the abundance or survival of different species vary with X_2 probably differ among species. At present these mechanisms can be guessed, but none is known with any certainty (Estuarine Ecology Team 1996). Knowing these mechanisms may permit more precise, effective, or economical management of the estuarine ecosystem and may prevent the enactment of costly and ineffective measures for ecosystem protection.

For species resident in and near the entrapment zone, the correlation with X_2 may be due to variations in intensity of trapping mechanisms with position of the entrapment zone (Estuarine Ecology Team 1996). Entrapment zone residents include species of interest such as delta smelt, longfin smelt, and young striped bass, as well as several ecologically important species in lower trophic levels. Therefore, it is worthwhile to investigate these trapping mechanisms, the nature of the entrapment zone

as habitat, and the responses of the entrapment zone to changes in X_2 or delta outflow.

Particle-tracking models are having increasing utility for examining the effects of alternative flow regimes on the movement of salt and particles. Future versions of these models may prove essential for predicting the effects of alternative flow regimes in the delta or elsewhere, provided they can be modified to depict flows in stratified portions of the estuary. To extend these models to any motile organisms such as larval fish, however, requires understanding of the interaction of vertical movements of these organisms with the tidal flow regime. The entrapment zone study presented here was motivated partly by the need to know more about these movements.

From a strictly scientific perspective, the entrapment zone is an excellent location to study a fundamental issue in ecology: how organisms are able to cope with a particularly demanding physical environment. To what extent are the populations resident in the entrapment zone influenced by patterns of circulation, and to what extent by food limitation or other biotic interactions?

Finally, we are motivated to conduct studies of the entrapment zone by technological development. Modern computers, acoustic doppler current profilers, and conductivity-temperature-depth instruments with additional sensors permit a much more finely resolved assessment of the physical environment than was heretofore possible. These advances in technology have permitted the development of more detailed mathematical and conceptual models of circulation (see Burau, this volume), which in turn allow the development of improved models of biological/physical interactions.

Background

The traditional concept underlying an entrapment zone is as follows (Postma and Kalle 1955; Festa and Hansen 1976, 1978; Officer 1976, 1980; Arthur and Ball 1979; Kimmerer 1992). Near the landward limit of salt penetration into the estuary, fresh water flowing out to sea entrains some saltier water, resulting in a longitudinal gradient in salinity. Surface flow is seaward because of a tidally averaged slope in surface elevation from the river mouth to the sea. The salinity gradient also results in a density gradient, which tends to move saltier water landward near the bottom. This two-layer net or tidally averaged flow is believed to trap living and non-living particles near the landward limit of salt penetration, resulting in a maximum in turbidity and living particles.

The main problem with this simple conceptual model is that it treats the estuary as static except for the net flows near the surface and the bottom. It ignores the role of tidal influence on mixing and longitudinal transport. The most important aspect of tides in this context is the periodic breakdown of stratification through turbulent mixing generated by shear stress near the bottom. Without stratification, two-layer flow or gravitational circulation is generally weak, because momentum is transferred throughout the water column unhindered by the buoyancy effects that occur in a stratified water column. The velocity profile in an unstratified water column therefore approximates a simple boundary layer, following a log profile; the average of this profile over time is a unidirectional, seaward velocity profile because of the barotropic mean flow (essentially delta outflow).

The horizontal density gradient that drives gravitational circulation is negligible land-

ward of the position of 2-psu bottom salinity (X_2); therefore, landward of X_2 stratification is weak except at high freshwater flows (Jassby *et al* 1995). Horizontal density gradients produce a density current that can create stratification depending on the strength of the vertical shear, which depends on strength of tidal currents (slack versus maximum current, spring versus neap). The strength of the density currents, and therefore the stratification, peak at slack water when vertical shear and therefore mixing is at a minimum. Conversely, stratification virtually disappears on every tidal cycle when the currents reach their maxima. If the time-average of these density currents exceeds the barotropic mean flow, then we observe gravitational circulation.

The traditional model of the entrapment zone also neglects other mechanisms for creating a maximum in turbidity or particles. These include local sources of materials (*eg*, shoals), complex shoal-channel circulation patterns (*eg*, Lucotte and d'Anglejan 1986), landward transport of particles through Stokes drift, and local minima in dispersive energy, such as at a wide place in the channel (Giese and Jay 1989). In addition, maxima can occur through the interaction of vertical distribution of particles and stratification-induced ebb/flood shear asymmetries (see Burau, this volume).

Finally, the simple model of the entrapment zone is based on limited information about patterns of velocity on a time and space scale relevant to the measurement of fluxes. Improvements in these measurements, specifically with the use of acoustic doppler current profilers, now make it possible to resolve the actual fluxes and determine the mechanisms underlying them.

Conceptual Model of Concentration Maxima

Maxima in turbidity and in the abundance of several species of organism persist across a wide range of conditions of fresh-water flow. Without a mechanism to maintain these maxima, longitudinal dispersion produced mainly by tidal currents would erode them, resulting in a monotonically sloping concentration profile with distance along the axis of the estuary. A resident population of estuarine planktonic organisms cannot be maintained without a maximum somewhere in the estuary. Maxima in concentrations or abundance can be maintained by one of the following mechanisms:

- A source of the material, such as a shoal discharging sediment, or an elevated growth rate in a restricted region of the estuary.
- A local minimum in longitudinal dispersion rate.
- A flux of material toward the maximum, sufficient to offset dispersion away from the concentration maximum. This flux could occur through:
 - Advection (*ie*, flow toward the maximum in at least part of the water column).
 - Stokes drift (due to the phase difference between sea level and velocity).
 - Directed movement (*ie*, swimming landward or seaward by larger organisms).
 - Vertical or lateral movement in synchrony with tides resulting in net movement toward the maximum.

I include as “particles” all non-living particles as well as living particles with a swimming speed much lower than current velocities; *ie*, plankton and larval fish. Since they cannot swim very fast, their primary control over longitudinal or lateral position is through vertical movement. The longitudinal transport or flux of particles past a point along the estuarine channel can be described simply as:

$$Flux = \overline{UCA}$$

where U is velocity along the channel (positive is landward), C is the concentration of particles (or abundance of organisms), and A is cross-sectional area. All three variables may vary with time. The overbar indicates averaging of the product over time, and the brackets indicate averaging over the cross-sectional area. The tidally averaged value of this flux is the net transport; if this is negative, then on average the material will be washed seaward of this section.

If the velocity U were always negative, as in a river, the flux would always be seaward. However, in the San Francisco estuary, U reverses tidally and is typically much larger than the net, river-derived water velocity. Thus, an opportunity exists for fluxes to develop in either direction, depending on how U and C covary.

The velocity and concentration (U and C above) can each be described as a mean value plus a component that fluctuates in space and time. We will ignore fluctuations in A with tide, meaning we ignore Stokes drift, which is probably unimportant to transport in the channels (see Burau, this volume). Then the above equation can be decomposed into:

$$Flux = \left(\overline{U} \overline{C} + \overline{U_x C_x} \right) A$$

where U_x and C_x are the fluctuating (*ie*, varying tidally, vertically, and across the section) parts of U and C respectively. These fluctuating parts, by definition, have an average value of zero.

Typically the mean velocity is negative (seaward) and much smaller than the tidal velocities. The tidal velocities U_x vary in time and also in position within the cross section. In the absence of stratification, velocity generally has a logarithmic profile with depth, so that it is highest near the

surface and is also lower near the sides and over shoals than in the channels. It can be asymmetrical on ebb and flood, so that it is stronger in a seaward direction in one part of the cross section and stronger landward in another. Gravitational circulation is a case of vertical asymmetry, in which the time-averaged velocity near the bottom is positive (landward) even though the cross-sectionally averaged velocity is seaward.

If the concentration C is constant or fluctuates randomly, the average value of the right-hand term above will be zero, and the flux of particles will be seaward. Any mechanism that causes the fluctuating parts of U and C to covary positively can cause landward transport. This can happen in three ways (Figure 1):

- The concentration of particles in the water column is highest where flow is flood-dominated; this can occur if the particles sink or swim downward, and there is either two-layer estuarine circulation or a pronounced flood dominance in the deeper parts of the water column and ebb dominance in the shallower locations. (Figure 1A)
- The concentration of particles in the water column increases on the flood, either by resuspension of sediments from the bottom or off shoals or by the migration or tidal resuspension of demersal organisms off the bottom. (Figure 1B)
- The concentration of particles is the same throughout the tide, but the particles are higher in the water column on the flood than on the ebb; this will put the highest concentration at a higher velocity on the flood than on the ebb. (Figure 1C)

An additional mechanism for apparent landward movement applies to biological particles, which can increase in abundance through reproduction:

- The reproductive minus death rate of biological particles is sufficiently higher landward (*ie*, in the entrapment zone) to

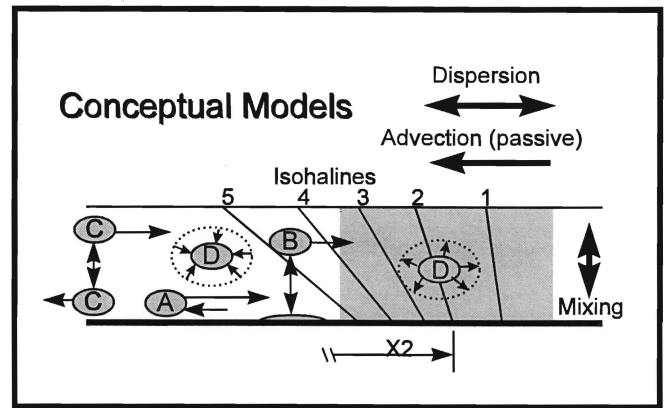


Figure 1
SCHEMATIC LONGITUDINAL SECTION OF THE ESTUARY
SHOWING ISOHALINES AND CONCEPTUAL MODELS OF
INTERACTION BETWEEN BEHAVIOR OF PARTICLES AND
LONGITUDINAL MOVEMENT

With a maximum in abundance of particles (shaded area), dispersion will tend to move particles away from the maximum and advection due to streamflow will move particles seaward. Tidal shear generates mixing that tends to remove vertical gradients, particularly in shallow areas. Particles can maintain a maximum by:

A, Remaining deep in the water column, provided there is sufficient ebb/flood asymmetry in velocity profiles (*ie*, landward transport dominates);

B, Migrating vertically off the bottom during flood currents and to the bottom on ebb currents;

C, Migrating higher in the water column on flood currents and deeper in the water column on ebb currents, provided shear in the currents is sufficient; or

D, Having a higher local net population growth (birth - death) in the region of the maximum than elsewhere.

offset the seaward losses to advection and dispersion. (Figure 1D)

The measurement of longitudinal fluxes in an estuary is complicated by great variability in tidal velocity (Kjerfve and Proehl 1979). Development of the acoustic doppler current profiler has provided a means of obtaining a large quantity of information on the distribution of velocity to help resolve the transport of particles. Now the greatest limitation to measuring fluxes is obtaining adequate resolution of the distribution of particles.

In the design of this study we have focused on vertical spatial variation with scales of meters as well as tidal time scales. We have also gathered some data on longitudinal variation and on variation among three cruises, two close to neap tides and one close to a spring tide. We have ignored the lateral component of variation for this study to keep the workload manageable.

Entrapment Zone as Habitat

Several estuarine species are most abundant in or near the entrapment zone for at least some life stages. For many of these species, the most significant aspects of the physical environment would appear to be related to the physical characteristics discussed above. That is, these species must have a way to offset losses to dispersion and seaward advection, either through high growth rate offsetting these losses (Ketchum 1954) or through behavioral interactions with the circulation pattern.

For small organisms such as bacteria, behavioral interactions would be limited to their ability to attach to particles that would be concentrated in the entrapment zone. Alternatively, the entrapment zone may represent a different and possibly more favorable environment for growth of bacteria than other regions of the estuary.

Thus our focus for bacteria is more on spatial variability in conditions for attachment and growth than on direct interactions with circulation patterns and, as discussed below, the sampling program for bacteria was quite different from those for other taxonomic groups.

For larger organisms such as zooplankton and larval fish, the entrapment zone could provide a physical environment where retention is possible, or a favorable biological environment. We focus in this study on the physical environment, while gathering data to interpret the biological environment in terms of the fine-scale distributions of bacteria, chlorophyll, and zooplankton that will be useful in modeling the feeding environment for entrapment zone species.

Study Objectives

The main goal of this study was to better understand the interaction of entrapment zone biota with their physical environment. Entrapment zone species examined included phytoplankton, bacteria, *Eurytemora affinis*, *Neomysis mercedis*, and larval fish that are sufficiently abundant in the entrapment zone, including striped bass, longfin smelt, and gobies.

Specific objectives were:

- To determine the relationship between vertical and longitudinal positions of common

entrapment zone species, salinity, and suspended solids and the velocity field under various conditions of tide and outflow.

- To determine the importance of particle-bound bacteria as a potential food supply for grazers and to bacterial community metabolism in and out of the entrapment zone.
- To obtain information on small-scale spatial (particularly vertical) distribution of larval fish and zooplankton.

Sample Design

The sampling program comprised continuous *in situ* monitoring of the physical environment, three spatially detailed investigations of the bacterial community, and three cruises to determine the distribution and movements of zooplankton. Continuous monitoring data were collected with acoustic doppler current profilers placed at the edge of the main shipping channel at Martinez (river kilometer 56), Port Chicago (64), Mallard Slough (74), and Antioch (83). In addition, CTDs recorded conductivity, temperature, depth, and optical backscatter at these and several other locations. Data used to interpret biological sampling were taken from the Mallard Slough ADCP, which was close to the center of the sampled area.

Bacterial samples were taken on April 19 and 28 from R/V *Questuary*, and on May 17 from R/V *Polaris*. Transects were run up the axis of the estuary from Martinez to Decker Island on the Sacramento River and Jersey Point on the San Joaquin River (Executive Summary, Figure 2).

Samples for zooplankton and phytoplankton were taken during cruises of R/V *San Carlos* on April 18-19 (Cruise A), April 26-27 (B), and May 17-18 (C). Our intent was to sample repeatedly in the same water mass over a period encompassing two full tidal cycles on each cruise. Use of drogues was not considered feasible in the restricted waters of the tidal channels with their heavy shipping traffic, so we used surface specific conductance as an indicator of the selected water mass.

Cruises A and C were conducted near neap tides and Cruise B near spring tide. During each cruise the vessel cycled for 27-28 hours among three stations defined by a surface specific conductance of about 1, 3, and 6 mS/cm (stations 1, 3, and 6). Each station was visited once per tidal cycle starting at station 6, with the timing set to arrive at station 3 (the "EZ" station) near the maximum flood and ebb. Station 3 was also visited as close as possible to slack water on most tides. Times of slack water were estimated using harmonic predictions. Surface specific conductance was measured using a continuous flow-through system.

The vessel was equipped with a GPS (global positioning satellite) receiver equipped with the MapTech program to allow users to record position on a computer disk. A 1200 kHz broadband ADCP was mounted on a swing arm on the starboard side of the vessel near the stern. At each station the ADCP was lowered into the water and secured, then turned on to record at about 5-second intervals and 25-centimeter depth bins starting at 1.25 meters depth. The ADCP was used to provide on-board read-outs of velocity profiles and also to attempt to detect scattering layers of organisms.

At each station the position was recorded on disk and on data sheets. Two casts were taken with a Seabird CTD (conductivity-temperature-depth) instrument. Samples were taken for large zooplankton and larval fish with Bongo sampling nets and for small zooplankton and phytoplankton with a pump. Details of sample collection and processing are provided in individual chapters.

Conditions During Cruises

Figure 2 in the Executive Summary shows the sample area with the locations of fixed ADCP sensors, bacterial sampling stations, and the range of ship's positions during the three cruises on R/V *San Carlos*. Table 1 lists times of stations and samples taken at each station from R/V *San Carlos*.

The hydrograph for the study period (Figure 2) shows a typical spring decline with several flow pulses in April and May. The first pulse, occurring around the time of Cruise B, probably did not affect conditions on that cruise because of the time (probably several days) for that pulse to reach the sample area. During cruise C the sampling area was shifted somewhat seaward (Executive Summary Figure 2) because of the cumulative effects of the flow pulses in late April and early May.

Figures 3-5 show the tidal speeds at Chipps Island, median ship's position as river kilometer index at each station, and wind speed and solar radiation at Chipps Island during the three cruises. Tidal speeds are water column means from the fixed ADCP at Chipps Island (river kilometer 74), calculated parallel to the channel axis. The nominal tidal stages at the times of sampling lagged slightly behind the actual tide; that is, most of the slack-water samples were taken somewhat after slack water. The ebb-dominance of the water column mean current speed is evident in all

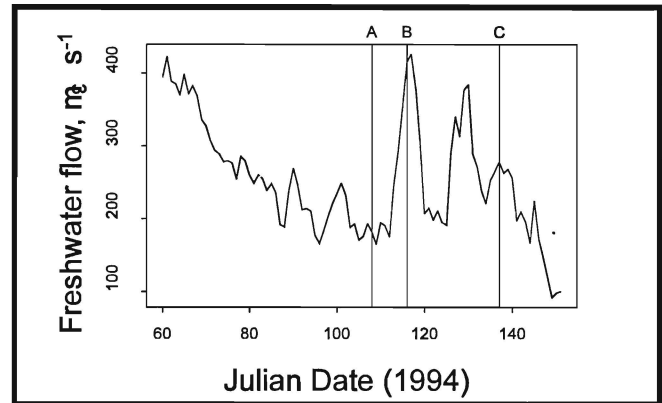


Figure 2
FRESHWATER OUTFLOW CALCULATED IN THE
DWR DAYFLOW PROGRAM FOR MARCH-MAY 1994

Vertical lines indicate the days on which each of the three cruises began.

three figures, and translates to tidally averaged speeds of -7 , -11 , and -6 cm/s, where negative speeds indicate westward (outward) flow. Wind was westerly during most of all three cruises, strongest during cruise A and weakest during cruise C.

Salinity showed increasing stratification with distance seaward on each cruise (Figures 6-8), but no consistent differences between ebb and flood at any of the nominal values. Optical backscatter voltage, related but uncalibrated to suspended solids, generally increased with depth, with occasional layers of backscattering particles near the bottom at all salinity values and tides (Figures 9-11).

Table 1
CONDITIONS DURING SAMPLING AND SAMPLES TAKEN

Columns show cruise, day (first or second day of the cruise), station, nominal specific electrical conductance (EC), tidal stage (high slack, ebb, low slack, flood), times over which stations were occupied, and whether samples were taken with the CTD, surface, middle, or bottom bongo net, and the pump.

Cruise	Day	Station	Nominal		Station Times		CTD	Bongo Samples			Pump Sample	Remarks
			EC	Tide	Start	End		S	M	B		
A	4/18	A	3	HS	10:57	12:10		S	M	B		
A	4/18	B	6	E	13:01	13:54		S	M	B	Y	
A	4/18	C	3	E	14:19	15:17		S	M	B	Y	
A	4/18	D	1	E	15:44	16:31		S	M	B	Y	
A	4/18	E	3	LS								No station
A	4/18	F	6	F	20:01	21:18	Y	S	M	B	Y	
A	4/18	G	3	F	21:50	22:46	Y	S	M	B	Y	
A	4/18	H	1	F	23:14	00:10	Y	S	M	B	Y	
A	4/19	I	3	HS	00:37	01:30	Y	S	M		Y	Bottom net failed
A	4/19	J	6	E	02:05	02:50	Y	S	M		Y	Bottom net failed
A	4/19	K	3	E	03:49	04:43	Y	S	M	B	Y	
A	4/19	L	1	E	05:12	06:17	Y	S	M	B	Y	
A	4/19	M	3	LS								No station
A	4/19	N	6	F	07:15	08:10	Y	S	M	B	Y	
A	4/19	O	3	F	09:00	09:58	Y	S	M	B	Y	
A	4/19	P	1	F	10:33	11:32	Y	S	M	B	Y	
A	4/19	Q	3	HS	11:59	12:57	Y	S	M	B	Y	
A	4/19	R	6	E	13:40	14:31	Y	S	M	B	Y	Davit broke
B	4/26	C	3	F	15:21	16:27	Y	S	M	B	Y	
B	4/26	D	1	F	16:53	17:39	Y	S		B	Y	Middle net failed
B	4/26	E	3	HS	18:10	19:04	Y	S	M	B	Y	
B	4/26	F	6	E	19:57	20:43	Y	S	M	B	Y	
B	4/26	G	3	E	21:22	22:06	Y	S	M	B	Y	
B	4/26	H	1	E	22:35	23:25	Y	S	M	B	Y	
B	4/27	I	3	LS	00:06	00:56	Y	S	M	B	Y	
B	4/27	J	6	F	01:29	02:16	Y	S	M	B	Y	
B	4/27	K	3	F	02:42	03:22	Y	S	M	B	Y	
B	4/27	L	1	F	03:49	04:31	Y	S	M	B	Y	
B	4/27	M	3	HS	05:43	06:32	Y	S	M	B	Y	
B	4/27	N	6	E		09:04	Y	S	M		Y	Bottom net failed
B	4/27	O	3	E	09:39	10:41	Y	S	M	B	Y	
B	4/27	P	1	E	11:06	11:55	Y		M	B	Y	
B	4/27	Q	3	LS	13:03	13:58	Y	S	M	B	Y	
B	4/27	R	6	F	14:50	16:06	Y	S	M	B	Y	
B	4/27	S	3	F	16:36	17:20		S	M	B	Y	
B	4/27	T	1	F	17:44	18:36		S	M	B	Y	
C	5/17	A	3	HS	10:05	11:19	Y		M		Y	Lost bottom net; moved middle down
C	5/17	B	6	E	11:42	12:42	Y	S		B		Pump failed
C	5/17	C	3	E	13:38	13:59	Y	S		B	Y	
C	5/17	D	1	E	15:20	16:03	Y	S		B	Y	
C	5/17	E	3	LS	17:14	17:56	Y	S		B	Y	
C	5/17	F	6	F	18:58	20:09	Y	S		B	Y	
C	5/17	G	3	F	20:28	21:28	Y	S		B	Y	
C	5/17	H	1	F	22:08	22:57	Y	S		B	Y	
C	5/17	I	3	HS	23:15	00:24	Y	S	M	B	Y	
C	5/18	J	6	E	01:16	01:56	Y	S		B	Y	
C	5/18	K	3	E	02:27	03:08	Y	S		B	Y	
C	5/18	L	1	E	03:42	04:27	Y	S		B	Y	
C	5/18	M	3	LS	05:10	05:53	Y	S		B	Y	
C	5/18	N	6	F	06:21	07:27	Y	S		B	Y	
C	5/18	O	3	F	08:12	09:07	Y	S		B	Y	
C	5/18	P	1	F	09:42	11:08	Y				Y	
C	5/18	Q	3	HS	11:09	11:43	Y				Y	
C	5/18	R	6	E	12:12	12:49	Y	S		B	Y	
C	5/18	S	3	E	13:26	14:16	Y	S		B	Y	

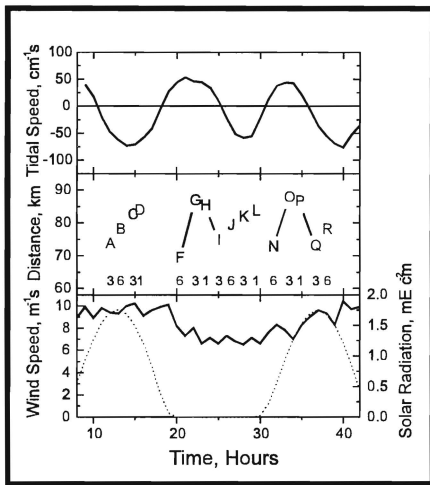


Figure 3
CRUISE A, APRIL 18-19, 1994

Top, tidal speed along channel axis averaged over the water column from ADCP data taken at Chipps Island; positive is the flood direction.

Middle, longitudinal position of the ship at each station,, midpoint of positions recorded during the station. Letters in the graph are station identifiers (Table 1); numbers below the curve give station (nominal specific conductance).

Bottom, hourly wind speed (solid line) and solar radiation (dashed line) at Chipps Island during the cruise.

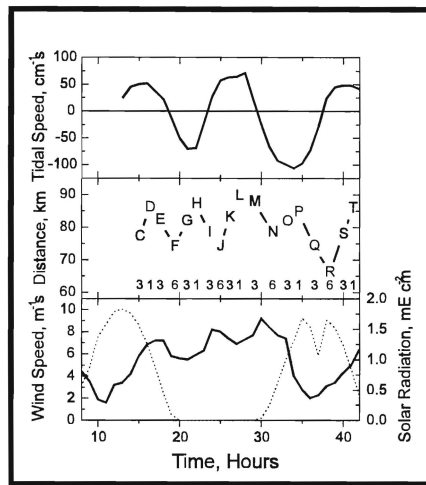


Figure 4
CRUISE B, APRIL 26-27, 1994

Top, tidal speed along channel axis averaged over the water column from ADCP data taken at Chipps Island; positive is the flood direction.

Middle, longitudinal position of the ship at each station, midpoint of positions recorded during the station. Letters in the graph are station identifiers (Table 1); numbers below the curve give station (nominal specific conductance).

Bottom, hourly wind speed (solid line) and solar radiation (dashed line) at Chipps Island during the cruise.

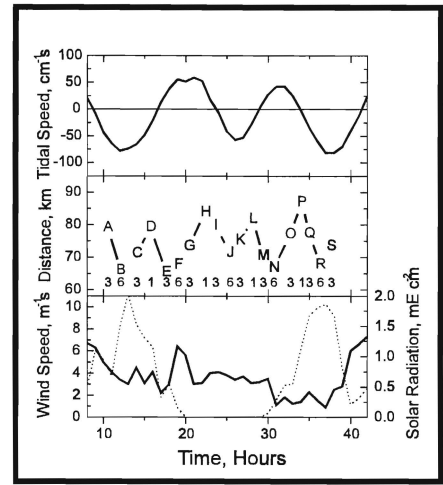


Figure 5
CRUISE C, MAY 17-18, 1994

Top, tidal speed along channel axis averaged over the water column from ADCP data taken at Chipps Island; positive is the flood direction.

Middle, longitudinal position of the ship at each station,, midpoint of positions recorded during the station. Letters in the graph are station identifiers (Table 1); numbers below the curve give station (nominal specific conductance).

Bottom, hourly wind speed (solid line) and solar radiation (dashed line) at Chipps Island during the cruise.

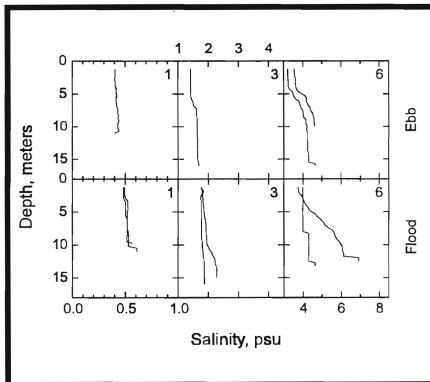


Figure 6
CRUISE A SALINITY PROFILES ON
EBB AND FLOOD TIDES AT
STATIONS 1, 3, AND 6

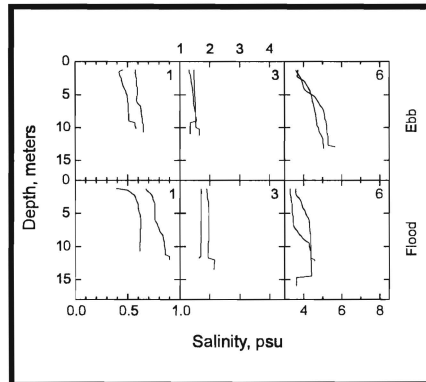


Figure 7
CRUISE B SALINITY PROFILES ON
EBB AND FLOOD TIDES AT
STATIONS 1, 3, AND 6

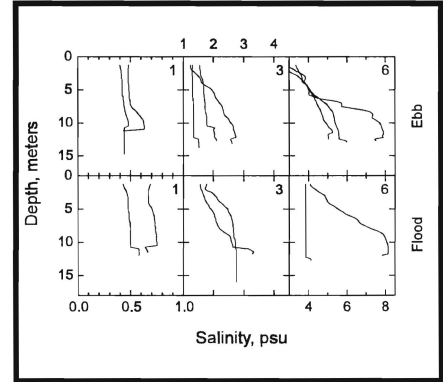


Figure 8
CRUISE C SALINITY PROFILES ON
EBB AND FLOOD TIDES AT
STATIONS 1, 3, AND 6

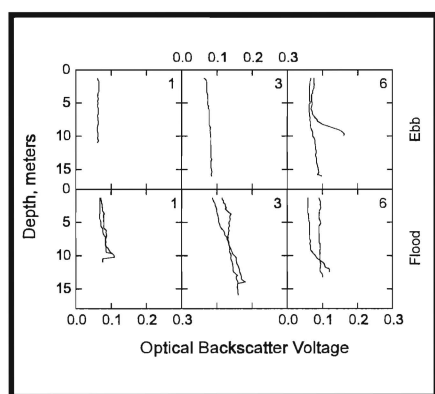


Figure 9
CRUISE A
OPTICAL BACKSCATTER VOLTAGE ON
EBB AND FLOOD TIDES AT
STATIONS 1, 3, AND 6

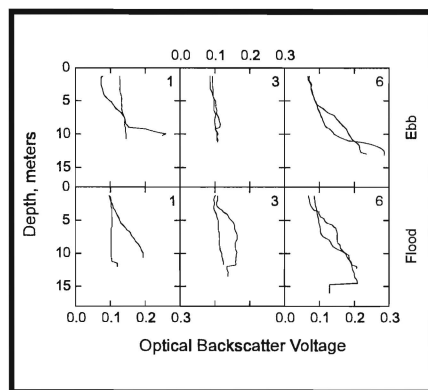


Figure 10
CRUISE B
OPTICAL BACKSCATTER VOLTAGE ON
EBB AND FLOOD TIDES AT
STATIONS 1, 3, AND 6

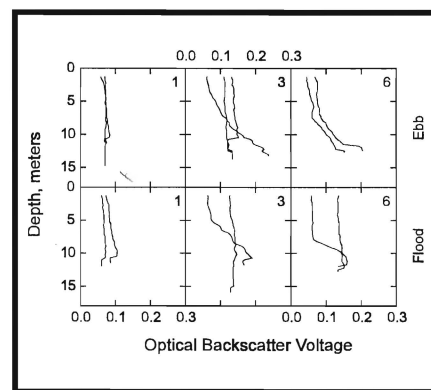


Figure 11
CRUISE C
OPTICAL BACKSCATTER VOLTAGE ON
EBB AND FLOOD TIDES AT
STATIONS 1, 3, AND 6

References Cited

- Arthur, J. A., and M.D. Ball. 1979. Factors influencing the entrapment of suspended material in the San Francisco bay-delta estuary. Pages 143-174. In T.J. Conomos [ed.], *San Francisco Bay: The Urbanized Estuary*. AAAS.
- Cloern, J., A. Alpine, B. Cole, R. Wong, J. Arthur, and M. Ball. 1983. River discharge controls phytoplankton dynamics in the northern San Francisco Bay estuary. *Estuar. Coastal Shelf Sci.* 16:415-429.
- Estuarine Ecology Team. 1996. *An Assessment of the Likely Mechanisms Underlying the "Fish-X2" Relationships*. Interagency Ecological Program Technical Report 52.
- Festa, J.F., and D. V. Hansen. 1976. A two-dimensional numerical model of estuarine circulation: the effects of altering depth and river discharge. *Estuar. Coastal Mar. Sci.* 4:309-323.
- _____. 1978. Turbidity maxima in partially mixed estuaries: a two-dimensional numerical model. *Estuar. Coastal Mar. Sci.* 7:347-359.
- Giese, B.S., and D.A. Jay. 1989. Modelling tidal energetics of the Columbia River Estuary. *Estuar. Coastal Shelf Sci.* 29:549-571.
- Jassby, A.D., W. J. Kimmerer, S.G. Monismith, C. Armor, J.E. Cloern, T.M. Powell, J.R. Schubel, and T.J. Vendliniski. 1995. Isohaline position as a habitat indicator for estuarine populations. *Ecological Applications* 5:272-289
- Ketchum, B.H. 1954. Relation between circulation and planktonic populations in estuaries. *Ecology* 35:191-200.
- Kimmerer, W.J. 1992. *An Evaluation of Existing Data on the Entrapment Zone of the San Francisco Bay Estuary*. Interagency Ecological Studies Program, Technical Report 33.
- Kjerfve, B., and J. Proehl. 1979. Velocity variability in a cross section of a well-mixed estuary. *J. Mar. Res.* 37:409-418.
- Lucotte, M., and B. D'Anglejan. 1986. Seasonal control of the Saint-Lawrence maximum turbidity zone by tidal-flat sedimentation. *Estuaries* 9:84-94.
- Officer, C.B. 1976. *Physical Oceanography of Estuaries (and Associated Coastal Waters)*. Wiley.

- _____. 1980. Discussion of the turbidity maximum in partially mixed estuaries. *Estuar. Coastal Mar. Sci.* 10:239-246.
- Peterson, D.H., T. Conomos, W.W. John Broenkow, and P.C. Doherty. 1975. Location of the non-tidal current null zone in northern San Francisco Bay. *Estuar. Coastal Mar. Sci.* 3:1-11.
- Postma, V.H., and K. Kalle. 1955. On the development of turbid zones in the lower course of rivers with special consideration of conditions in the lower Elbe. *Sond. Deutsch Hydr. Zeitschrift* 8:137-144.

Results from the Hydrodynamic Element of the 1994 Entrapment Zone Study in Suisun Bay

By Jon R. Burau, Jeffrey W. Gartner, and Mark Stacey
U.S. Geological Survey
Placer Hall, 6000 J Street
Sacramento, Ca 95819-6129

Abstract

The term entrapment zone has been used to describe a zone of elevated concentrations of particles, plankton, and juvenile fish observed in low-salinity areas of north (San Francisco) bay and the western Sacramento-San Joaquin Delta, California. The hypothesized mechanism for entrapment was a combination of particle aggregation, sinking and a residual current null zone. The null zone is a time-mean, near-bed flow convergence where riverine flow ends and gravitational circulation begins that was presumed to occur near a salinity of 2 psu. Current-meter measurements made prior to 1990 provide evidence of gravitational circulation and a null zone during autumn in the north bay of San Francisco Bay, including Suisun Bay and the western delta. Data collected after 1990, however, show an absence of gravitational circulation from most of Suisun Bay during spring, and the presence of multiple gravitational circulation cells between bathymetric constrictions elsewhere in the bay. Because null zones appear to be bathymetrically controlled, they often occur in areas far removed from the low salinity zone (near X2, the position of a bottom salinity of 2 psu). The presence or absence of gravitational circulation can be predicted with appropriate physical scaling, which explains the most recent and historical current-meter observations throughout the Bay/Delta system. In areas where gravitational circulation is weak or nonexistent, some other physical or biological mechanism(s) must be causing the observed concentration of particles and organisms in the low-salinity zone. Four physical mechanisms were evaluated: density-current pulses that occur near slack tide, ebb/flood shear stress asymmetries, vertical migration of organisms during the tidal cycle, and an upstream mass flux known as Stokes' drift. Stokes' drift was eliminated from further consideration because variations in sea level are small relative to the mean depth and because of the weak correlation between sea level and the tidal currents in Suisun Bay.

Introduction

From a broad perspective the studies described in this report are meant to uncover the underlying processes that cause the observed accumulations of suspended particulate matter and organisms in the low salinity zone in San Francisco Bay. Many possible accumulation mechanisms in es-

tuarine systems have been discussed in the literature that rely on the complex interaction between the tides, tidal currents, salt field, freshwater inflow, and biological behaviors at the tidal and residual timescales. Among them are: (1) gravitational circulation (Nichols and Poor 1967); (2)

shallow/channel exchange (Weir and McManus 1987); (3) wind-wave resuspension (Weir and McManus 1987); (4) stratification (Geyer 1993); (5) baroclinic flows that occur near slack water (Monismith and others 1996); (6) ebb/flood near-bed shear stress asymmetries (Stacey 1996); (7) ebb/flood vertical mixing asymmetries (Stacey 1996); (8) local minimums in energy [actually local energy flux divergence minimums] (Jay and others 1990); and finally (9) vertical or lateral migration (Kimmerer and Bennett, this volume).

In the San Francisco estuary, a gravitational-circulation based conceptual model of entrapment (Figure 2-1) has prevailed for the last few decades that was essentially borrowed from the other estuaries (Chesapeake: Pritchard 1952; Schubel 1968. Thames River: Ingles and Allen 1957. Mersey estuary: Bowden 1960) and was confirmed in a limited way in San Francisco Bay using (1) current meter data [Peterson and others (1975); Walters and Gartner (1985); Mortenson (1987); Smith (1987); and Nichol (1996)] and (2) drifter studies (Conomos and others 1971).

The data collected as part of the entrapment zone studies suggest, however, a

more complicated picture of the residual currents than is shown in Figure 2-1. The actual residual currents differ from this simplistic conceptual model because of the complex interaction between the seasonal landward migration of the salt field (in particular, the position of the horizontal salinity gradient) with the spatially variable geometry of north bay (a region including San Pablo Bay, Carquinez Strait, and Suisun Bay; Figure 2-2) and vertical mixing caused by the tidal currents. The idea that an (estuarine turbidity maximum occurs in the low-salinity zone that is directly derived from gravitational circulation (Figure 2-1) is useful because, based on the analysis of these data, this model applies in certain reaches of north bay (for example, seaward of Pinole Shoal and in Carquinez Strait) and in the western delta.

However, Figure 2-1 may be incorrectly interpreted to mean gravitational circulation directly advects nutrients and biota, somewhat like a conveyor belt, from the Pacific Ocean through north bay up in the low salinity zone. What the data in this chapter suggest instead is that gravitational circulation is rare in parts of the estuary (for example, the ship channel in Suisun Bay), and when gravitational circu-

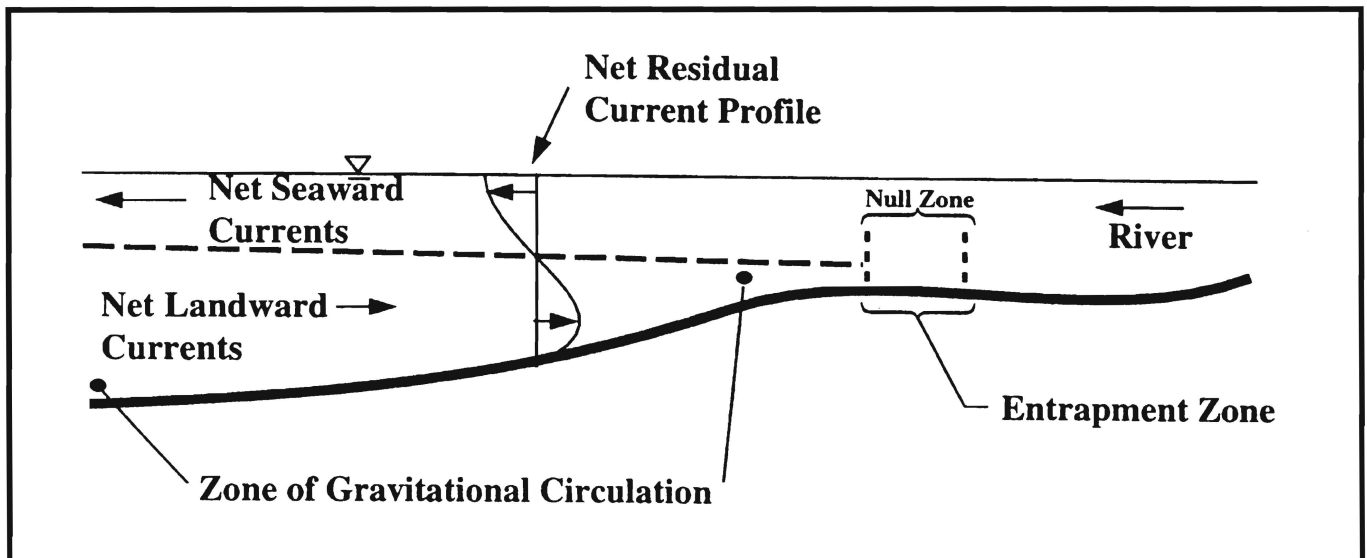


Figure 1
CONCEPTUAL MODEL OF THE ENTRAPMENT AND NULL ZONES

This chapter presents results of the analyses of U.S. Geological Survey (USGS) hydrodynamic data collected as part of the 1994 Interagency Ecological Program (IEP) entrainment zone study. The USGS took part in three 30-hour cruises in the north bay between April and June 1994. Prior to these cruises, *in situ* instruments that measured currents and salinity were deployed. This chapter focuses primarily on the analysis of data from five acoustic Doppler current profilers (ADCPs) deployed in Carquinez Strait, Suisun Bay, and the western delta (Figure 2-2). These analyses suggest a revision of the conceptual model of the entrainment zone. In this chapter, the existing conceptual model of entrainment based on a gravitational circulation hypothesis is discussed, and data inconsistent with this conceptual model are presented. A revised conceptual model of gravitational circulation based on the horizontal Richardson number is presented.

This revised model is consistent with the hydrodynamic data collected to date. Because the net currents in the channels cannot explain the observed accumulation

of suspended sediment (based on secchi disk data) and various organisms in the low salinity zone (~2 psu), alternate, tidal timescale, hydrodynamic (biological) processes were considered. (Salinities in this chapter's figures are given without units because, by definition, salinity is a conductivity ratio that has no physical units (Millerno 1993). For salinities greater than 2 psu, salinity is computed on the basis of the UNESCO standard (UNESCO 1985). Salinities less than 2 psu are computed after Hill and others (1986)). The lateral variation in the tides and tidal currents and the storage and release of waters into and out of the shallows substantially contribute to the distributions of salinity, suspended-sediment concentrations, and of nonmotile and feebly-swimming biota throughout the estuary. These processes, however, are beyond the scope of this chapter. This chapter focuses on three possible accumulation processes that act in the vertical plane: the first two processes involve the timing and structure of the velocity shear and vertical salinity stratification, and the third process examined is Stokes' drift.

Historical Perspective

Much of the conceptual understanding of the physics of the north bay was either inferred from detailed investigations of other estuaries or based on the velocity studies of Peterson and others (1975) and on the drifter studies of Conomos and others (1971). Peterson analyzed velocity measurements taken at eight stations throughout the estuary from 1956 to 1969. The measurements were taken at five depths during roughly 25-hour periods with Price AA¹ current meters. Based on these limited data, Peterson showed that

gravitational circulation existed seaward of Carquinez Strait. Conomos and others (1971) clearly show that gravitational circulation moved drifters released offshore (a drifter is a device designed to move with the current, often at preset density) landward into the bay. However, we now know that the residual currents seaward of Carquinez Strait are not indicative of the residual currents in the north bay as a whole, and the drifter studies provided little insight into the residual current patterns in

1 Use of the brand name in this chapter is for identification only and does not constitute endorsement by the U.S. Geological Survey.

Suisun Bay because no drifters were recovered landward of Carquinez Strait.

The USGS (Cheng and Gartner 1984), in collaboration with the National Oceanic Atmospheric Administration (NOAA) collected large amounts of current data throughout San Francisco Bay (Denton and Hunt 1986), including the north bay. Although these records were generally short (<1 month) relative to the typical deployment length of today (~3 months) and were collected during various times of the year, Smith (1987) analyzed these data for the presence of gravitational circulation and concluded that gravitational circulation is a dominant feature seaward of the null zone. Walters and Gartner (1985) analyzed a subset of these data collected during autumn 1978 and found strong gravitational circulation [~ 15 centimeters per second (cm/s)] in Suisun Cutoff and weak gravitational circulation (<10 cm/s) at Mallard Island, in the Reserve fleet channel, and in Carquinez Strait. In autumn 1986, Mortenson (1987) collected a remarkably complete data set in Suisun Bay following a relatively small runoff event [$\sim 21,000$ cubic feet per second (cfs)]. The residual currents measured by Mortenson showed a gravitational circulation cell in Suisun Cutoff during the falling limb of the hydrograph, a time when the horizontal salinity gradient was likely compressed and probably centered in the Suisun Cutoff area. Monismith and others (1996) confirm the observations made by Peterson and others (1975) and Cheng and Gartner (1984) that gravitational circulation dominates the residual flows in Carquinez Strait. Finally, data collected in the lower Sacramento River by the U.S. Army Corps of Engineers show a weak gravitational circulation cell in the western delta when salinities locally exceeded ~ 2 psu (Nichol 1996).

Therefore, ample hydrodynamic evidence existed in support of a gravitational-circulation-based conceptual model of entrap-

ment until 1993, when the USGS, in collaboration with Stanford University, began an annual series of detailed hydrodynamic studies in Suisun Bay. The methodology and purpose of these investigations were consistent with the work of Peterson and others (1975), Cheng and Gartner (1984), Mortenson (1986), and Nichol (1996). The only significant improvement on the previous studies was in the sophistication and amount of oceanographic equipment used. ADCPs that can measure a complete velocity profile of as much as 0.5-meter (m) intervals and Conductivity-Temperature-Depth (CTDs) sensors, capable of being continuously and autonomously deployed for as long as 3 months, were simultaneously deployed to capture the temporal and spatial variability in the tidal and residual currents in Suisun Bay.

Definitions

A review of the entrapment zone literature (primarily U.S. Bureau of Reclamation or California Department of Water Resources reports) suggests that confusion exists about the definition of the entrapment zone (Arthur and Ball 1979; Kimmerer 1993). Although Kimmerer (1993) rigorously defines the entrapment zone as “the area of the estuary where flow convergence results in the concentration of particulate matter; this [process] usually operates through the interaction of particle (or organism) sinking and net-landward flow at depth,” much of the literature is remarkably vague on exactly what the entrapment zone is. In general, however, it seems to be a catchall term that has been used synonymously with, and seems to encompass the terms such as turbidity maxima, biological maxima, null zone, and low salinity zone (or X2). Unlike the term entrapment zone, these other terms have precise definitions that are well documented in the literature. These terms are not synonymous, even though they describe related phenomena. For example, the null zone has nothing to

do with elevated concentrations of suspended sediment (or elevated concentrations of anything else). The null zone is simply the area where net landward flow near the bottom ceases and just downstream of where net flow throughout the water column is seaward (Figure 2-1).

An important element of the gravitational-circulation-based conceptual model of accumulation (Figure 2-1) is that the phenomena described by these related terms are co-located. An overarching term that generally describes a zone where all of these terms apply is useful if these things are actually occurring at the same place and time. On the basis of the analysis of the data described in this chapter, the null zone, turbidity and biological maxima and X2 can often occur at entirely different locations in the estuary. Therefore, if the primary utility of the term, entrapment zone, was to describe a region where these related phenomena were occurring simultaneously, then the term is misleading. Analysis of these data suggests that these related phenomena are not occurring at the same place and time, at least with respect to the residual currents, turbidity maximum, and X2.

Timescales

Another reason for the ambiguity in the use of the term entrapment zone, and the difficulty in understanding the underlying mechanisms that may create it, is the pervasive mixing of timescales in papers in which the entrapment zone is discussed. For example, from the Kimmerer (1993)

definition of the entrapment zone, one could infer that the entrapment zone primarily evolves from the net landward flow at depth. It follows that if the entrapment zone evolves from a residual process such as the net currents determined through time averaging, then the entrapment zone itself is realizable only in a time-mean sense. Therefore, if the entrapment zone is defined in this way, the location of the entrapment zone cannot be determined from a single cruise, but from several cruises taken throughout a complete tidal cycle to be consistent with this definition.

Furthermore, Kimmerer (1993) defines the operational definition of the entrapment zone as having a surface salinity range of 1 to 6 psu without specifying the timescale. To be consistent with a gravitational circulation conceptual model of entrapment, the operational definition of the entrapment zone should be the position of the time-mean salinity range of 1 to 6 psu. In this chapter, an operational definition of the entrapment zone was used that follows the movement of the salt field (Lagrangian) and is consistent with the Kimmerer (1993) definition. This definition is consistent with the timescale of cruise data that form the basis of most of the entrapment zone literature to date, but is inconsistent with the Eulerian-based conceptual model of gravitational circulation and the null zone because the residual timescale is used in this conceptual model.

Given the confusion over the term entrapment zone some key terms used in this chapter are defined in a glossary of terms given at the end of this chapter.

Existing Conceptual Model of Entrapment in the North Bay

The generally accepted conceptual model of the entrapment zone is of an area in the estuary where a flow convergence results in an increased concentration of particulate matter through the interaction of particle (or organism) aggregation and sinking and net landward flow at depth (Arthur and Ball 1979; Kimmerer 1993). For this chapter, the terms, net, tidally averaged, and residual, imply timescales whose periods are significantly longer than the diurnal tidal period of about 25 hours. The null zone, which generally is believed to coincide with the landward limit of the entrapment zone, is a location in the estuary just landward of the cessation of residual landward flow near the bottom (Figure 2-1). The entrapment zone and null zone have been associated with the low salinity zone (salinity of 1 to 6 psu, Arthur and Ball 1979; Kimmerer 1993) and more recently associated with X2, the position of the near-bed, 2 isohaline (Jassby and others 1995). This model of the entrapment zone assumes the presence of gravitational circulation, a landward residual flow along the bottom of

the estuary seaward of the low salinity zone.

Gravitational Circulation

The physics of gravitational circulation have been understood for at least four decades (Pritchard 1952; Postma and Kalle 1955) and have been well documented (Hansen and Rattray 1965; Peterson and others 1975; Officer 1976). For this chapter, gravitational circulation is a residual (tidally averaged), two-layer flow in which low-salinity water flows seaward in the surface layer, whereas denser, more saline water flows landward in the bottom layer. This two-layer flow results from the balance between the free surface slope acting in a down-estuary direction, and the longitudinal density (salinity) gradient acting in the landward direction (Officer 1976). See the appendix for the details of barotropic (free surface slope) and baroclinic (longitudinal density gradient) flows.

Principal Findings

Many of the principal findings in this report evolve directly from interpretations of the residual currents measured at fixed sites along the axis of north bay. Although the interaction of the tides and tidal currents with the residual currents are inherently nonlinear, the instantaneous current at any point in the estuary can be thought of as the sum of the currents from several independent processes (Figure 2-3). Except for the tidal currents, all the currents depicted in Figure 2-3 evolve from residual processes, which are at least an order of magnitude smaller than the tidal currents.

In this chapter we are primarily interested in the gravitational circulation component of the residual currents (Figure 2-3a) because gravitational circulation forms the basis of the historical conceptual model of entrapment in the north bay. In the following paragraphs, however, we place gravitational circulation in the context of the many other physical factors that can contribute to the residual currents. In practice, it is difficult, if not impossible, to separate out the individual contributions to the measured residual currents from the various mechanisms shown in Figure 2-3.

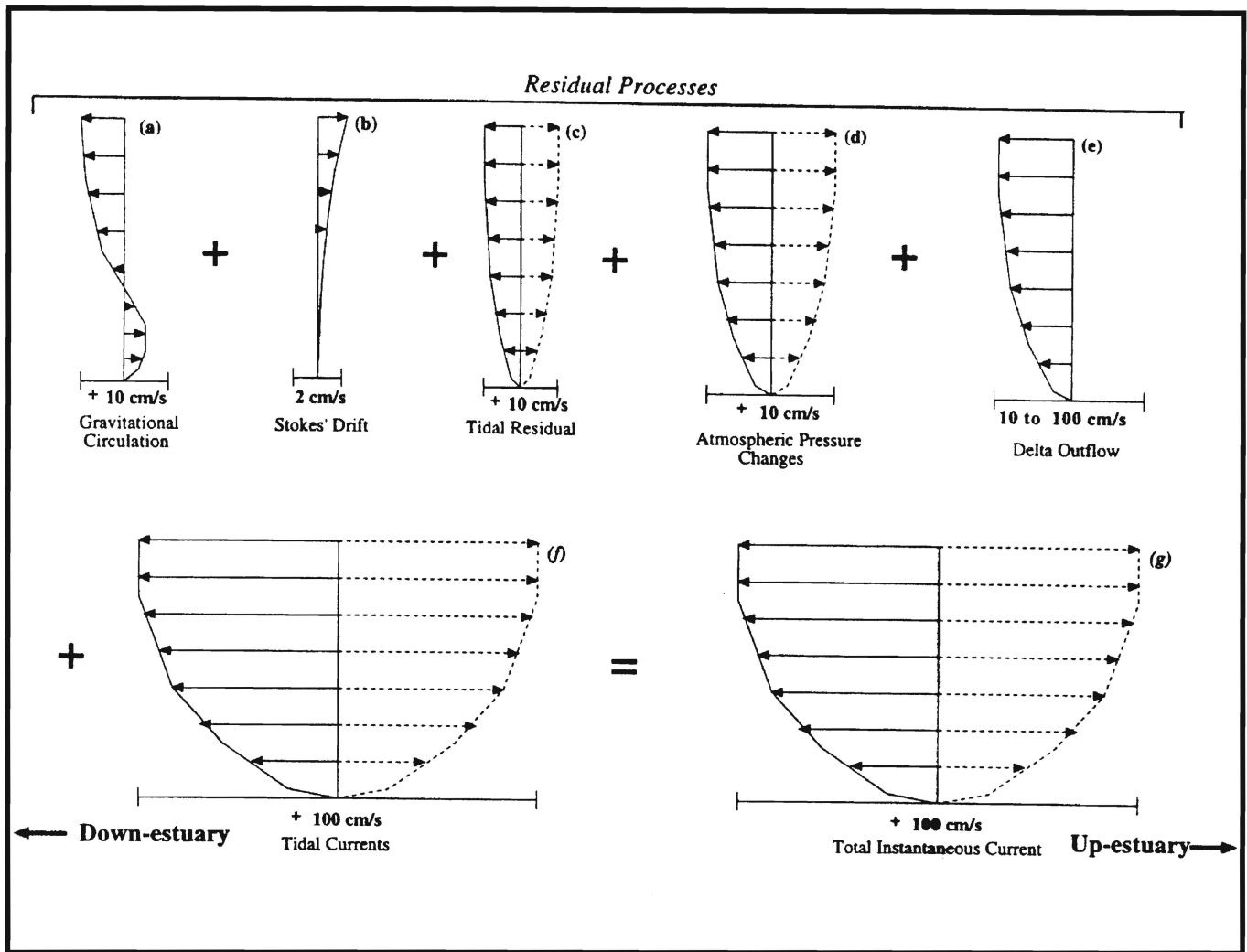


Figure 3
CONCEPTUAL MODEL OF THE TIDAL AND RESIDUAL CURRENTS IN THE NORTH BAY

Current magnitudes are approximate and vary considerably in time and space.

Dashed profiles in the landward direction are indicative of a process that can operate in either direction. The magnitudes of the tidal and residual currents given in this figure are order of magnitude estimates. Many of these values can vary, depending on location and season. The tidal residual evolves from the interaction of the tides with the bathymetry. ($x = \langle x \rangle + x'$, where $\langle x \rangle$ is a residual and x' is a deviation from the residual.) Current speed is shown in centimeters per second (cm/s).

However, in the final analysis, if the baroclinic pressure gradients are unable to create a net upstream residual current, we say that gravitational circulation is weak or nonexistent because without a net upstream residual current, entrapment from gravitational circulation is impossible, as defined.

The low-pass-filtered, or residual, velocities presented in this chapter represent the net result of all the residual processes depicted in Figure 2-3. So when the net near-bed currents are pointing in a land-

ward direction on a low-pass-filtered stick (velocity) plot, we state that “no gravitational circulation was observed.” What we really mean is that the sum total of the residual processes at a given location was such that the net near-bed currents were down-estuary (for example, gravitational circulation was weak relative to the other residual processes). A horizontal density

gradient ($\frac{\partial \rho}{\partial x}$, where ρ is the velocity and x is the along-channel distance) driven flow (Figure 2-3a) may actually exist, but may

be overshadowed by the other residual processes, such as a barotropic mean flow (for example, delta outflow). Gravitational circulation is the only residual process that depends on the gradients in the density field.

Stokes' drift depends on the correlation between tidal timescale water surface fluctuations (the tides) (ζ) and the tidal current, u' , which creates a convex-shaped Eulerian residual profile that is landward directed (Figure 2-3b) (Najarian and others 1984). Tidal residuals are generated through the interaction of the tides and tidal currents with the basin bathymetry (Figure 2-3c). Atmospheric pressure changes can induce exchanges between the Pacific Ocean and the entire San Francisco Bay system (Figure 2-3d). The water level in the delta can be raised as much as 0.4 m by a large atmospheric pressure drop. Delta outflow introduces a residual current throughout the north bay that varies with the amount and timing of the outflow. Residual currents, on the order of the tidal currents [~ 1 meter per second (m/s)], caused by delta outflow, can occur in the channels during large, uncontrolled winter flows (Figure 2-3e).

Three of the residual processes shown in Figure 2-3 have fortnightly (spring/neap) components. Gravitational circulation varies with the intensity of the vertical mixing; during spring tides, vertical mixing is strong and gravitational circulation, if it exists, is weaker. Because the tide-induced residual involves nonlinear interaction between the tides, tidal currents, and the basin bathymetry, it is expected that spring tides enhance this interaction (Walters and others 1985). The same is true for Stokes' drift; greater tidal range and tidal-current magnitudes during spring tides increase the magnitude of their correlation.

Except for gravitational circulation and Stokes' drift, the remaining residual processes are forced by water-surface slopes, which essentially yield a characteristic log

profile, as shown in Figure 2-3. Barotropic pressure gradients in the presence of strong vertical stratification can yield non-log profiles; however, these nonlinear interactions are beyond the scope of this chapter. Even though these interactions may be important in creating ebb/flood asymmetries in near-bed shear and vertical mixing that could contribute to concentration maxima in regions in the bay where gravitational circulation is weak, the study of these interactions is in its infancy and a topic of active research.

Because the position of the salt field and the strength of its gradients depend primarily on the uncontrolled winter freshwater flows into Suisun Bay, the timing and strength of gravitational circulation depend primarily on the hydrology in a given year. During 1994, a fairly dry year when peak delta outflows were less than 1,000 cubic meters per second (m³/sec) (Figure 2-4), the salt field was relatively far landward and X2 was near, or landward of, Mallard Island. Mallard Island has a river kilometer index (RKI) of 75 kilometers (km).

Gravitational Circulation

Approximate locations of the ADCPs deployed during the 1994 entrapment zone study are shown in Figure 2-2. ADCPs measure the velocity at a sequence of evenly spaced intervals above the bed. These measurement locations are referred to as "BINs" where BIN 1 is the velocity measurement nearest to the bottom. Data collected from ADCPs deployed in the southern channel of Suisun Bay (stations: CONC, CNCRD, MAL) and the western delta (stations: ANTCH, MK8) indicate little evidence of gravitational circulation, even though the mean position of the near-bed 2 isohaline was near or landward of Mallard Island (Figure 2-5). Specifically, ADCP data collected near Concord (Figure 2-6) and Mallard Island (Figure 2-7) indicate near-bed residual currents that were di-

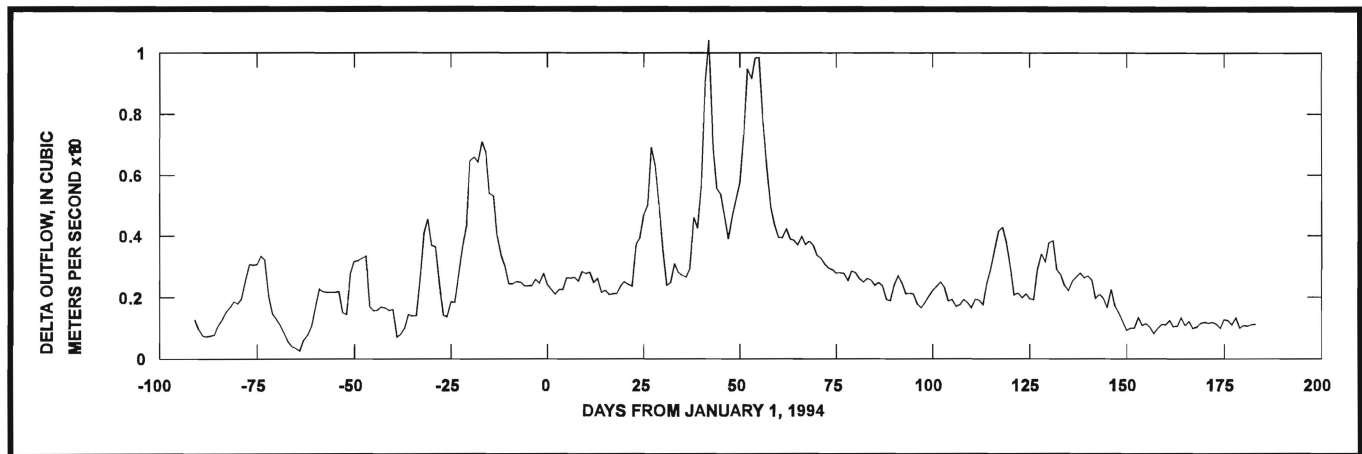


Figure 4
DELTA OUTFLOW ESTIMATES (DAYFLOW), OCTOBER 1, 1993, TO JULY 1, 1994, SUISUN BAY

CONC, CNCRD, MAL) and the western delta (stations: ANTCH, MK8) indicate little evidence of gravitational circulation, even though the mean position of the near-bed 2 isohaline was near or landward of Mallard Island (Figure 2-5). Specifically, ADCP data collected near Concord (Figure 2-6) and Mallard Island (Figure 2-7) indicate near-bed residual currents that were directed seaward, indicating a lack of, or relatively weak, gravitational circulation. In contrast, the ADCP data collected in Carquinez Strait near Martinez (station MRTNZ) from April 22 to June 15, 1994, show strong residual near-bed currents of 15 to 20 cm/s directed landward (Figure 2-8). ADCP data collected by NOAA in Carquinez Strait (Figure 2-9) and near Concord (Figure 2-10) from April 22 to May 22, 1992, are consistent with the data collected in 1994 in that near-bed residual currents in Carquinez Strait were landward, and near-bed residual currents were seaward at Concord, even though these data were collected during different water year types. During the 1992 NOAA deployments, X2 was also landward of Mallard Island.

The observed magnitude of landward near-bed residual currents in the Carquinez Strait ADCP (CAR in Figure 2-2) data, coupled with the seaward near-bed residual currents in the southern channel

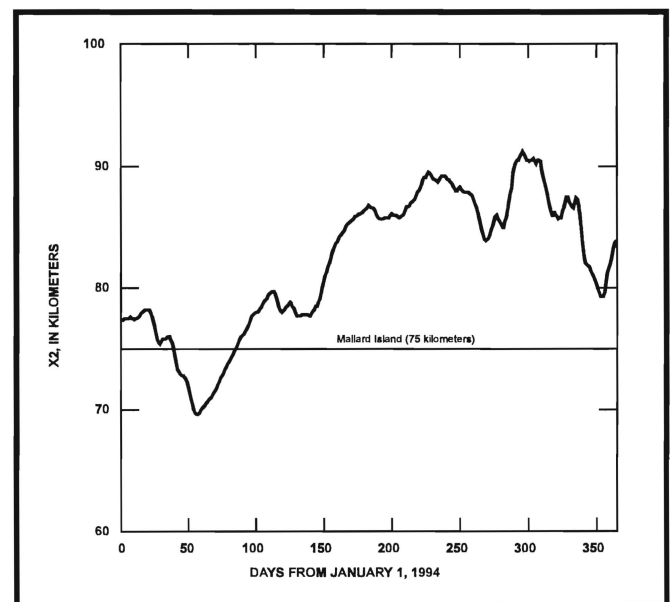


Figure 5
X2 COMPUTED FROM AN ARIMA MODEL THAT PREDICTS X2 FROM LOG DELTA OUTFLOW AND YESTERDAY'S X2 (Jassby and others 1995)
X2 is the along-channel distance from the Golden Gate of the near-bed salinity of 2 psu. (KM=kilometers.).

of Suisun Bay, indicates the possibility of a topographic control of the gravitational circulation at the Benicia Bridge (Figure 2-2) where the depths change from about 19 m in Carquinez Strait to about 11 m in Suisun Bay. The concept of topographic control is well known (Armi 1986; Farmer and Armi 1986). The large decrease in depth, coupled with a large decrease in width just landward of the Benicia Bridge, likely is responsible for the reduction in

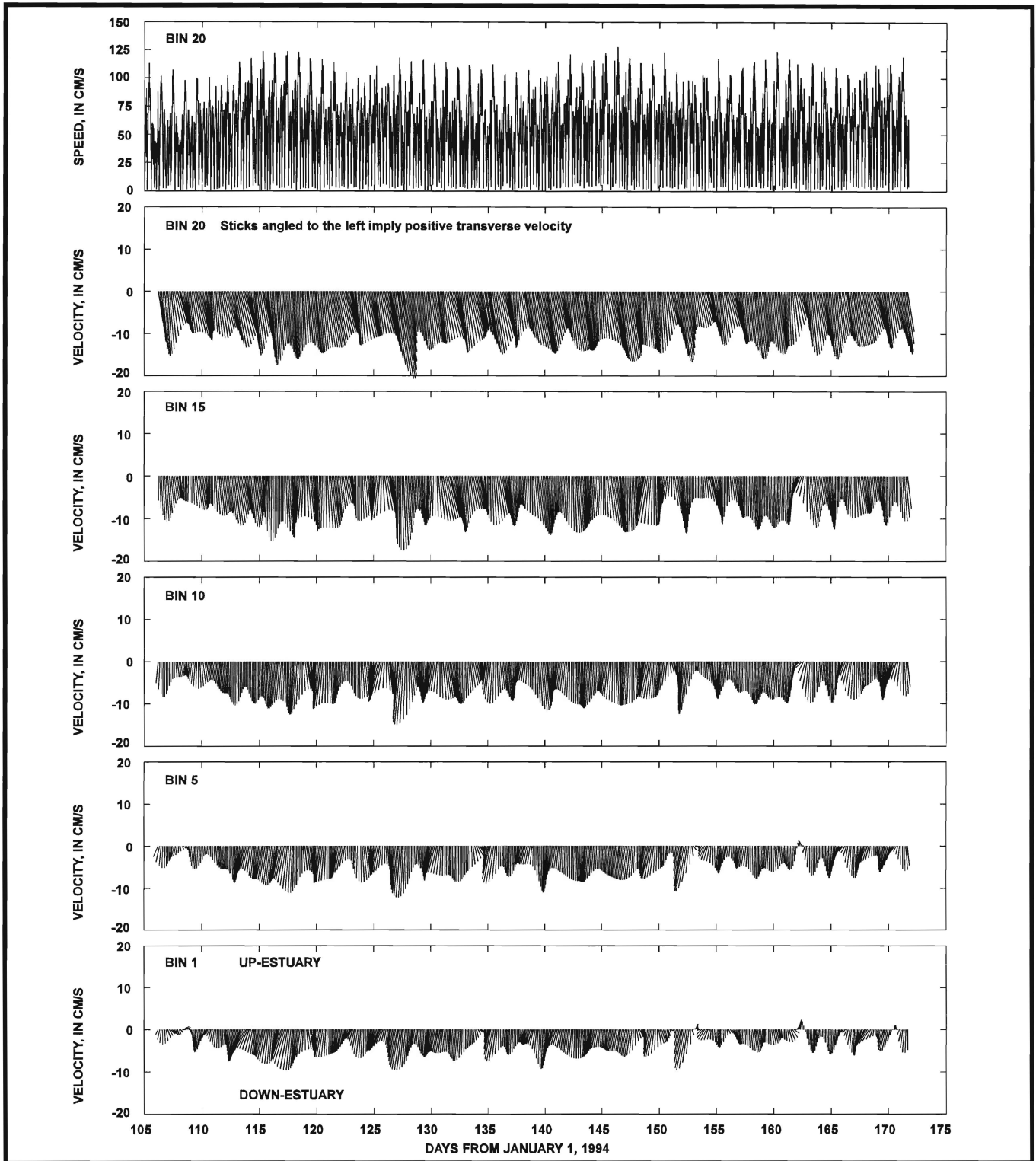


Figure 7
 STICK PLOTS OF RESIDUAL CURRENTS AT STATION MAL (near Mallard Island),
 APRIL 14 THROUGH JUNE 20, 1994, SUISUN BAY

Tidal current speed at velocity measurement location (BIN 20) is shown in the top panel for reference.

The velocity measurement at BIN 1 is located 1.9 meters off the bed. The remaining BINS are evenly spaced toward the surface at 0.5-meter intervals (for example, BIN 2 is at 2.4 meters, etc.). Principal direction is 107.0 degrees relative to true north.

Velocity and speed are given in centimeters per second (cm/s).

mean position of the 2-psu near-bed isohaline was near or landward of Mallard Island during these time periods. These data conflict directly with the idea that a null zone is located near X2. Moreover, other data indicate that vertical constrictions of the channels (Pinole Shoal, for example; Figure 2-2) can create local null zones (Walters and Gartner 1985). These results suggest the possibility of several distinct gravitational circulation cells in the north bay separated by sills in the channels. An explanation of barotropic and baroclinic flows is given in the appendix.

Delta Acoustic Doppler Current Profiler Data

As part of the 1994 entrapment zone study, two ADCPs were deployed in the delta (ANTCH and MK8, Figure 2-2). Residual currents in the Sacramento River at channel marker 8 and the San Joaquin River near Antioch are shown in Figures 2-11 and 2-12, respectively. Although these data show weak landward residual currents (<5 cm/s) near the estuary bed, they do not indicate the presence of gravitational circulation because a dynamically significant horizontal salinity gradient was absent (for example, time-mean salinities in excess of 2 psu). Such a gradient was not present at either of these locations during the 1994 study (Figures 2-13 and 2-14). The near-bed landward flows observed in the MK8 data near day 115 and day 150 (Figure 2-11) likely were caused by atmospheric pressure drops that occurred during these times (Figure 2-15). Atmospheric-pressure-induced residual velocities are distinguishable (1) from gravitational circulation because atmospheric pressure changes affect the entire water column (barotropically-driven log profile), and (2) from delta outflow because of the relatively short duration of atmospheric pressure-change induced residuals relative to delta outflow induced residuals.

The residual current profiles observed in the delta (Figures 2-11 and 2-12) exhibit a greater shear than would be expected from a pure barotropic flow. Two possible explanations for this are: (1) lateral ebb/flood current asymmetries could exist at both stations because both stations were located relatively close to channel bends, and (2) tidal timescale baroclinicity occurred near high water slack tide. The first explanation also could account for the residual surface current flowing at right angles to the channel.

Atmospheric pressure changes appear to produce a greater response at the San Joaquin River station than at the Sacramento River station. Atmospheric pressure-related net upstream currents can be seen near days 115, 135, 150, and 160 in the Antioch data (Figure 2-12), whereas the Sacramento River data indicate little or no response (Figure 2-11). A likely explanation for the apparent greater atmospheric coupling on the San Joaquin River is the greater surface area on the San Joaquin side of the delta. Because of the relatively small size of San Francisco Bay [$\sim 1.04 \times 10^9$ square meters (m^2)], Conomos (1979) compared with the spatial scale of atmospheric pressure fluctuations (Walters and Gartner 1985), water-level changes that occur in this system are driven by exchanges with the Pacific Ocean, which means that water levels throughout the bay and delta rise and fall approximately coherently (for example, without spatial gradients) with changes in atmospheric pressure. Therefore, if the delta rises approximately uniformly, then the volume of water that must flow through a given delta channel depends entirely on its upstream surface area. Because the San Joaquin River has the greater surface area, it has the greater response to atmospheric pressure fluctuations.

Wind has a significant effect on the circulation in lakes and in estuaries. For example, many micro-tidal estuaries are almost

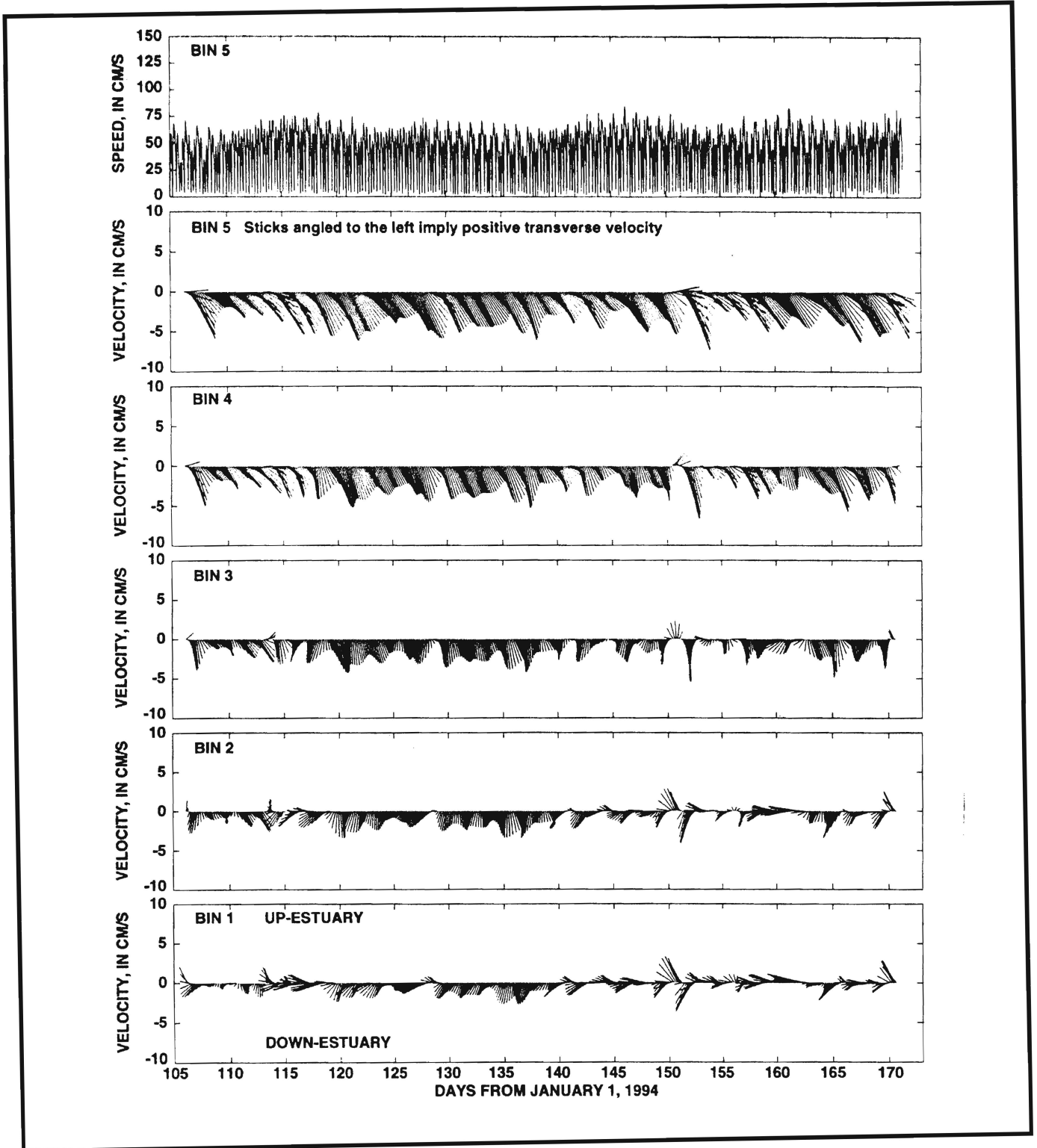


Figure 11
 STICK PLOTS OF RESIDUAL CURRENTS AT STATION MK8 (Sacramento River near channel marker 8),
 APRIL 14 THROUGH JUNE 20, 1994, SACRAMENTO RIVER
 Tidal current speed at velocity measurement location (BIN) 5 is shown in the top panel for reference.
 The velocity measurement at BIN 1 is located 1.9 meters off the bed. The remaining BINS are evenly spaced toward the surface at 1-meter intervals
 for example, BIN 2 is at 2.9 meters, etc.). Principal direction is 99.0 degrees relative to true north.
 Velocity and speed are given in centimeters per second (cm/s).

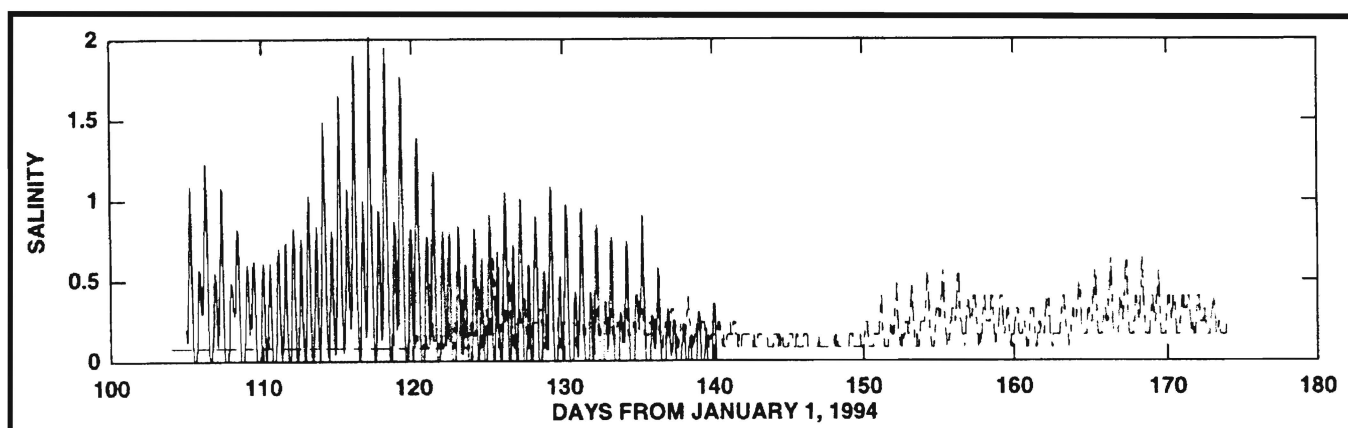


Figure 13
TIME SERIES PLOT OF NEAR-BED (solid) AND NEAR-SURFACE (dashed) SALINITY AT ANTIOCH

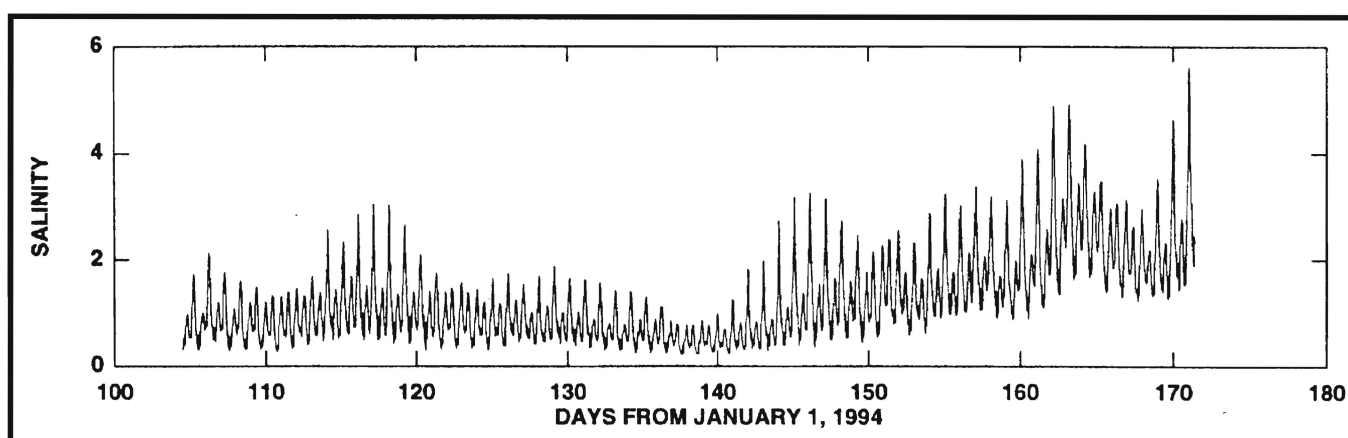


Figure 14
TIME SERIES PLOT OF NEAR-BED SALINITY ON THE SACRAMENTO RIVER AT CHANNEL MARKER 8, SACRAMENTO RIVER

completely wind driven. In San Francisco Bay, however, no correlation between the wind and the residual currents for summer conditions has been observed in the north bay (Walters and Gartner 1985). Also, periods of large persistent winds in San Francisco Bay usually are caused by significant atmospheric pressure changes, making it difficult to separate the effects of wind from the effects of atmospheric pressure. Although Warner and others (1997) found a correlation between the wind and residual currents at a single location in Honker Bay, current/wind correlations need to be done on the more recently collected hydrodynamic data.

In summary, analysis of the data described in this chapter and a review of all historical near-bed current-meter data collected in

Suisun Bay (Peterson and others 1975; Cheng and Gartner 1984; Walters and Gartner 1985; Mortenson 1987; Monismith and others 1996) and in the Sacramento River (Nichol 1996) indicate the following spatial and temporal characteristics of gravitational circulation in the north bay of San Francisco Bay:

1. Gravitational circulation dominates residual currents in Carquinez Strait unless freshwater inflows are so high that the waters in Carquinez Strait are completely fresh. Recently collected indirect evidence (decreased stratification and suspended-sediment concentrations in the autumn at the Benicia Bridge) suggests that gravitational circulation decreases in the autumn as the horizontal

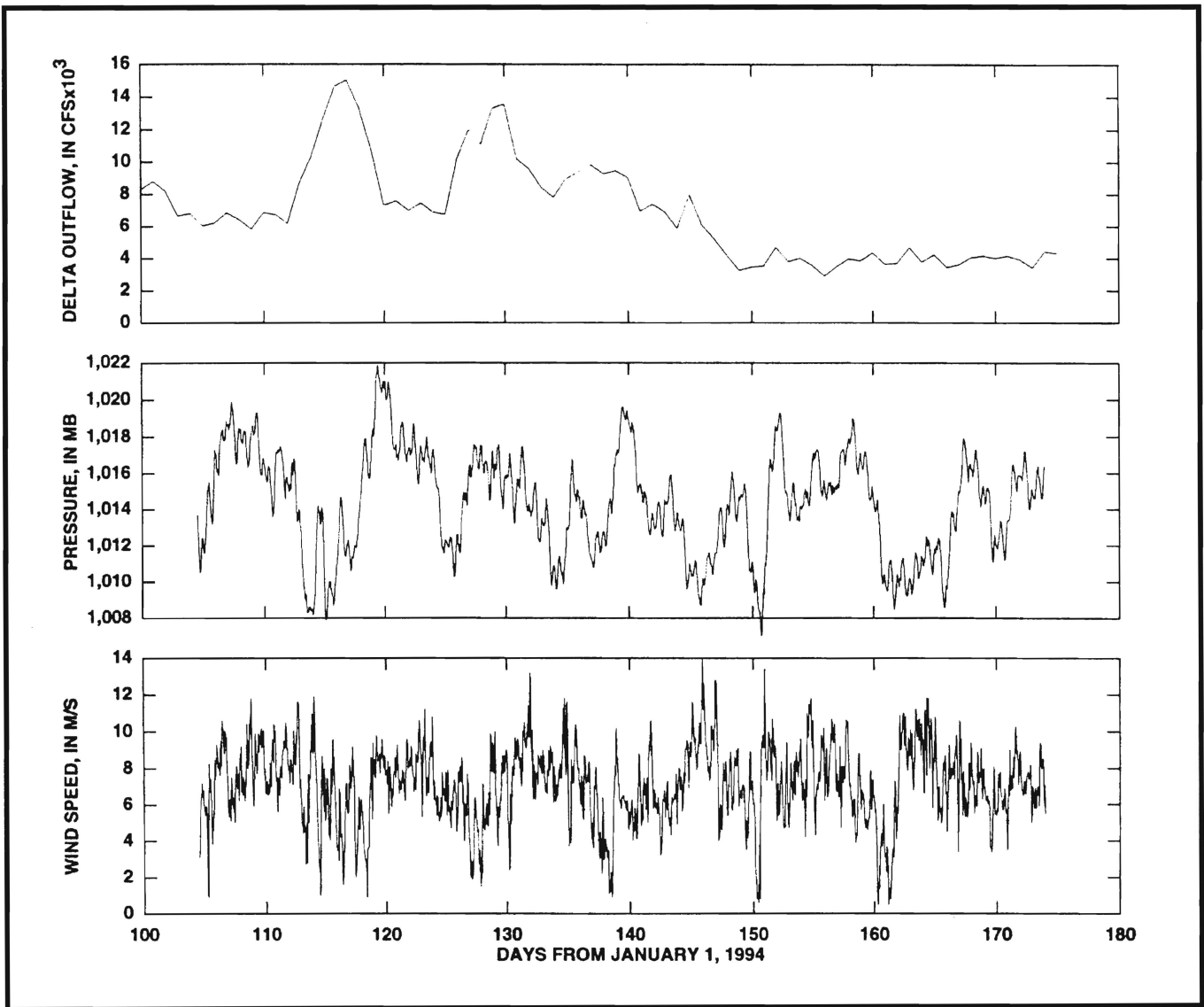


Figure 15
 DELTA OUTFLOW INDEX (DAYFLOW) (top), ATMOSPHERIC PRESSURE (middle), AND WIND SPEED (bottom)
 AT CHANNEL MARKER 27 IN SUISUN BAY

Winds during this period generally were from the east. Direction is about 270 degrees.
 (M/S=meters per second; MB=millibar; CFS=cubic feet per second.)

- salinity gradient moves landward of Carquinez Strait.
 - 2. Gravitational circulation is rare in Suisun Bay during the spring, but has been consistently measured during the autumn in the northern part of Suisun Bay (Walters and Gartner 1985; Mortenson 1987; Stacey 1996).
 - 3. Gravitational circulation has been measured in the Sacramento River at channel marker 14 (not shown in Figure 2-2) when local near-bed salinities have exceeded about 2 psu (Nichol 1996).
 - 4. When gravitational circulation is present in the north bay, its magnitude is modulated by the fortnightly (14-day period) spring/neap cycle. Gravitational circulation is weakest during spring tides and strongest during neap tides (Burau and others 1993).
- The available data indicate a seasonal variability in the strength of the gravitational

circulation in the eastern portion of Suisun Bay, which is tied through the salt field (horizontal density gradient) to winter freshwater flows that control the location and strength of the horizontal salinity gradient. Throughout most of the year, gravitational circulation appears to be weak or absent in the ship channel in Suisun Bay. Gravitational circulation is not likely to be the principal mechanism responsible for accumulation of particles and organisms

in the low salinity zone (~2 psu) when this zone is located in the ship channel of Suisun Bay. In the following sections, a revised conceptual model based on scaling arguments (stratification timescale) is discussed that demonstrates how gravitational circulation works in Suisun Bay and at least qualitatively explains the depth, fortnightly, and seasonal variability observed. Finally, alternate entrapment mechanisms are discussed.

Revised Conceptual Model of Entrapment

In the following section, a conceptual model is presented that predicts the rarity of gravitational circulation in the southern channel of Suisun Bay, but predicts that gravitational circulation can occur in Suisun Cutoff and in the western delta during autumn.

Revised Conceptual Model of Gravitational Circulation

On the basis of one-dimensional (1D) modeling of stratified water columns, a nondimensional parameterization of gravitational circulation strength can be constructed (Monismith and others 1996) known as the horizontal Richardson number

$$Ri_x = \frac{g H^2}{\rho_o U_s^2} \frac{\partial \rho}{\partial \chi} \quad (1)$$

where g is gravitational acceleration, H is the mean depth, ρ is density and ρ_o is a reference density (freshwater) and “ x ” is a distance in the along-channel direction, and U_s is the near-surface velocity. A more intuitive form of equation 1 is

$$Ri_x = \frac{\left(\frac{g}{\rho_o} \right) \frac{\partial \rho}{\partial \chi}}{\left(\frac{U_s}{H} \right)^2} \quad (2)$$

In this form, Ri_x can be thought of as a balance (or ratio) between two competing mechanisms. The numerator contains the horizontal density gradient $\left(\frac{\partial \rho}{\partial \chi} \right)$ that

drives the gravitational circulation, which also stratifies and thereby stabilizes the water column. The tendency of the horizontal density gradient to stratify the water column is balanced against the (water column average) vertical shear $\left(\frac{U_s}{H} \right)$ squared,

which tends to break down the stratification through vertical mixing, ultimately reducing the strength of the gravitational circulation.

To reinforce the idea of the horizontal Richardson number representing the ratio of two competing processes, this nondimensional number can be thought of as the squared ratio of two timescales (Figure 2-16). The inverse of the horizontal Brunt-Väisälä frequency (Nunes Vaz and others 1989),

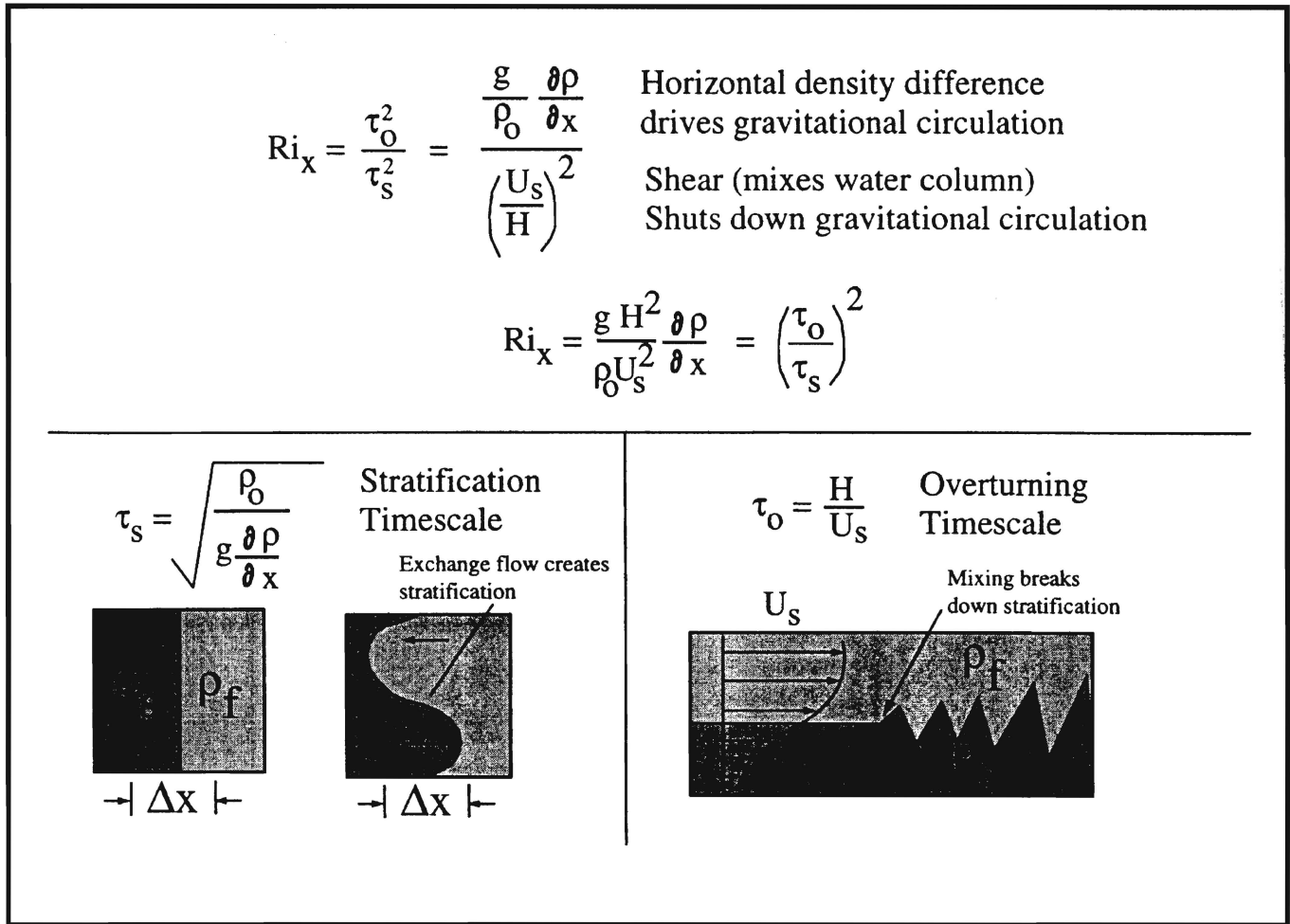


Figure 16
HORIZONTAL RICHARDSON NUMBER: A RATIO OF TWO TIMESCALES

$$\tau_s = \sqrt{\frac{1}{\frac{g}{\rho_o} \frac{\partial \rho}{\partial x}}}, \tag{3}$$

$$Ri_x = \left(\frac{\tau_o}{\tau_s}\right)^2 \tag{5}$$

represents what is referred to as the stratification timescale. This timescale, for example, represents the time it takes for two fluids of different densities separated by a wall to exchange after the wall is removed. The straining or overturning timescale,

$$\tau_o = \frac{H}{U_s}, \tag{4}$$

is a representative time for vertical mixing to break down stratification. The square of the ratio of the overturning timescale to the stratification timescale is the horizontal Richardson number given in equation 1,

If the stratification timescale is short (stratification occurs rapidly—small τ_s) and vertical mixing is weak (overtuns take a long time—large τ_o), the Richardson number will be large, indicating the possibility of gravitational circulation. Conversely, if τ_s is large and τ_o is small, gravitational circulation likely will not occur. An alternate interpretation is given by Monismith and others (1996) and Stacey (1996).

Horizontal Richardson number

The stratification timescale, τ_s , depends on the salt field, which in turn depends on delta outflow that varies from year-to-year, depending on winter runoff. The overturning timescale, τ_o , on the other hand, is easy to estimate because the mean depth, H , and the near-surface (top meter) tidal current speed, U_s , can be easily measured and remain fairly constant.

Overturning or Straining Timescale

An estimate of the overturning timescale, based on the root-mean-square (RMS) surface current speed and the mean depth, as a function of the RKI, is plotted in Figure 2-17. Large values of τ_o (longer mixing timescale) have a greater probability of supporting a gravitational circulation cell for a given horizontal density gradient. Therefore, based on a horizontal Richardson number scaling, gravitational circulation is likely to occur (from left to right on Figure 2-17): (1) seaward of RKI 25, (2) in Carquinez Strait, (3) in the Reserve Fleet Channel, (4) in Suisun Cutoff, and (5) landward of Mallard Island.

Basically, gravitational circulation occurs seaward of RKI 25 and in Carquinez Strait because both are deep (relative to the strength of the tidal currents). Gravitational circulation occurs in the Reserve Fleet/Suisun Cutoff channel and landward of Mallard Island because the tidal currents are relatively weak in these locations. Friction (primarily) reduces the tidal current by about half across Suisun Bay, and the shallows (~3 m) at both ends of Suisun Cutoff reduce the tidal currents. In contrast, locations on the overturning timescale plot, where the curve is low, are locations where gravitational circulation is not likely to occur (from left to right on Figure 2-17): (1) Pinole Shoal, (2) the ship channel in Suisun Bay (bounded by the Benicia Bridge to the west and Mallard

Island to the east), and (3) the shallow areas to the northeast and southwest of Suisun Cutoff. Therefore, Pinole Shoal, the Benicia Bridge, and the shallow areas to the northeast and southwest of Suisun Cutoff are likely null zone locations when X2 is landward of these locations. The overturning timescale explains why gravitational circulation in Carquinez Strait has been measured, but is rarely observed, in the shipping channel in Suisun Bay.

The overturning timescale also explains several apparently anomalous data sets. It explains, for example, why gravitational circulation was measured in Suisun Cutoff by Mortenson (1987) and by Stacey (1996). This timescale also explains why Nichol (1996) measured gravitational circulation at RKI 90 in the Sacramento River in 1987, 1989, and 1991-93 (all dry years when X2 was landward of this location).

Figure 2-17 shows that Carquinez Strait, Suisun Cutoff, and, interestingly, upstream of Mallard Island have a greater potential to produce a gravitational circulation cell for a given horizontal salinity gradient than does the ship channel in Suisun Bay where the overturning timescale is shorter. The weaker tidal currents in Suisun Cutoff and in the delta account for the long overturning timescales observed at these locations in the estuary. The tidal current magnitudes are reduced by roughly a factor of two between the west end of Carquinez Strait and Decker Island on the Sacramento River (bottom panel, Figure 2-17).

Moreover, sections of the Sacramento and San Joaquin rivers are deeper than the shipping channel in Suisun Bay, which adds to the potential for gravitational circulation in these locations. Figure 2-18 summarizes the basic residual current patterns that might be observed when X2 is landward of the confluence. Regardless of bottom topography, gravitational circulation is always seaward of X2; therefore, X2 must be landward of each of the gravi-

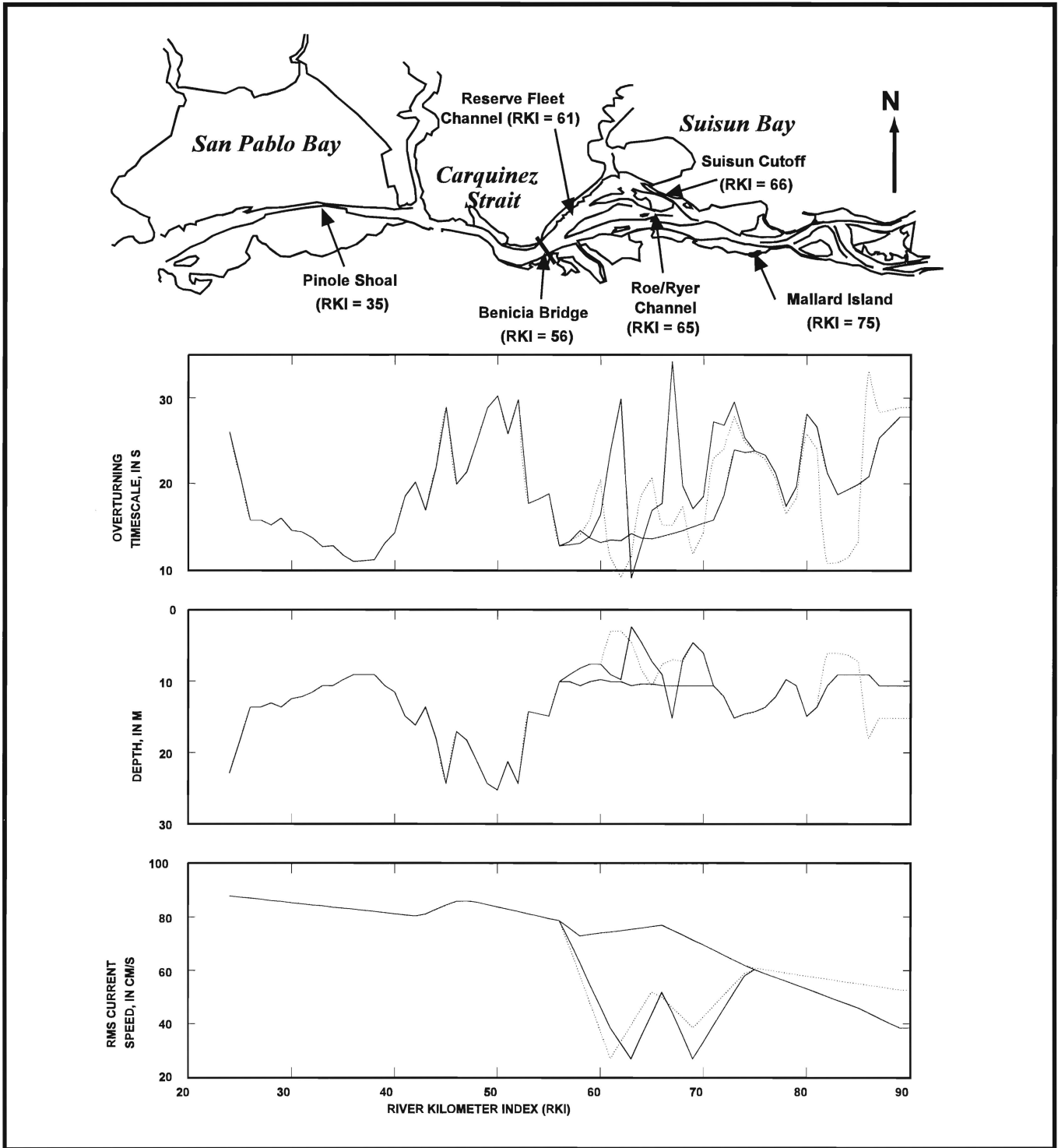


Figure 17. OVERTURNING TIMESCALE $\tau_0 = \frac{H}{U_s}$ ESTIMATED USING THE ROOT-MEAN-SQUARED NEAR-SURFACE CURRENT

AND DEPTHS FROM ACOUSTIC DOPPLER CURRENT PROFILER DATA AS A FUNCTION OF ESTUARINE POSITION, SUISUN BAY
 There are several distinct channels in Suisun Bay and the western delta; these channels are represented in this figure by different line types. The solid line represents the ship channel and the Sacramento River, the dashed line is the Reserve Fleet/Suisun Cutoff channel, and the dotted line is the Roe/Ryer Island Channel, and finally, the chain-dashed line represents the San Joaquin River. River kilometer index (RKI) is the channel distance in kilometers from the Golden Gate Bridge. (CM/S=centimeters per second; M=meters; S=seconds.)

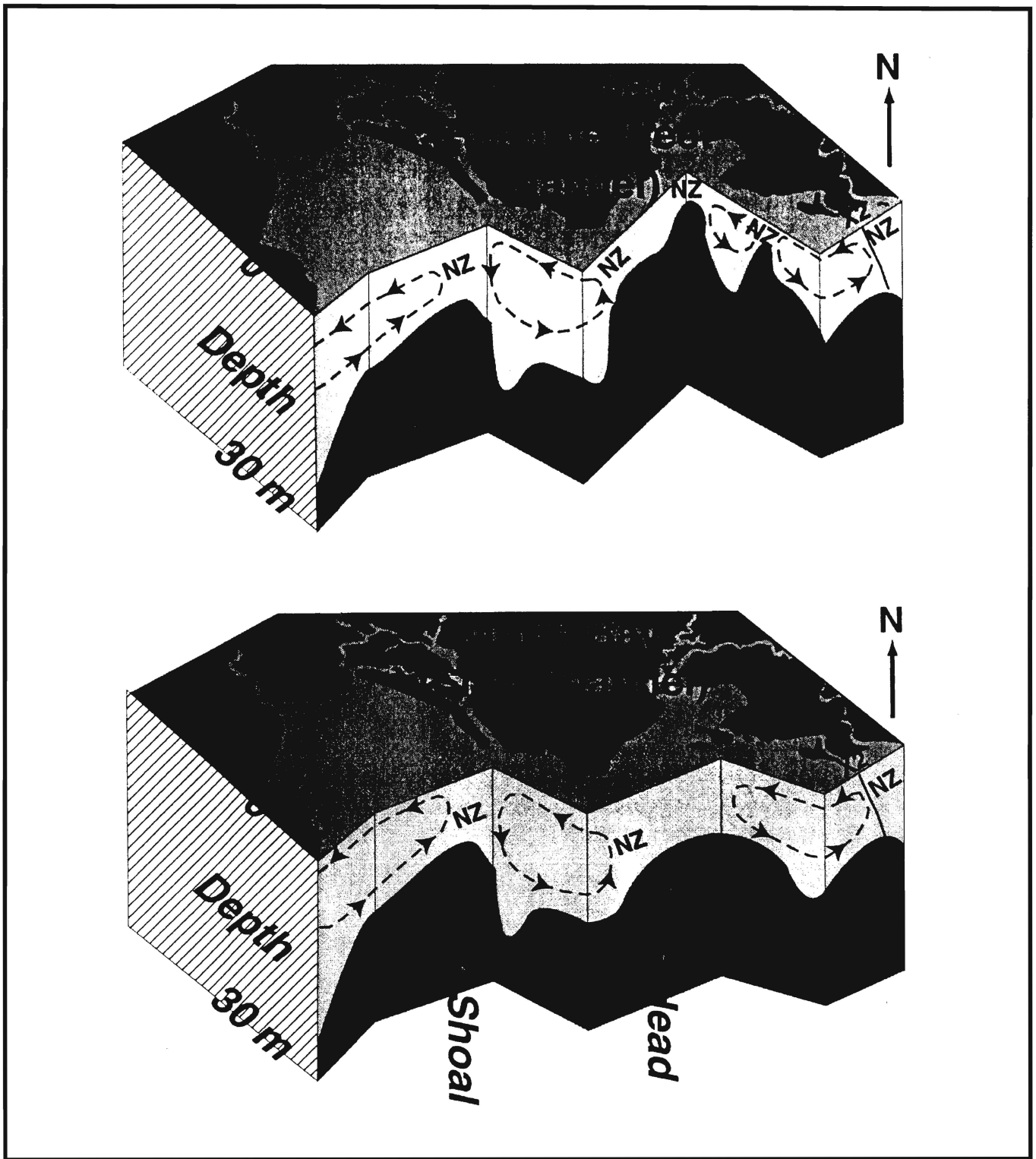


Figure 18

CONCEPTUAL MODEL OF GRAVITATIONAL CIRCULATION IN THE NORTH BAY, BASED ON THE OVERTURNING TIMESCALE

A longitudinal slice up the axis of the (a) Reserve Fleet/Suisun Cutoff channel and
 (b) the ship channel of Suisun Bay and the San Joaquin River are shown.

Salient features of this revised conceptual model of gravitational circulation include the possibility of multiple gravitational circulation cells that terminate near restrictions in depth and a modulation of gravitational circulation cell strength with the spring/neap cycle.

(NZ=null zone; M=meters.)

of bottom topography, gravitational circulation is always seaward of X2; therefore, X2 must be landward of each of the gravitational circulation cells shown in Figure 2-18 for the gravitational circulation cells to occur.

The overturning timescale not only varies in space, but can vary considerably with the fortnightly spring/neap cycle. According to Cheng and Gartner (1984), the maximum tidal current speed at spring

tide can be estimated by $(M2+S2) + (O1+K1)$, and the maximum speed at neap tide is estimated to be not less than $(M2S2) + (O1K1)$ where M2, S2, O1, and K1 are the principal partial tides computed from harmonic analysis. By using these estimates for the spring and neap tidal currents, a large variation in the tidal currents exists between spring and neap tides, which, in turn, affects the overturning timescale shown in Figure 2-19. Because the over-

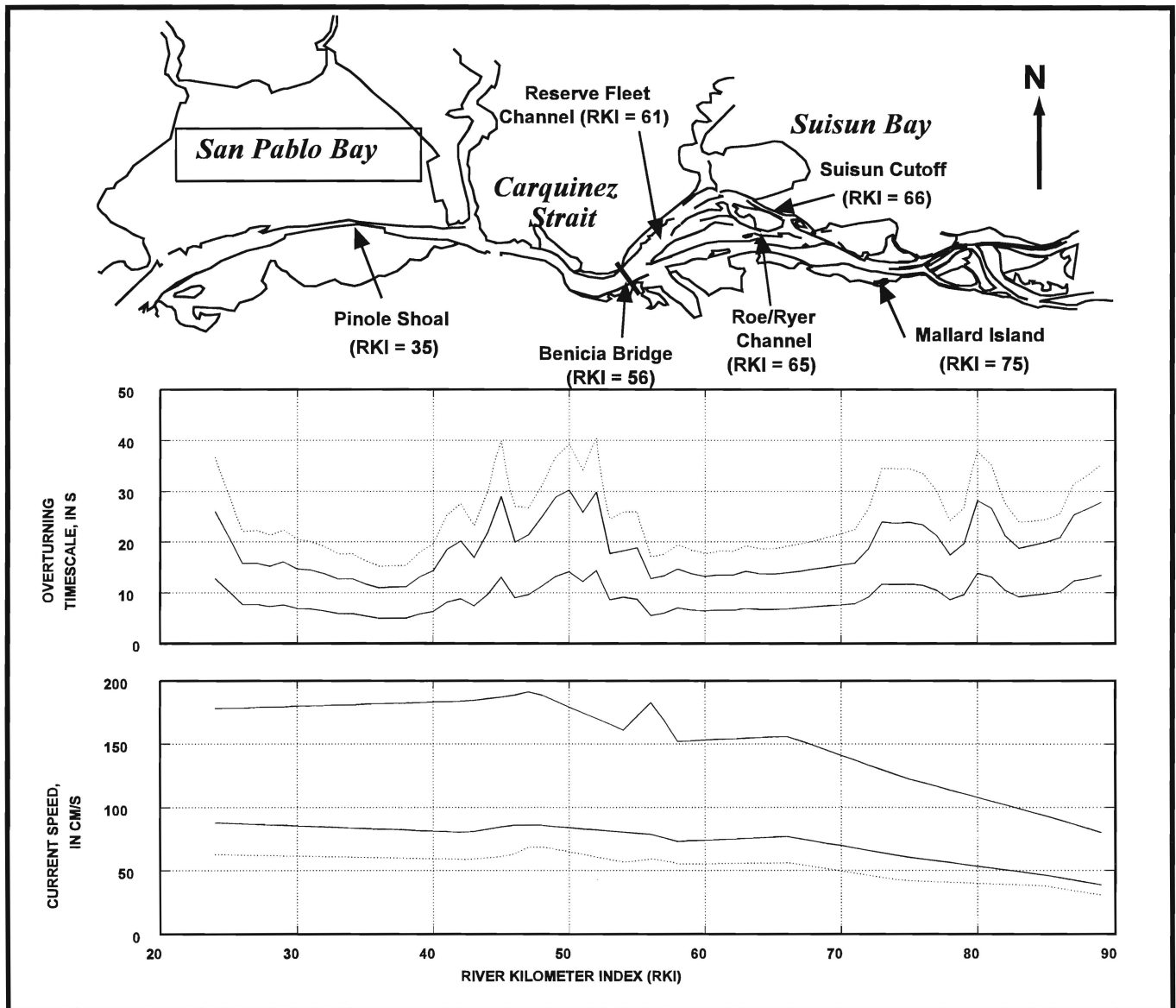


Figure 19
OVERTURNING TIMESCALE AND CURRENT SPEED DURING SPRING CURRENT MAXIMUMS (solid), ROOT-MEAN-SQUARED CURRENT (dash), AND NEAP CURRENT MINIMUMS (dash-dot), SACRAMENTO RIVER TO SUISUN BAY

River kilometer index (RKI) is the channel distance in kilometers from the Golden Gate Bridge.

(CM/S=centimeters per second; S=seconds.)

tational circulation cells shown in Figure 2-18 for the gravitational circulation cells to occur.

The overturning timescale not only varies in space, but can vary considerably with the fortnightly spring/neap cycle. According to Cheng and Gartner (1984), the maximum tidal current speed at spring tide can be estimated by $(M2+S2) + (O1+K1)$, and the maximum speed at neap tide is estimated to be not less than $(M2S2) + (O1K1)$

where M2, S2, O1, and K1 are the principal partial tides computed from harmonic analysis. By using these estimates for the spring and neap tidal currents, a large variation in the tidal currents exists between spring and neap tides, which, in turn, affects the overturning timescale shown in Figure 2-19. Because the overturning timescale is squared in the horizontal Richardson number, a factor of two difference in the overturning timescale

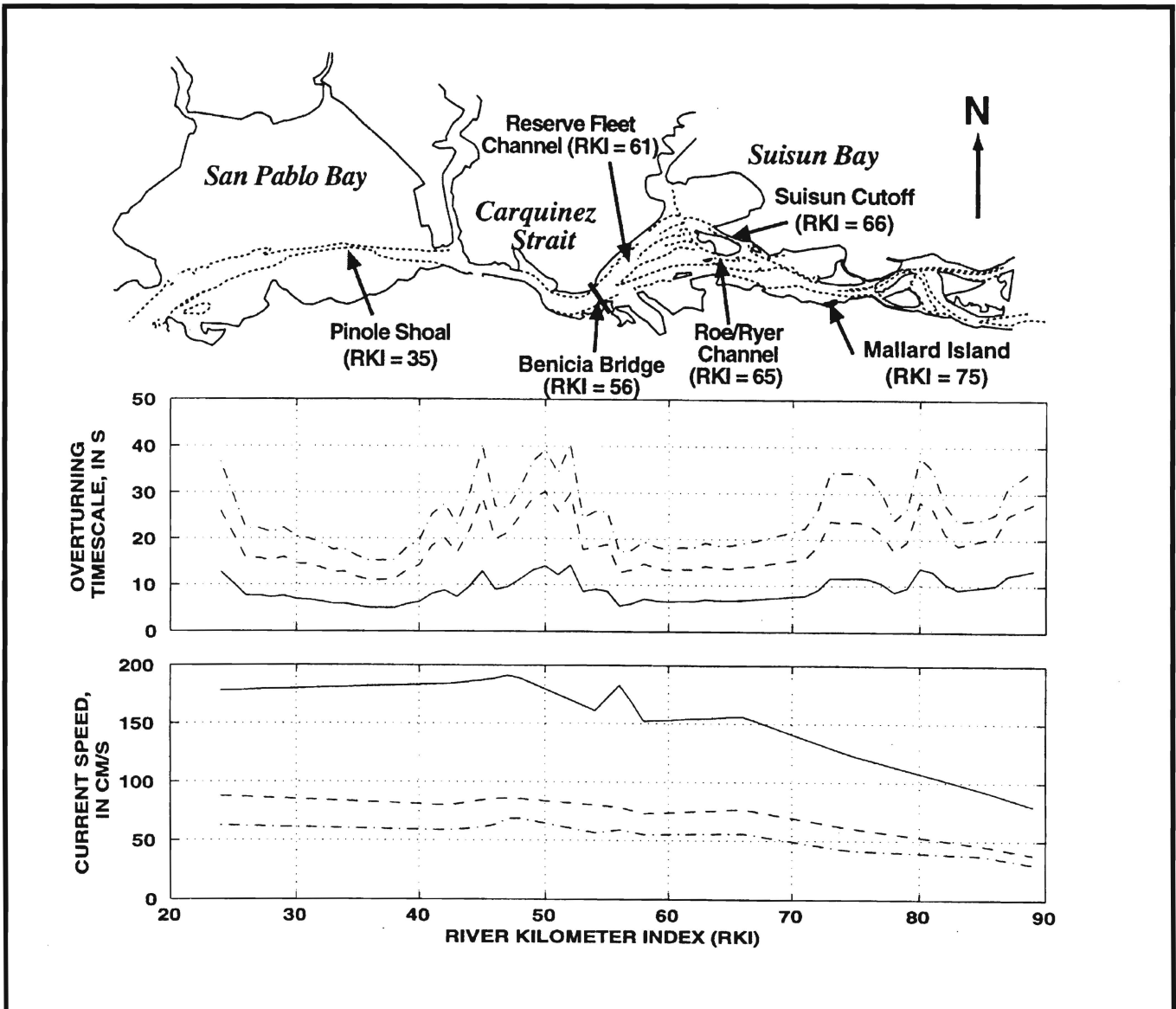


Figure 19
 OVERTURNING TIMESCALE AND CURRENT SPEED DURING SPRING CURRENT MAXIMUMS (solid), ROOT-MEAN-SQUARED CURRENT (dash), AND NEAP CURRENT MINIMUMS (dash-dot), SACRAMENTO RIVER TO SUISUN BAY
 River kilometer index (RKI) is the channel distance in kilometers from the Golden Gate Bridge.
 (CM/S=centimeters per second; S=seconds.)

means a factor of four difference in the Richardson number.

Stratification Timescale

The low-pass-filtered salinities at Mallard Island and the low-pass-filtered basinwide horizontal salinity gradient, $\frac{\partial S}{\partial x}$ (see appendix for the computational details), are

shown in Figure 2-20. The time mean horizontal salinity gradient is highly variable throughout the winter-spring period, depending on delta outflow for a given year. Even though 1992, 1993, and 1994 represent significantly different water year types, the basin-wide horizontal salinity gradient, on which the stratification timescale depends, approaches about 0.4 psu/km in late summer-early autumn during each year. The large tidal fluctua-

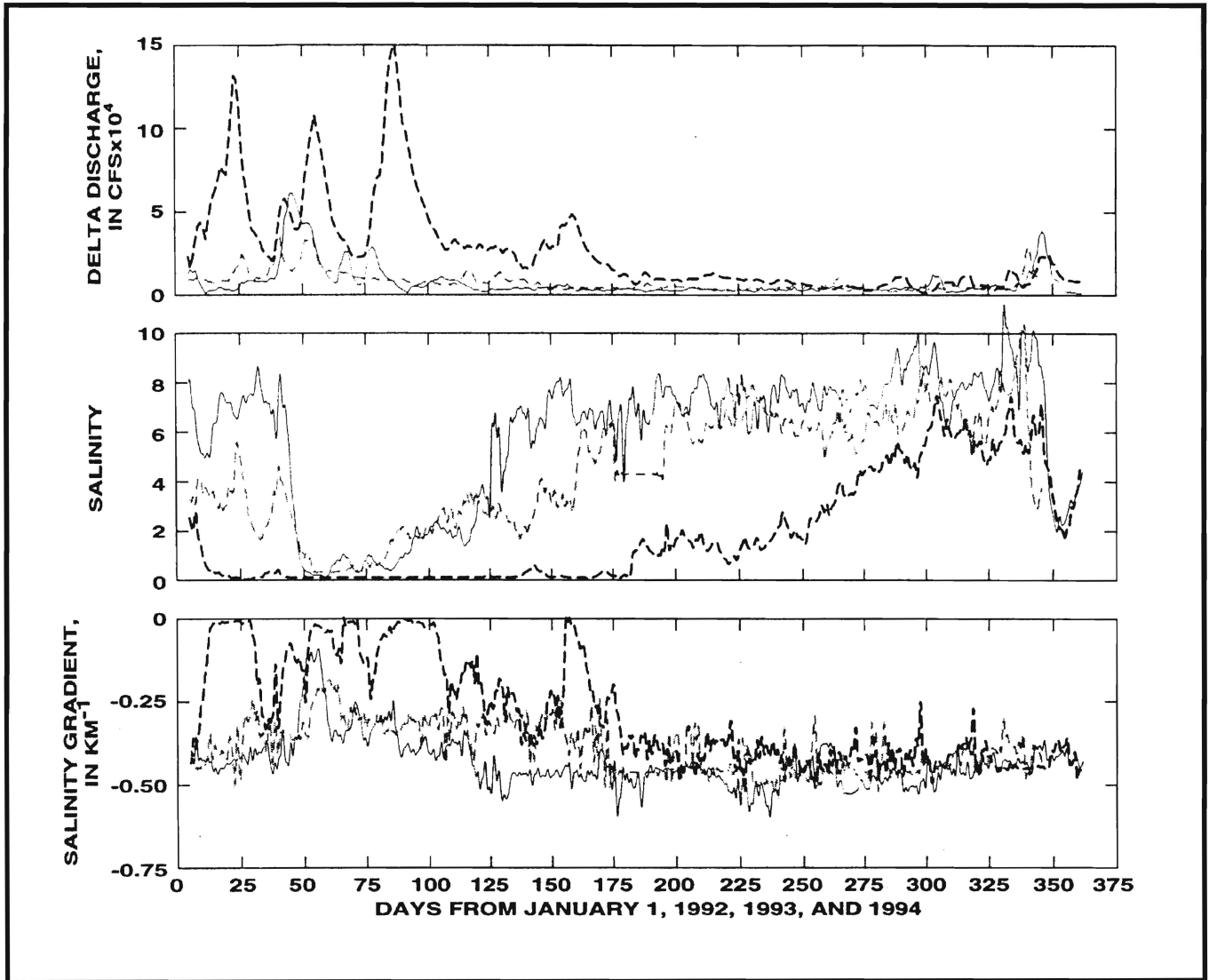


Figure 20

TIME SERIES PLOTS OF DELTA OUTFLOW (DAYFLOW) (top), MALLARD ISLAND LOW-PASS-FILTERED SALINITY (middle), AND THE BASINWIDE HORIZONTAL LOW-PASS-FILTERED, NEAR-BED SALINITY GRADIENT, dS/dx , (bottom) FOR 1992 (solid), 1993 (light dash), AND 1994 (dark dash), MALLARD ISLAND.

The horizontal salinity gradient is computed by taking the difference between the Mallard Island near-bed salinity and subtracting it from the Martinez near-bed salinity divided by the distance between the station locations. The units in the middle and lower panel could have been given as psu per kilometer, but salinity has no units (see glossary).

(KM=kilometer; CFS= cubic feet per second.)

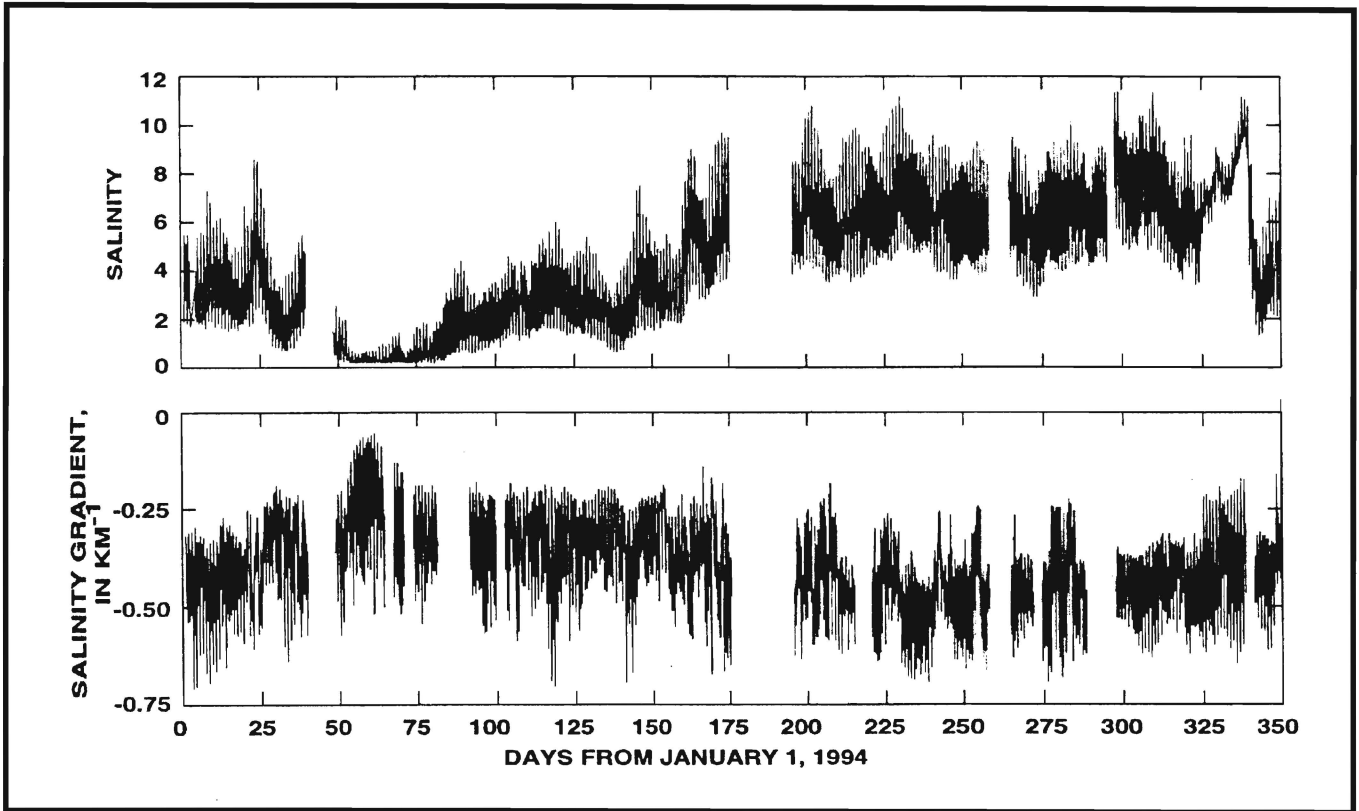


Figure 21
 TIME SERIES PLOTS OF SALINITY (top) AND THE BASINWIDE HORIZONTAL SALINITY GRADIENT, dS/dx , (bottom),
 MALLARD ISLAND

The basinwide horizontal salinity gradient fluctuates tidally. The units in the lower panel could have been given as psu per kilometer, but salinity has no units (see glossary.)
 (KM=kilometer.)

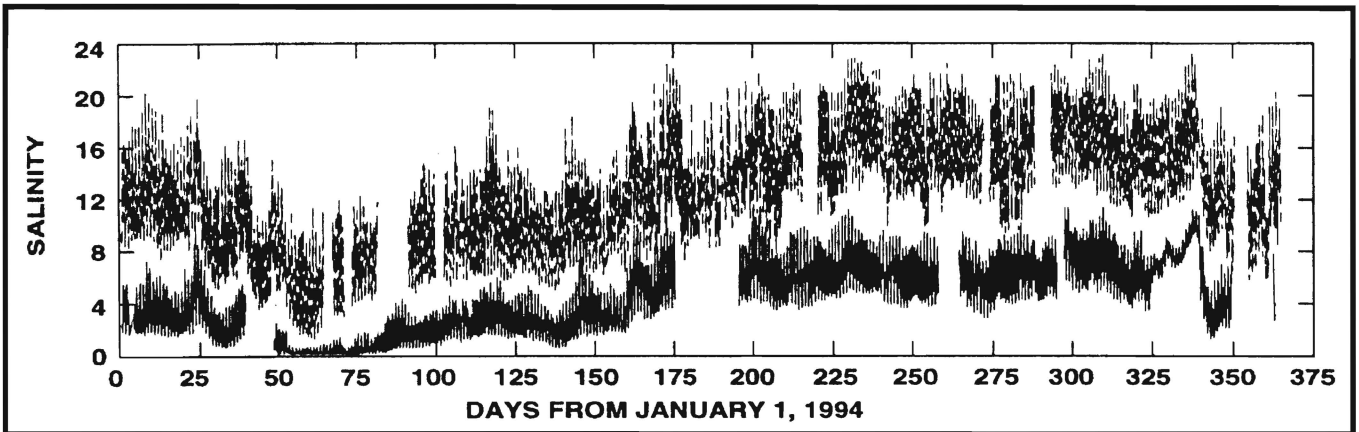


Figure 22
 TIME SERIES PLOTS OF THE SALINITIES AT MARTINEZ (dash) AND MALLARD ISLAND (solid)
 The tidal variation in salinity is much greater at Martinez. Salinity has no units (see glossary).

tions in the horizontal gradients shown in Figure 2-21 are, in part, because of the much larger tidal fluctuation in salinity at Martinez (Figure 2-22). The basinwide and the local horizontal salinity gradients are nearly always greater on flood than on ebb in Suisun Bay, indicating a contraction of the salt field on flood and an expansion on ebb because there is a greater change in salinity over the tidal cycle at Martinez

than at Mallard Island $\frac{\partial S}{\partial t}_{Mart} > \frac{\partial S}{\partial t}_{Mal}$. This

expansion and contraction is due to a combination of the greater velocities at Martinez over Mallard Island $U_{Mart} > U_{Mal}$ and the horizontal salinity gradient at Martinez is greater than the basin-wide mean horizontal salinity gradient, which, in turn, is greater than the gradients at Mallard Island

$$\frac{\partial S}{\partial \chi}_{Mart} > \frac{\partial S}{\partial \chi}_{Basin} > \frac{\partial S}{\partial \chi}_{Mal}.$$

The time variability in the basinwide horizontal salinity gradient indicates that this gradient may be useful in looking at long-term trends, but is of little use in studying local dynamics because the local horizontal salinity gradient also is tidal timescale dependent and likely different than the basin mean shown in Figure 2-20.

As previously discussed, the horizontal salinity gradients at a given location can vary tidally, but fortnightly and seasonal variations also are important in understanding when and where gravitational circulation occurs. For example, several roughly four-fold increases in the horizontal salinity gradient during neap tides were observed during summer 1995 in Suisun Cutoff (Figure 2-23).

The low-pass-filtered surface current squared, $\overline{u^2}$, is a measure of the tidal energy. Peaks in $\overline{u^2}$ are spring tides, and valleys correspond to neap tides. In Figure 2-23, the neap tides correspond directly to

increases in the horizontal salinity gradient (but with a noticeable time lag).

Seasonal variations in the time-mean horizontal salinity gradient also have been observed. Figure 2-24 plots low-pass-filtered salinity, which generally increases as the summer and autumn progress, as a function of the horizontal salinity gradient. Although there are many physical forcing

mechanisms that control S and $\frac{\partial S}{\partial \chi}$, the

$\frac{\partial S}{\partial \chi}$ magnitude increases as salt intrudes into the system.

In summary, gravitational circulation is dependent primarily on the horizontal salinity gradient that varies seasonally with the position of the salt field. The position of the salt field depends primarily on the uncontrolled winter inflows from the delta; however, the horizontal gradients in the salt field also appear to have a secondary dependence on local effects (primarily bathymetry) and the spring/neap cycle. The spatial distribution of gravitational circulation also depends strongly on the ratio of the tidal currents to the depth, or overturning timescale given in Figure 2-17. On the basis of this timescale, gravitational circulation is likely to occur in the Reserve Fleet Channel and Suisun Cutoff and landward of Mallard Island, and null zones are predicted to occur at Pinole Shoal (needs to be confirmed with data), the Benicia Bridge, and the shallow areas northeast and southwest of Suisun Cutoff (these also need to be confirmed with data) when the time mean position of X2 is significantly landward of these locations.

Our revised conceptual model of the north bay, based on Eulerian measurements, is as follows:

- The depth dependence in equation 1 explains, in part, why there is strong gravitational circulation in Carquinez Strait ($H \geq$

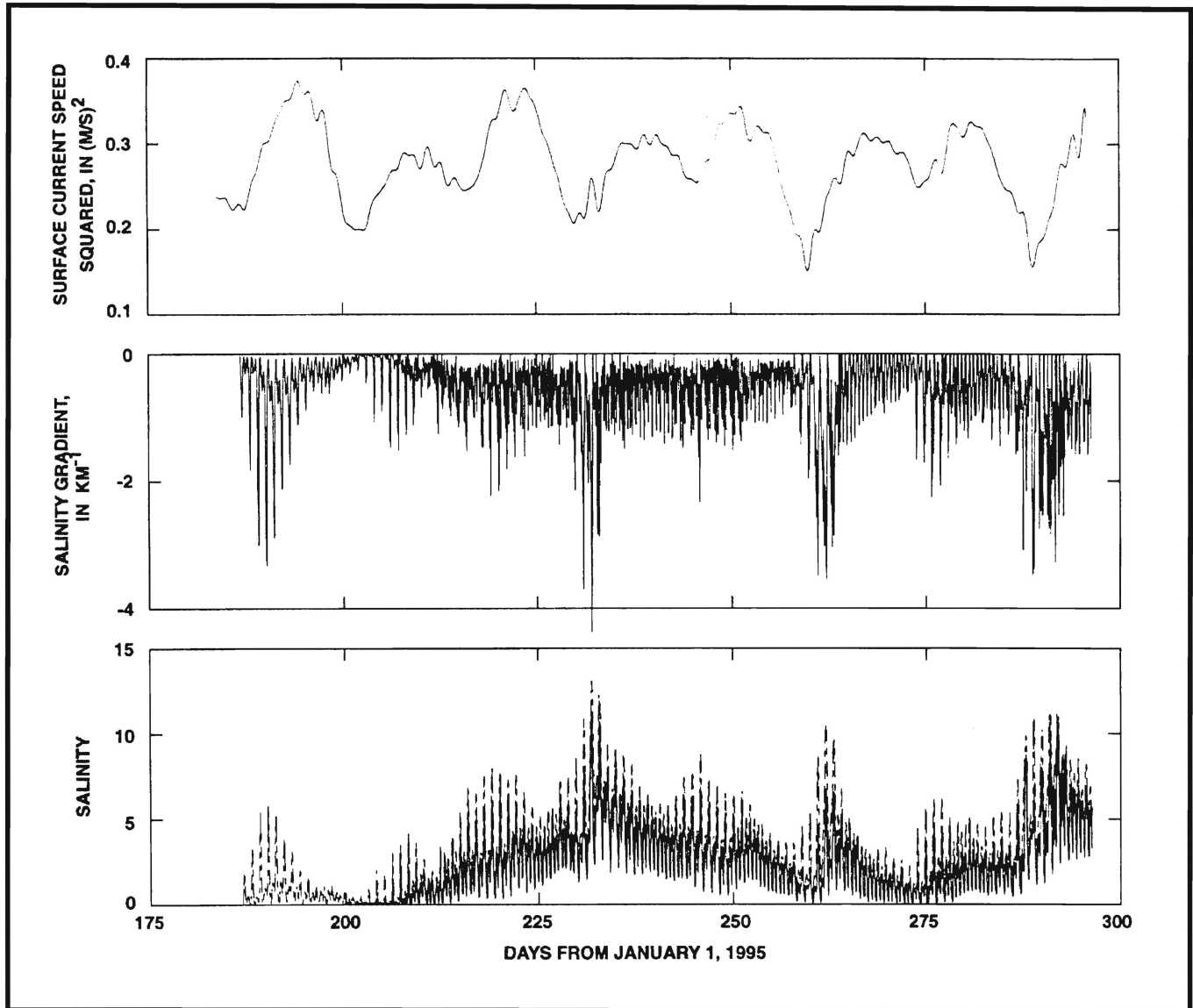


Figure 23

TIME SERIES PLOTS OF THE LOW-PASS-FILTERED ALONG-CHANNEL COMPONENT OF THE SURFACE CURRENT SQUARED,

u^2 (top), THE LOCAL HORIZONTAL SALINITY GRADIENT, dS/dx , IN SUISUN CUTOFF AS COMPUTED BY CONDUCTIVITY/TEMPERATURE INSTRUMENTS DEPLOYED 1.5 KILOMETERS APART ALONG THE AXIS OF SUISUN CUTOFF (middle), AND THE SALINITY IN SUISUN CUTOFF (bottom).

The bottom sensor is represented by the solid line and the surface sensor by the dashed.

The units in the middle panel could have been given as psu per kilometer, but salinity has no units (see glossary).

(KM=kilometer; M/S= meters per second; (M/S)² = square meters per second.)

19 m) and none in Suisun Bay is (H ~ 11 m) during spring.

- A semipermanent null zone (and possibly a turbidity maximum) is located near the Benicia Bridge during spring. At the very least, net near-bed currents are reduced significantly in the channels of western Suisun Bay from what they are in Car-

quinez Strait. Based on the horizontal Richardson number scaling, geographically fixed null zones also may exist in the shoal between the Reserve Fleet Channel and Suisun Cutoff and in the shoal south of Honker Bay (see the null zone designations on Figure 2-2 and the conceptual model in Figure 2-18).

- The inverse relation to velocity squared, U^2 , in equation 1 accounts for the spring-neap modulations in gravitational circulation strength (Burau and others 1993). The velocity squared is an index of the tidal energy available for vertical mixing. Increased vertical mixing from the increased tidal energy available during spring tides breaks down stratification, which effectively short circuits the gravitational circulation-induced two-layer flow.
- The horizontal density gradient, $\frac{\partial \rho}{\partial \chi}$, drives

the gravitational circulation; without it, by definition, gravitational circulation does not exist.

Alternate Entrapment Mechanisms

Given that gravitational circulation was not measured in Suisun Bay during the spring of 1992 and 1994, what does this imply about the existence of a turbidity maximum or entrapment zone based on existing conceptual models? Numerous publications (Arthur and Ball 1979; Peterson and others 1975, among others) have explained the turbidity maximum as resulting from a hydrodynamic null zone. The lack of measured net landward bottom currents in Suisun Bay during spring suggests that, if a turbidity maximum or entrapment zone does exist during the spring, a mechanism other than gravitational circulation must be responsible. The low-salinity region of the estuary is also characterized by abundance maxima of several species of planktonic organisms (Kimmerer, this volume), and maxima in the proportion of bacteria that are attached to particles (Hollibaugh, this volume). Entrapment mechanisms must, therefore, explain not only maxima in concentration of particles (for example, turbidity) but also maxima in organism abundance. In the remaining sections, several possible entrapment mechanisms are discussed from a hydrodynamic perspective.

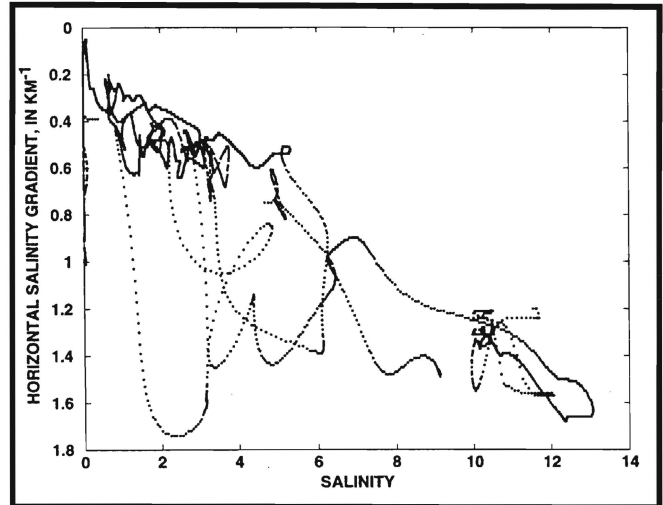


Figure 24
HORIZONTAL SALINITY GRADIENT DATA VERSUS
TIDALLY-FILTERED SALINITY CONDUCTED AT SUISUN
CUTOFF, DURING AUTUMN 1994 AND SPRING 1995.

The units in this figure could have been given as psu per kilometer, but salinity has no units (see glossary). (KM=kilometer.).

Vertical Migration

Because gravitational circulation is rare in Suisun Bay, three possible entrapment mechanisms are discussed that involve the correlation between the vertical distribution of organisms (or suspended solids) and vertical shear. The first two mechanisms discussed that could account for increased concentrations near X2 do not involve the assumption of biological behavior, but instead rely completely on the physics of shear-buoyancy interaction. These mechanisms are differentiated from each other, for the purposes of discussion, by the exact timing between the vertical concentration distribution (whether it be organisms or suspended solids) and the vertical shear, even though both mechanisms evolve from the same highly non-linear interaction between the salt field and vertical mixing.

The first mechanism discussed simply requires the centroid of the concentration distribution to be higher in the water column during flood tides than during ebb tides. There are two possible ways (that we know of) in which the centroid of the concentration distribution can shift vertically

over the tidal cycle: one includes biological behavior, which is discussed in Kimmerer and Bennett (this volume); the other, a purely physical mechanism, is discussed in this chapter. In terms of suspended sediment transport, preliminary evidence suggests that there may be greater resuspension of bottom sediment in the channels during flood tides than during ebbs in a stratified water column because the near-bed shear stress appears to be greater during flood (Stacey 1996). Moreover, increased near-bed shear during flood would also suggest that organisms attached to the bed or that are trying to remain near the bed would have a more difficult time remaining on or near the bed during flood in the presence of a horizontal salinity gradient. Therefore, ebb/flood asymmetry in the near-bed shear is a purely physical explanation that could explain increased flood water column concentrations over ebb, and could thereby explain a vertically averaged net landward transport of suspended sediment and biota at locations seaward of X2.

A conceptually satisfying outcome of this mechanism is that the ebb/flood asymmetry in the near-bed shear would end just seaward of X2, where the horizontal salinity gradient, for practical purposes, ends, which means the positive correlation between elevated water column concentrations and the flood tidal current would also end near X2. This purely physical mechanism could, therefore, explain the observed accumulations of suspended sediment and biota near the low salinity zone. Collaborative studies between the USGS (David Schoellhamer and Jon Burau) and Stanford University (Stephen Monismith, Matthew Brennan, and Jessica Lacy) of this mechanism, with respect to suspended in sediment transport, are currently (1998) under way.

The second purely physical mechanism that could account for accumulations near X2 depends on a sequence of tidally driven

shear-buoyancy interactions in the presence of a weak horizontal salinity gradient. Although this mechanism is related to the first, it is different because all of the action occurs during a short (1- to 4-hour) interval around low slack water and the subsequent flood tide. The sequence is as follows:

(1) the water column naturally tends to become stratified during ebb tides through a process known as Strain Induced Periodic Stratification or SIPS (Simpson and others 1990). Weaker vertical mixing that occurs near slack water permits (a) a two-layer density driven exchange flow to occur that further stratifies the water column and (b) negatively buoyant particles to accumulate in the lower part of the water column through settling.

(2) During the period of weak vertical mixing near low slack water, the 1- to 4-hour density driven exchange flow advects the elevated concentrations of particles near the bottom landward. This intermittent advective process could ultimately lead to a net landward transport of particles up to a position near X2, where stratification dynamics cease to play an important role. The two-layer density driven flow is limited to slack water because the intense vertical mixing that occurs during the tidal current maximums breaks down stratification, which effectively short-circuits the density driven exchange flow.

The third and final vertical transport mechanism discussed involves biological behavior. This process, which is limited to organisms that can swim, depends on the correlation between vertical shear and organism position. Kimmerer (this volume) and Bennett (this volume) present evidence for vertical movement of organisms on a tidal cycle, with abundance higher in the water column on the flood than on ebb. This pattern appears to be universal in those species residing in this part of the estuary, implying that it is important to position maintenance.

For an organism to achieve a net upstream movement from vertical migration in synchrony with the tides, the water column must be sheared. If the shear is weak, as it is in a vertically well-mixed water column, little net upstream movement is derived from vertical migration. Conversely, when the water column is stratified, large local shears develop near the density interface that could easily be exploited by organisms to position themselves within the estuary. The greater the vertical shear, the shorter the vertical migration is needed to achieve net upstream movement. If the flow is strongly stratified, organisms only would have to travel through the salinity (density) interface; a distance that often can be measured in centimeters rather than meters. Moreover, if the vertical distance required to achieve net upstream movement is minimal, it suggests that either less effort is required for an individual organism or that weaker organisms can succeed in achieving a net upstream benefit from vertical migration. In this section, the magnitude and timing of the stratification and shear in the ship channel in Suisun Bay is described in support of the vertical migration hypothesis.

Because flow reversals occur twice daily, differentiating between shear created on flood or ebb is desirable. For this chapter, the tidal current direction is based on the depth average currents where the shear is computed using the following relation:

$$\Delta U = \frac{\bar{U}}{|\bar{U}|} |U_S - U_B| \quad (6)$$

where $|U_S - U_B|$ gives the magnitude of the shear and is strictly positive by definition

and the term $\frac{\bar{U}}{|\bar{U}|}$ is either +1 or -1 when

the depth-averaged, along-channel currents are flooding or ebbing, respectively.

U_S , U_B , and \bar{U} are the near-bed, near-sur-

face, and depth-averaged currents, respectively.

The near-bed and near-surface salinities, the along-channel speeds, and ΔU are plotted in Figure 2-25, which shows a typical tidal cycle when locally weak salinity gradients were present. The timing of the shear and stratification is markedly different when the horizontal density gradient is strong (for example, strong enough to produce a gravitational circulation cell).

The water column rapidly stratifies as the flood begins to decelerate and continues to stratify through high water slack. The water column begins to destratify as the ebb begins to accelerate. Stratification reduces the vertical transfer of along-channel momentum causing a partial decoupling of the upper layer from the lower layer; thereby, increasing the shear in the water column. Even though stratification starts with the flood [in contrast to a strain-induced periodic stratification (SIPS) model], the greatest stratification and concomitant shear ΔU , occurs during the acceleration phase of the ebb (negative along-channel speed).

This pattern of stratification, with most of the shear occurring on ebb, is shown on Figure 2-26, where the bottom panel shows that the low-pass-filtered (tidally averaged) vertical shear is negative (for example, the shear occurs on ebb because of the way the shear in equation 6 is computed). If suspended-sediment concentrations, or biota, were to concentrate in the lower layer during stratification, their progress down-estuary would be considerably less (by about 50 cm/s for ~3 hours or ~5.5 km near day 146.25 in Figure 2-25) than the upper layer during this period. If suspended sediment, or biota, were concentrated in the lower layer during these times, and, if the concentrations could then become evenly distributed throughout the water column or were concentrated in the upper layer during the remainder of the tidal cycle, a vertically averaged, landward net flux

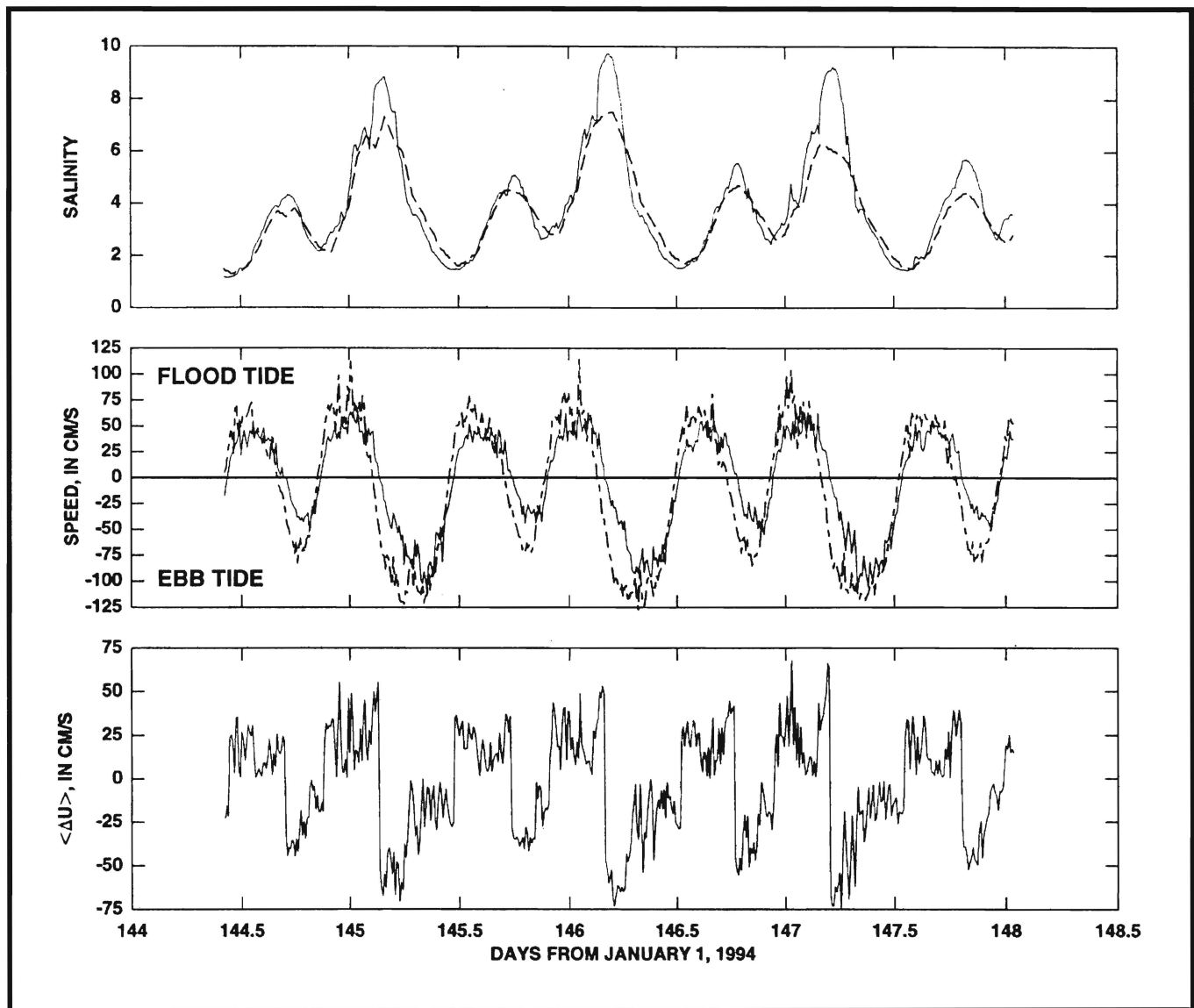


Figure 25
 TIME SERIES PLOTS OF THE NEAR-BED (solid) AND NEAR-SURFACE (dash) SALINITIES (top);
 THE NEAR-BED (solid) AND NEAR-SURFACE (dash) ALONG-CHANNEL SPEED (middle);
 AND THE FLOOD/EBB NORMALIZED SHEAR (bottom) AT MALLARD ISLAND

The units in the middle and bottom panels could have been given as psu per kilometer, but salinity has no units (see glossary). (CM/S=centimeters per second).

could be achieved depending on the thickness and concentration in the lower layer).

The conditions for this upstream migration mechanism would abruptly end near X2, where dynamically significant salinities and the increased shear that occurs on ebb cease to exist. Because the water column naturally mixes vertically during the tidal current maximums, the only unknowns in this alternate entrapment process are (1)

whether elevated concentrations actually occur in the lower layer when the water column is stratified, and (2) what the thickness of the lower layer. Zooplankton (Kimmerer, this volume) and larval fish (Bennett, this volume) appear to migrate vertically such that abundance is higher in the upper layer on the flood and higher on the lower layer on ebb. For copepods, this migration appears to be insufficient, at least for the period of our data collection, to overcome the net transport (Kimmerer,

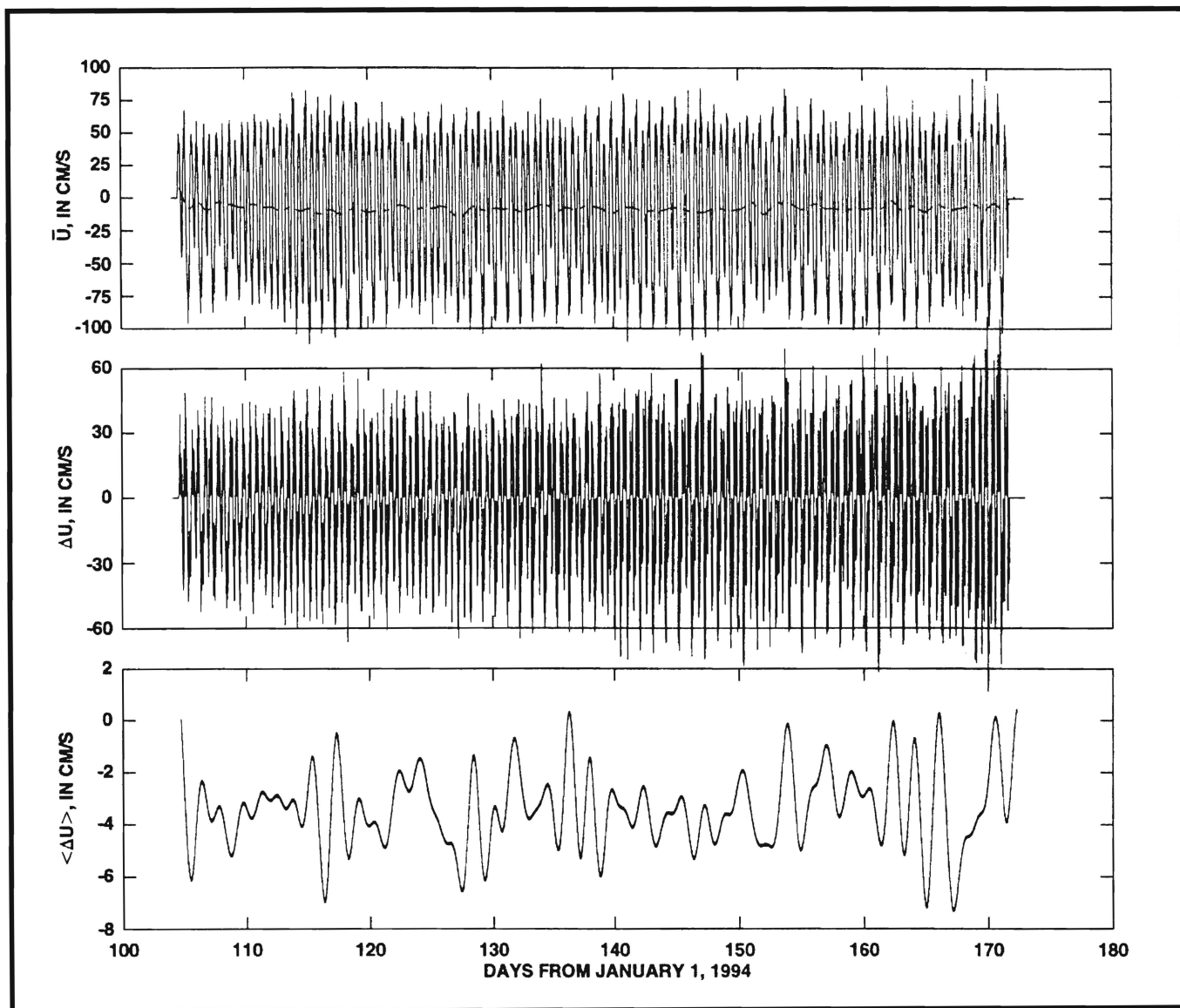


Figure 26
 TIME SERIES PLOTS OF THE DEPTH-AVERAGED, ALONG-CHANNEL CURRENT (\bar{U}); THE VERTICAL SHEAR (ΔU); AND
 THE TIDALLY AVERAGED VERTICAL SHEAR, ($\langle \Delta U \rangle$), AT MALLARD ISLAND
 (CM/S=centimeters per second.)

this volume), because of the weak stratification and concomitant shear referred to above. An alternate migratory mechanism appears to exist for mysids and amphipods (Kimmerer, this volume) by which these organisms are apparently less abundant throughout the water column on ebb than on flood. If they are on the bottom on ebb, where seaward transport would be negligible, their migratory behavior could overcome the lack of vertical shear and result

in net landward movement (Kimmerer, this volume).

Stokes' Drift

An upstream residual current, Stokes' drift, can occur in progressive wave systems like the north bay of San Francisco Bay. Stokes' drift creates a flux in the direction of wave propagation that evolves from the correlation of sea level and the tidal current. For example, the residual

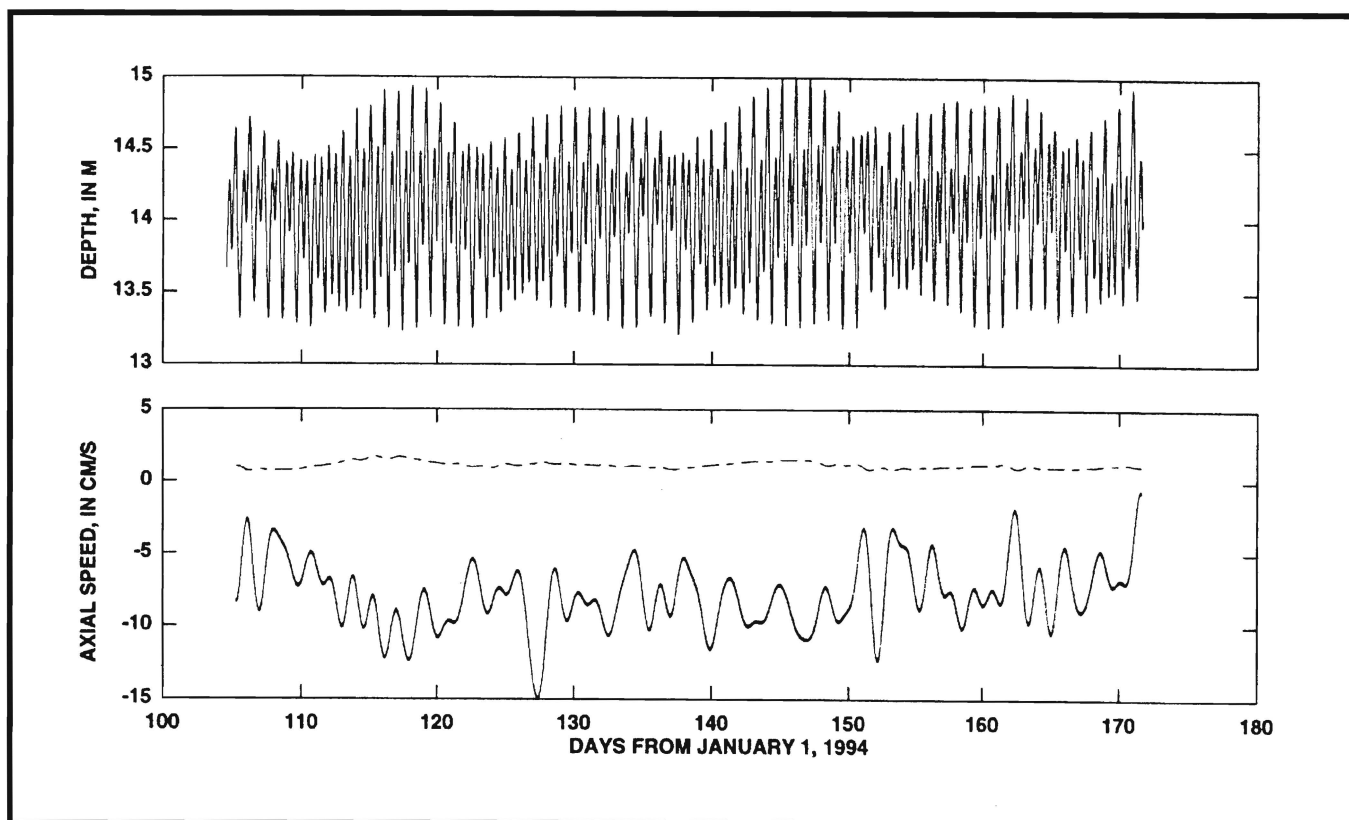


Figure 27

TIME SERIES OF DEPTH AT MALLARD ISLAND, (top) AND THE LOW-PASS-FILTERED, DEPTH-AVERAGED, ALONG-CHANNEL SPEED (bottom, solid) AND THE STOKES' DRIFT VELOCITY (bottom, dashed)
(CM/S=centimeters per second; M=meters.)

(time average) mass flux past an ADCP location is

$$\langle \bar{u}H \rangle = \langle \bar{u} \rangle h + \langle \bar{u}'\zeta \rangle \quad (7)$$

where $\bar{u} = \langle \bar{u} \rangle + \bar{u}'$ is the depth-averaged velocity, $H = h + \zeta$ is the total depth, h is the tidally averaged depth, and ζ is sea level where the operators ($\langle \rangle$, $'$) represent a time average and the tidal fluctuation components, respectively. The overbar represents a depth average.

Dividing the Stokes' drift by the time-mean depth allows the Stokes' drift to be cast in terms of a velocity. The time-mean, depth-averaged velocity, $\langle \bar{u} \rangle$, and the Stokes'

drift velocity, $\frac{\langle \bar{u}'\zeta \rangle}{h}$, are shown in Figure 2-27. The Stokes' drift profile is vertically

nonuniform (Ianniello 1977), and simple modeling studies indicate that the vertical Eulerian velocity profile attributed to Stokes' drift is strictly positive (landward) throughout the water column (Najarian and others 1984) (Figure 2-3). To compute the Stokes' drift profile from data, estimates of the stream-wise velocity, the vertical and along-channel derivatives in the stream-wise velocity, and the vertical velocity component are needed. These parameters could not be measured in 1994 with the instrumentation available at that time; therefore, the Stokes' drift contribution could not be vertically partitioned. Nonetheless, the depth-averaged Stokes' drift velocity is small (<2 cm/s) with greater magnitudes on spring tides than on neap tides (Figure 2-27), which is consistent with previous research (Walters and Gartner 1985).

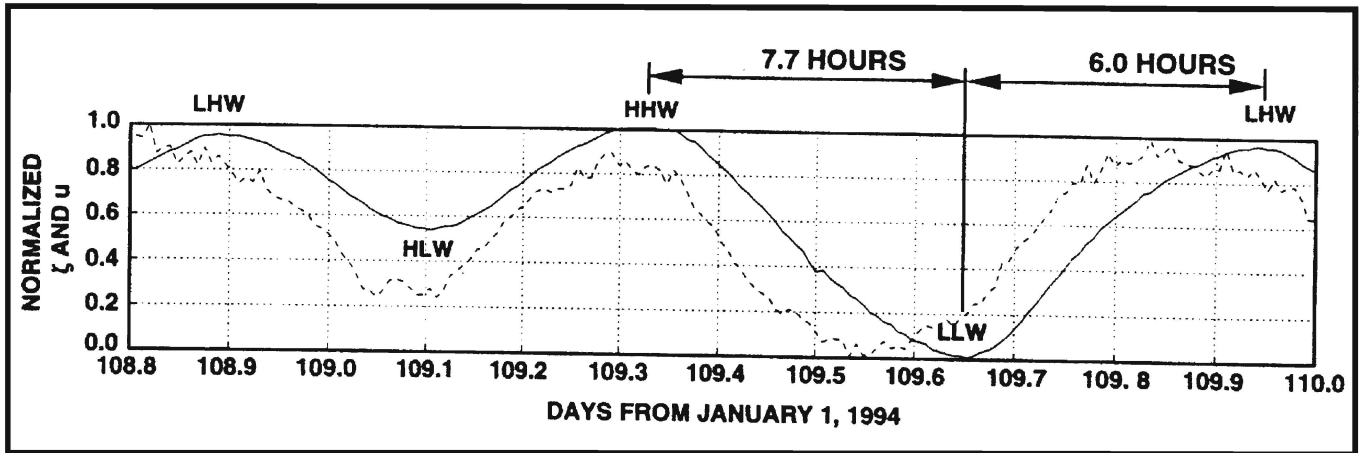


Figure 28

NORMALIZED SEA LEVEL, ζ (solid), AND DEPTH-AVERAGED VELOCITY, u (dashed), AT MALLARD ISLAND
The abbreviations are, from left to right: LHW, lower high water; HLW, higher low water; HHW, higher high water; LLW, lower low water.

Two things are relevant in determining whether Stokes' drift is important: (1) the magnitude of the tidal range, ζ , relative to the mean depth, h (if $\frac{\zeta}{h} \ll 1$, Stokes' drift is not important), and (2) the phase between the tide (sea level) and the tidal currents. If the phase between the tide and tidal currents is 90 degrees (standing wave), then the sea-level variations and the currents are uncorrelated and Stokes' drift is not important. Conversely, if the phase between the tide and tidal current is 0 degrees, then the tide and tidal currents are perfectly correlated and Stokes' drift may be important depending on the magnitude of $\frac{\zeta}{h}$. Using Mallard Island data as an example, the tidal range is $\zeta = 1.2$ m and the mean depth is $h = 13$ m, so $\frac{\zeta}{h} \ll 1$.

The idea of a purely progressive or purely standing wave system is a conceptual construct. In real estuarine systems, the phase between the tides and the tidal currents changes spatially and temporally. The normalized sea level and along-channel velocities at Mallard Island for a typical tidal cycle are shown in Figure 2-28. These time series are normalized so they can be

overlaid and easily compared. The timing of the tidal currents, relative to the tide, changes over the tidal cycle (Figure 2-28). For example, the decline from higher high water (HHW) to lower low water (LLW) takes 7.7 hours, whereas the rise from LLW to lower high water (LHW) takes 6.0 hours. Moreover, the shape of the decline is not only longer but more gradual than the rising tide, which shows evidence of wave steepening indicative of more rapid progress of LHW upstream. This tidal distortion is caused primarily by interaction between the incoming tidal currents and the outgoing time-mean current (delta outflow) (Godin 1991).

In terms of the phase between the tide and the tidal currents, the weak tides (day 108.8 to 109.35 in Figure 2-28) represent periods when sea levels are closer to being in phase (correlated) than they are during the strong tides (day 109.35 to 109.95 in Figure 2-28). The difference between the correlation during spring versus neap tides is shown in Figure 2-29 where the time difference between the tidal currents and sea level are plotted and in Figure 2-30 where the phase lag ($phase_{currents} - phase_{tide}$), assuming a semidiurnal period of 12.42 hours (principal lunar component of the tide referred to as the M2 tide), is

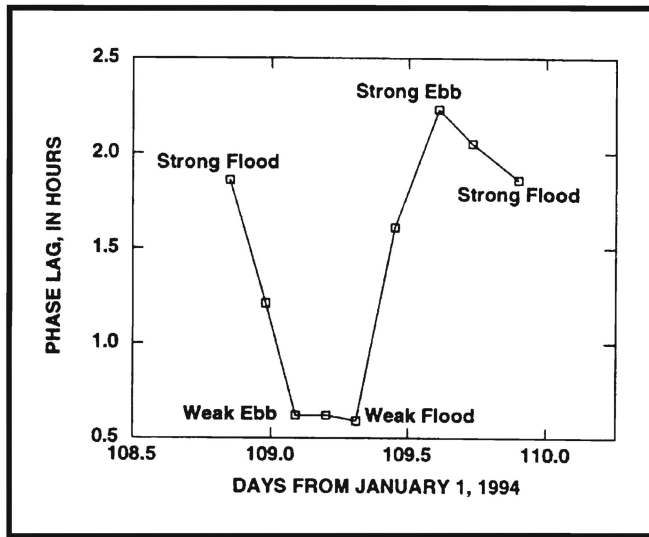


Figure 29
PHASE LAG ASSUMING A SEMIDIURNAL TIDAL PERIOD OF 12.42 HOURS (M2 tide) BETWEEN SEA LEVEL AND THE CURRENTS AT MALLARD ISLAND

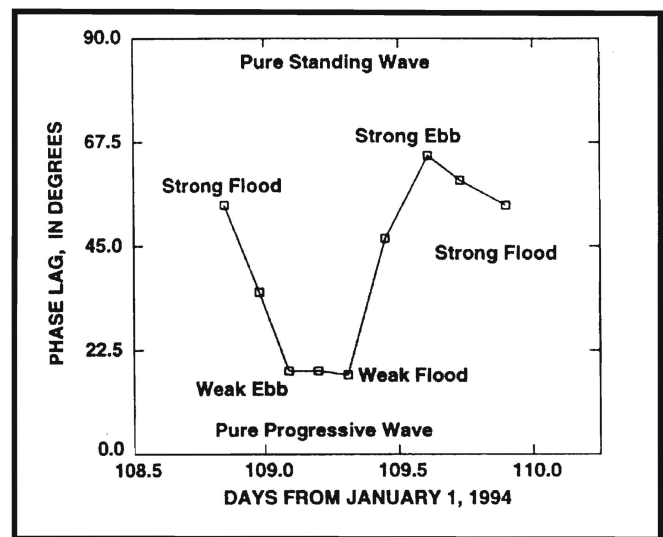


Figure 30
PHASE LAG, ASSUMING A SEMIDIURNAL TIDAL PERIOD OF 12.42 HOURS (M2 tide) BETWEEN SEA LEVEL AND THE CURRENTS AT MALLARD ISLAND

plotted. The tides and tidal currents in the north bay are, on average, only weakly correlated [$\phi_{ave} = 40^\circ$, $\cos(40^\circ) = 0.77$]; the weakest correlation occurs during the period of maximum tidal exchange.

In summary, Stokes' drift is weak in Suisun Bay (Mallard Island specifically) because sea level variations are small relative to the mean depth ($\zeta \ll h$) and the correlation between sea level and the tidal currents is weak (particularly during the maximum flood and ebb periods).

Management Implications

The revised conceptual model of gravitational circulation has significant implications to proposed dredging in Suisun Bay and to the generally accepted hydrodynamic explanation for the turbidity maximum and the entrapment zone. Observation of residual currents and theoretical analysis of the horizontal Richardson number indicate the importance of bathymetry and variations in depth in the establishment of gravitational circulation cells. The modification of the existing bathymetry as proposed as part of the John R. Baldwin and Stockton ship channel dredging projects (U.S. Army Corps of

Engineers 1989) would significantly lower the channel depths near the Benicia Bridge (dredged from 11 m deep and 92 m wide to 14 m deep and 183 m wide). The horizontal Richardson number scaling discussed in this chapter suggests that deepening the ship channel in this area could locally increase gravitational circulation, which could result in elevated salinities in Suisun Bay and the western delta. A detailed hydrodynamic study in the area adjacent to the Benicia Bridge is needed, however, to verify the importance and extent of this topographic control.

Acknowledgments

This study was done in cooperation with the San Francisco Bay ecosystem initiative of the USGS, DWR, and the USBR, as part of the Interagency Ecological Program. The authors greatly appreciate the help of Randall Brown (DWR) and James Arthur (USBR) in arranging the funding for this work. The guidance and encouragement

from Steve Monismith, Jeffrey Koseff (Stanford University) and Ralph Cheng and Peter Smith (USGS) were essential in the design and execution of this study. The field study described in this chapter required the help of a number of people. Jim Burau; Rick Oltmann, Rick Adorador, and Scott Posey (USGS); and Doug Ball and Jim Arthur (USBR) put in many hours in the field to obtain the data.

References

- Armi, L. 1986 The hydraulics of two flowing layers with different densities: *Journal of Fluid Mechanics*, v. 163, p. 27-58.
- Arthur, J.F. and M.D. Ball. 1979. Factors influencing the entrapment of suspended material in the San Francisco Bay Estuary, Conomos, T.J., editor, *San Francisco Bay: The Urbanized Estuary*. San Francisco, Pacific Division, American Association for the Advancement of Science, p. 143-174.
- Bowden, K.F. 1960. Circulation and mixing in the Mersey estuary. International Association of Scientific Hydrology Committee of Surface Waters, *Publication 51*, p. 352-360.
- Buchanan, P.A., D.H. Schoellhamer, and R.C. Sheplaine. 1996. Of suspended-solids concentration data, San Francisco Bay, California, water year 1994. U.S. Geological Survey *Open-File Report 95-776*, 48 p.
- Burau, J.R., M.R. Simpson, and R.T. Cheng. 1993. Tidal and residual currents measured by an acoustic Doppler current profiler at the west end of Carquinez Strait, San Francisco Bay, California, March to November 1988. U.S. Geological Survey *Water-Resources Investigations Report 82-4064*, 79 p.
- Cheng, R.T., V. Casulli, and J.W. Gartner. 1993. Tidal, residual, intertidal mudflat (TRIM) model and its applications to San Francisco Bay, California. *Estuarine, Coastal and Shelf Science*, v. 36, p. 235-280.
- Cheng, R.T. and J.W. Gartner. 1984. Tides, tidal and residual currents in San Francisco Bay, California-Results of measurements, 1979-1980: pt. 2, Results of measurements in Suisun Bay region. U.S. Geological Survey *Water-Resources Investigations Report 84-4339*, 231 p.
- Conomos, T.J., D.H. Peterson, D. S. McCulloch, and P.R. Carlson. 1971. Drift of surface and near-surface bottom waters of the San Francisco Bay system: March 1970 through April 1971. U.S. Geological Survey Open-File map.
- Conomos, T.J. 1979. Properties of circulation of San Francisco Bay waters material in the San Francisco Bay Estuary, T.J. Conomos, editor. *San Francisco Bay: The Urbanized Estuary*. San Francisco, Pacific Division, American Association for the Advancement of Science, p. 47-84.
- Denton, R.A. and J.R. Hunt. 1986. Currents in San Francisco Bay-Final report. University of California and Berkeley, *Hydraulic and Coastal Engineering Report No. UCB/HEL-86/01*, 99 p.

- Downing, J.P. 1983. An optical instrument for monitoring suspended particulates in ocean and laboratory: Abstract, *OCEANS 1983*, San Francisco, California, August 29-September 1, 1983, p. 199-202.
- Dyer, K.R. 1973. *Estuaries: A physical introduction*. New York, John Wiley, 140 p.
- Farmer, D.M. and L. Armi. 1986. Maximal two-layer exchange over a sill and through the combination of a sill and contraction with barotropic flow: *Journal of Fluid Mechanics*, v. 164, p. 53-76.
- Fischer, H.B., E.J. List, R.C.Y. Koh, J. Imberger, and N.H. Brooks. 1979. *Mixing in Inland and Coastal Waters*. Academic Press, New York, 483 pp.
- Geyer, W.G. 1993. The importance of suppression of turbulence by stratification on the Estuarine Turbidity Maximum. *Estuaries*, v. 16, no. 1, p. 113-125.
- Godin, G. 1991. Frictional effects in river tides, in Parker, Bruce, editor, *Tidal hydrodynamics*. New York, John Wiley, p. 379-402.
- Hansen, D.V. and M. Rattray. 1965. Gravitational circulation in straits and estuaries. *Journal of Marine Research*, v. 23, p. 104-122.
- Hill, K.D., T. M. Dauphinee, and D.J. Woods. 1986. The extension of the practical salinity scale 1978 to low salinities. Institute of Electrical and Electronics Engineers, *Journal of Oceanic Engineering*, v. OE-11, no. 1, p. 109-112.
- Ingles, C. and F.H. Allen. 1957. The regimen of the Thames estuary. *Proceedings of the Institute of Civil Engineers (London)* v. 7, p. 827-868.
- Jassby, A.D., W.M. Kimmerer, S.G. Monismith, C. Armor, J.E. Cloern, T.M. Powell, J. Shubel, and T. Vendliniski. 1995. Isohaline position as a habitat indicator for estuarine resources: San Francisco Bay-Delta, California, U.S.A. *Ecological Applications*, v. 5, p. 273-289.
- Jay, J.A., B.S. Giese, and C.R. Sherwood. 1990. Energetics and sedimentary processes in the Columbia River estuary. *Prog. Oceanography*, v. 25, p. 157-174.
- Kimmerer, W.M. 1993. An evaluation of existing data in the entrapment zone of the San Francisco Bay Estuary. Biosystems Analysis, Inc., *Technical Report 33*, 49 p.
- Millero, F.J. 1993. What is a psu? *Oceanography*, v. 6, no. 3, p. 67.
- Monismith, S.G., J.R. Burau, and M. Stacey. 1996. Hydrodynamic transport and mixing processes in Suisun Bay, Hollibaugh, J.T., editor, *San Francisco Bay: The Ecosystem*. San Francisco, Pacific Division, American Association for the Advancement of Science, p. 123-153.
- Mortenson, W.E. 1987. Investigation of estuarine circulation in Suisun Bay: The Bay Institute of San Francisco Exhibit 49, *State Water Resources Control Board Hearing 13*, 70 p.
- Najarian, T.O., D.P. Wang, and P.S. Huang. 1984. Lagrangian transport model for estuaries. American Society of Civil Engineers, *Journal of Waterway, Port, Coastal and Ocean Engineering*, v. 110, no. 3, p. 321-333.
- Nichol, G.D. 1996. Estuarine circulation cell of lower Sacramento River: Reno, University of Nevada, Ph.D. thesis, 197 p.
- Nichols, M., and G. Poor. 1967. Sediment transport in a coastal plain estuary. American Society of Civil Engineers, *Journal of Waterways and Harbors Division*, v. 93, p. 83-95.
- Nunes Vaz, R.A., G.W. Lennon, and J.R. de Silva Samarasinghe. 1989. The negative role of turbulence in estuarine mass transport. *Estuarine, Coastal and Shelf Science*, v. 28, p. 361-377.

- Officer, C.B. 1976. *Physical oceanography of estuaries (and associated coastal waters)*. New York, John Wiley, 465 p.
- Peterson, D.H., T.J. Conomos, W.W. Broenkow, and P.C. Doherty. 1975. Location of the nontidal current null zone in northern San Francisco Bay. *Estuarine and Coastal Marine Science*, v. 3, p. 111.
- Postma, H., and K. Kalle. 1955. One the development of turbid zones in the lower course of rivers with a special consideration of the conditions in the lower Elbe. *Sonde. Deutche Hydr. Zeitschrift*, v. 8, p. 137-144.
- Pritchard, D.W. 1952. Salinity, distribution, and circulation in Chesapeake Bay estuarine system. *Journal of Marine Research*, v. 11, p. 106-123.
- Schubel, J.R. 1968. Turbidity maximum of northern Chesapeake Bay. *Science*, 8, v. 161, p. 1013-1015.
- Simpson, J.H., J. Brown, J. Mathews, and G. Allen. 1990. Tidal straining, density currents, and stirring in the control of estuarine stratification. *Estuaries*, v. 13, no. 2, p. 125-132.
- Smith, L.H. 1987. A review of circulation and mixing studies of San Francisco Bay California. U.S. Geological Survey *Circular 1015*, 18 p.
- Smith, T.A., and G.V. Bogle. 1993. Three dimensional particle tracking model for the Sacramento-San Joaquin Delta. *Proceedings, American Association of Civil Engineers Hydraulic Engineering Conference*, San Francisco, California, p. 827-832.
- Stacey, M.T. 1996. Turbulent mixing and residual circulation in a partially stratified estuary: Stanford University, California, Ph.D. thesis, 209 p.
- UNESCO. 1985. The international system of units (SI) in oceanography. Paris, France, *UNESCO Technical Paper in Marine Science*, no. 45, 53 p.
- U.S. Army Corps of Engineers. 1989. Hydraulic model study for the salinity impact of the John F. Baldwin, Stockton, and Sacramento ship channel projects, dynamic salinity tests. U.S. Department of the Army, Corps of Engineers, San Francisco District *Technical Memorandum 2*, 53 p.
- Walters, R.A., R.T. Cheng, and T.J. Conomos. 1985. Timescales of circulation and mixing processes in San Francisco Bay waters, in Temporal dynamics of an estuary: San Francisco Bay, Cloern, J.E. and Nichols, F.H. (eds.). *Hydrobiologia*, v. 129, p. 13-36.
- Walters, R.A., and J.W. Gartner. 1985. Subtidal sea level and current variations in the northern reach of San Francisco Bay. *Estuarine, Coastal and Shelf Science*, v. 21, p. 17-32.
- Walters, R.A., and C. Heston. 1982. Removing tidal-period variations from time-series data using low-pass digital filters. *Journal of Physical Oceanography*, v. 12, no. 1, p. 112-115.
- Warner, J.C., D.H. Schoellhamer, and J.R. Burau. 1997. A sediment pathway in the back of a nearly semi-enclosed subembayment of San Francisco Bay, California. *Proceedings, 27th International Association for Hydraulic Research*, San Francisco, California, August 10-15, 1997, v. 2, p. 1096-1101.
- Weir D.J. and J. McManus. 1987. The role of wind in generating turbidity maxima in the Tay Estuary, *Continental Shelf Research*, v. 7, p. 1315-1318.

Glossary

- Baroclinic flow. Circulation driven by the pressure gradient caused by horizontal differences in salinity. The baroclinic pressure gradient increases with depth under most conditions. See appendix for more details.
- Barotropic flow. Circulation that is driven by the pressure gradient caused by slope in the water surface. The barotropic pressure gradient is constant with depth. See appendix for more details.
- Bathymetry. Topography of the bottom of the estuary (Kimmerer 1993).
- Density Gradient. Spatial density difference.
- Dispersion. The scattering of particles (or mixing of salt) or a cloud of contaminants by the combined effects of shear and transverse mixing (Fischer and others 1979).
- Entrapment zone. The area of the estuary where flow convergence results in the concentration of particulate matter; this usually operates through the interaction of particle (or organism) sinking and net up-estuary flow at depth (Kimmerer 1993).
- Estuarine turbidity maximum (ETM). An area of the estuary where turbidity is enhanced either by entrapment or by other mechanisms (Kimmerer 1993).
- Eulerian. An Eulerian method of description uses a fixed point in space as a reference. All of the properties of interest are measured with respect to, or are referenced to, this location. Therefore, measurements are made as the fluid and its properties move past the measurement location.
- Gravitational circulation. A residual, two-layer flow, in which low salinity water flows seaward in the surface layer, whereas denser, more saline water flows landward in the bottom layer; this two-layer flow results from the balance between the free surface slope acting in a down-estuary direction and the longitudinal density (salinity) gradient acting in the landward direction (Officer 1976).
- Lagrangian. A Lagrangian method of description takes a fluid particle world view where all of the fluid properties of interest (temperature, salinity, suspended sediment, etc.) are measured with respect to, or referenced to, a single unique parcel of water. Therefore, a Lagrangian description goes with the flow.
- Null zone. The location in the estuary at which net landward flow near the bottom ceases and all tidally averaged flow throughout the water column is seaward (Kimmerer 1993).
- OBS. Acronym for optical backscatterance sensor. This sensor can be calibrated to measure suspended-solids concentrations (Downing 1983; Buchanan and others 1996).
- Operational definition of the entrapment zone. The salinity range of 1 to 6 (Arthur and Ball 1980).
- Practical salinity units (psu). Salinities in this report are given in practical salinity units computed based on the 1985 UNESCO standard (UNESCO 1985) for salinities greater than 2. Salinities that are less than 2 are computed as in Hill and others (1996). Salinity is a conductivity ratio; therefore, has no physical units (Millero 1993). Use of psu in this report is for clarification.
- Pressure gradient. Spatial pressure difference.
- Residual. This term often represents the difference between a data value and the value predicted by a regression line or other statistical model (Kimmerer 1993). In a hydrodynamic context, residual is synonymous with tidally averaged and is used to describe processes whose time scales are longer than the tidal period (30 hours).

- RMS. Acronym for root mean square; computed by squaring the values in a time series, calculating a mean value, then taking its square root.
- Shear. A spatial difference (gradient) in velocity. For example, a large vertical shear indicates a large difference between surface and near-bed velocities.
- Spring/neap tidal cycle. Fortnightly (period of 14 days) oscillation in tidal energy that principally results from constructive and destructive interference between the diurnal (24-hour) and semi-diurnal (12-hour) partial tides. During spring tides, the ebb and flood tides are roughly equal in magnitude; however, during neap tides, two weaker and two stronger tides occur during a roughly 24-hour period. This is known as the diurnal inequality. The largest spring-neap tidal difference occurs during the summer (~June 21) and winter (~December 21) solstices.
- Stokes' drift. A Eulerian residual current that is created when the tidal variation in cross-sectional area (sea level) and the tidal currents are correlated (in phase). See the Stokes' drift section in this report.
- Tidally averaged. Refers to a time series that is time averaged over a tidal cycle so that signals in the data with periods equal to or less than the tidal period are removed. This is usually accomplished through the use of a digital filter (Walters and Heston 1982).
- X2. Position, measured as the distance in kilometers from the Golden Gate along the axis of the estuary, of the 2-psu near-bottom isohaline (Jassby and others 1995).

Fundamentals of Baroclinic and Barotropic Flows

The flows in estuaries are intrinsically more complicated than other surface water flows (rivers, lakes) because estuaries are where freshwater and salty water mix. The spatial density differences that occur in estuaries create an additional pressure gradient that drives flows that are wholly absent in rivers and lakes. Understanding how this pressure gradient interacts with the tides and freshwater inflow is fundamental to understanding estuaries. This section presents the background necessary to interpret the hydrodynamic data collected in Suisun Bay.

Water moves in surface waters (primarily) because of horizontal pressure differences (gradients). In the absence of a pressure gradient, water will not move (except for an applied shear stress like wind). The flow in rivers results from a pressure difference that involves a change in elevation of the water surface. For example, the Sacramento River flows from Redding to Sacramento because the water level in Redding, ζ_R , is much higher than in Sacramento, ζ_S . Oceanographers refer to this gradient as a barotropic pressure gradient, which can be written mathematically for the Sacramento River example as

$$\text{Pressure gradient} \sim \frac{\zeta_R - \zeta_S}{\text{distance from Redding to Sacramento}} \quad (8)$$

If the distance from Sacramento to Redding is Δx (where Δ represents a discrete difference and x is the along-channel distance assumed positive in the upriver direction) and the water surface difference between Sacramento and Redding is represented by $\Delta\zeta = \zeta_R - \zeta_S$,

then the horizontal pressure gradient, $\frac{\partial P}{\partial \chi}$, that drives the flow in rivers can be written

$$\frac{\partial P}{\partial \chi} \sim \frac{\Delta\zeta}{\Delta\chi} \sim \frac{\partial\zeta}{\partial\chi} \quad (9)$$

where we have made the leap from discrete, Δ , to continuous mathematics; the “ ∂ ” represents a partial derivative, $\frac{\partial\zeta}{\partial\chi}$ represents a water-surface slope, and “ \sim ” means

proportional. The proportionality is replaced with an equivalence in equation 9 through the addition of gravity, g , and the density of water, ρ_0 ,

$$\frac{\partial P}{\partial \chi} = g\rho_0 \frac{\partial\zeta}{\partial\chi} \quad (10)$$

If the water-surface gradient, $\frac{\partial \zeta}{\partial \chi}$, is zero, then the pressure gradient, $\frac{\partial P}{\partial \chi}$, is zero, and no barotropic flow occurs. In the absence of wind, a lake is a good approximation of this condition.

The flows in estuaries are more complex than in rivers or lakes because estuaries typically are the geographic location where saltwater and freshwater mix. The density difference between salty and freshwater along the axis of the estuary creates an additional pressure gradient, the so-called baroclinic pressure gradient, that also can drive flow in estuaries. Therefore, the horizontal density difference must be considered in the pressure gradient relation, which is given here without proof (Dyer 1973):

$$\frac{\partial P(z,t)}{\partial \chi} = g\rho_0 \frac{\partial \zeta}{\partial \chi} + g \int_z^H \frac{\partial \rho(z,t)}{\partial \chi} dz \quad (11)$$

where the pressure now varies with depth depending on the stratification (for example, what $\rho(z,t)$ looks like), H is the total depth, z is the vertical direction; z is zero at the bed and positive up. In words, equation 11 states that the total pressure gradient at any depth, z , is the sum of a water-surface slope (term 1) and the along-channel difference in the “weight” of water (the “weight” of water at any point in the water column is $g \int_z^H \rho(z,t) dz$). Simply put, if there is a difference in pressure between adjacent water parcels, the water with the higher pressure will move toward the water with the lower pressure. Depth dependent pressure variation is the primary reason for the additional complexity of estuarine flows.

The flow of water derived from term 1 in equation 11 is referred to as barotropic flow, and the flow that results from the second term is called baroclinic flow. The tides, delta outflow, atmospheric pressure changes, and wind create water-surface slopes that produce barotropic flows in estuaries. Because the barotropic pressure is constant with depth (for example, no integral in term 1 in equation 11), barotropic pressure gradients produce classic log velocity profiles (assuming a well-mixed water column).

Gravitational and estuarine circulations (defined below), on the other hand, result from horizontal density differences and are therefore baroclinic flows. Because the pressure from the baroclinic pressure gradient varies with depth (the integral in term 2 in equation 11), baroclinic motions can stratify the water column, which creates distinctly nonlog velocity profiles (more on this later).

Horizontal density differences not only drive a two-layer flow (gravitational circulation), but also can drive a depth average flow that will be referred to as estuarine circulation. Estuarine circulation, for this chapter, is defined as the depth average flow that results from a baroclinic pressure gradient. Gravitational and estuarine circulations can occur in the channels. Because the shallows are well mixed, estuarine circulation only occurs there.

To understand how baroclinic processes contribute to strictly depth-averaged circulation, consider the following simple example. Figure 2-31a shows a tank filled with two fluids of different densities, $\rho_s > \rho_f$, separated by an initially immovable wall. The water levels across the wall are initially identical, $h_s = h_f = H$. Figure 2-31b shows the pressure exerted on the wall by each of the fluids. Because density does not vary with depth in this example, the pressure at any level, z , in the water column is $P(z) = \rho g(z - H)$.

Because salty water has a greater density than freshwater, the net pressure on the gate is directed toward the freshwater (Figure 2-31c). When the gate is released, it moves toward the lower salinity fluid until the net pressure on the gate is zero (Figure 2-31d). As the gate moves, the depth of the lower salinity water is increased relative to the high salinity water until the pressure difference across the gate, caused by the difference in water level, just balances the pressure difference caused by the difference in density across the gate (for example, the barotropic and baroclinic pressures are equal) (Figure 2-31e). This example shows a density-driven flow (the gate moves from the higher density water to the lower density water) that is strictly in the horizontal plane, what is referred to in this report as estuarine circulation (Figure 2-31f). In Suisun Bay, estuarine circulation can be important when the water column is well mixed in the presence of a horizontal density gradient. A well-mixed water column typically occurs in the shallows and in the channels during the tidal current maximums.

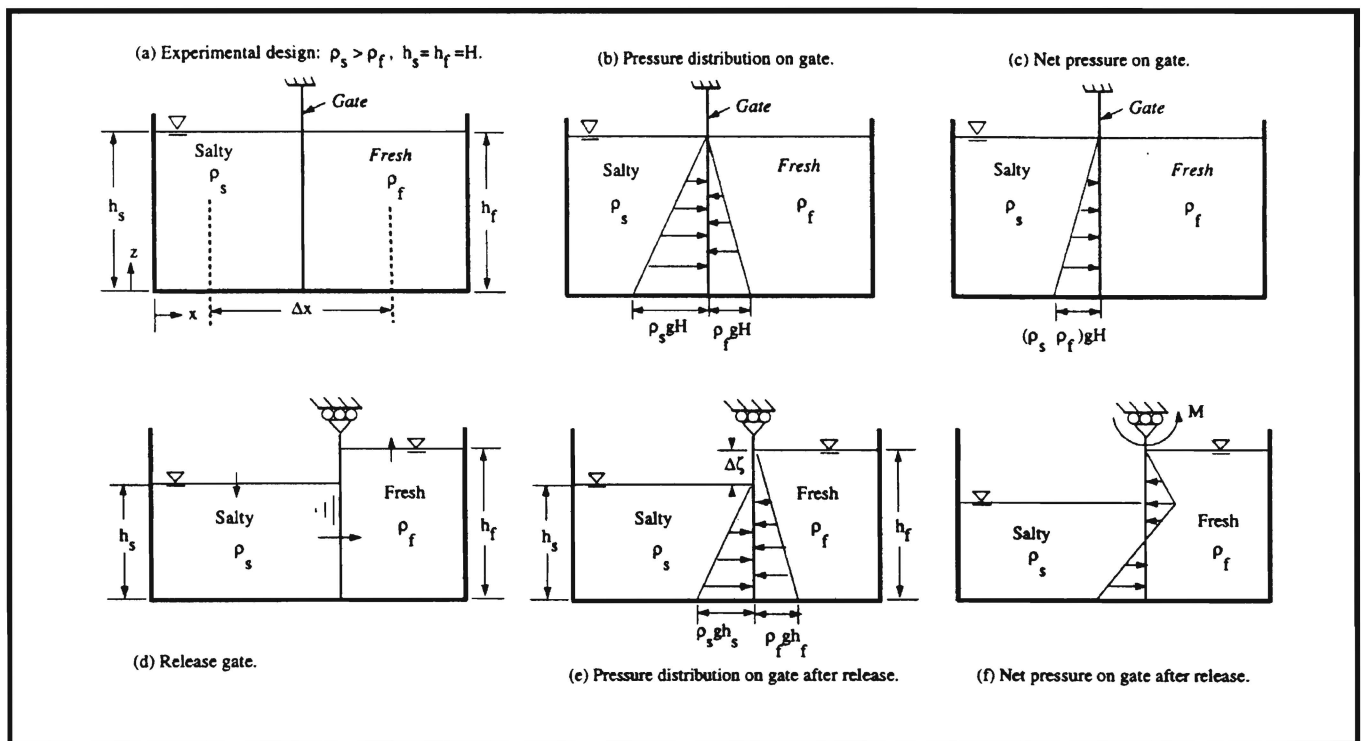


Figure 31

EXAMPLE OF THE PRESSURE DISTRIBUTIONS ON A GATE THAT SEPARATES TWO FLUIDS OF DIFFERENT DENSITIES, where (ρ_s, ρ_f) are the densities, (h_s, h_f) are the water-surface heights of the salty water and freshwater, respectively. H , the undisturbed water surface height; g , gravity; Δh , the water-level difference between the salty water and freshwater; and M , the moment created on the gate from the density difference across the gate.

The net pressure distribution on the gate shown in Figure 2-31f shows why seaward flow at the surface and landward flow near the bed occur when a horizontal salinity gradient is present because that is the way the net pressures are directed on the gate. Therefore, if the gate were removed, a classic gravitational circulation cell would develop.

How are horizontal salinity and density gradients computed? Using Suisun Bay as an example, the typical summer, depth-averaged salinity at Martinez, S_{mart} , is about 16 psu [$\rho_{mart} \sim 1012$. kilograms per cubic meter (kg/m^3)] and at Mallard Island, S_{mal} is about 7 psu ($\rho_{mal} \sim 1002$. kg/m^3), and the distance along the channel between Martinez and Mallard Island is $\Delta x \sim 21$ km (Figure 2-20). The (depth-averaged) horizontal salinity gradient between Martinez and Mallard Island is $\Delta S = S_{mal} - S_{mart} = -9$ psu, then the

$$\text{horizontal salinity gradient across Suisun Bay} = \frac{\Delta S}{\Delta x} \sim \frac{-9 \text{ psu}}{21 \text{ km}} \sim -0.4 \text{ psu/km} . \quad (12)$$

The low-pass-filtered Mallard Island salinity gradient shown in Figure 2-20 are computed as the difference between the Mallard Island and Martinez DWR monitoring stations.

Because density is a known function of salinity and (to a lesser extent) temperature (UNESCO 1985), the summer mean density gradient across Suisun Bay is easily estimated as

$$\frac{\Delta S}{\Delta x} \rightarrow \frac{\Delta \rho}{\Delta x} \sim -0.35 \text{ kg}/\text{m}^3 / \text{km} \quad (13)$$

The flow of water from the delta into and through the bay is accomplished by a net (tidally averaged, positive) water-surface slope. That is, the water surface in the delta is, on average, higher than in Carquinez Strait. At the same time, the horizontal density gradient across Suisun Bay creates a baroclinic pressure gradient that opposes (negative) the delta outflow-derived barotropic pressure gradient. Therefore, if there is actually to be a net flow through Suisun Bay equal to delta outflow, the net “tilt” across Suisun Bay must be greater than the equivalent “tilt” created by the horizontal density gradient. The equivalent incremental rise in mean tide level to just balance a constant longitudinal salinity (density) gradient is

$$\Delta \zeta \sim \frac{H \Delta \rho}{2 \rho_0} \sim \frac{10 \cdot (1012 - 1002)}{2(1000)} \sim 5 \text{ cm} . \quad (14)$$

Numerical Modeling Implications

Various numerical models have been applied to the delta/Suisun Bay system, including two dimensional (2D)_{xy} (depth-averaged) and 1D models. 2D models, like TRIM2D (Cheng and others 1993), account for estuarine circulation by including the depth average of term 2 in equation 12, $\frac{g}{2\rho_0} \frac{\partial \rho}{\partial \chi}$, directly in the momentum equations. Current (1998) versions of the Fischer Delta model and DSM1 do not include this baroclinic forcing in their formulations, even though these models are applied in the western delta and Suisun Bay where baroclinic forcing is important during the autumn and winter. One could argue that the baroclinic term is negligible in the delta; however, data collected near Decker Island indicate that gravitational circulation was present, although weak (>5 cm/s), during the autumn of 1987, 1989, 1992, and 1993, and the water column was weakly stratified (Nichol 1996). Stratification implies that the baroclinic pressure gradient is significant. Moreover, during periods where the water column is stratified, typically seaward of X2, a log profile poorly approximates a stratified water column, fundamental assumption of DWR current particle tracking model (Smith and Bogle 1993).

Net Tilt Scaling

In this section, an estimate of the net "tilt," $\Delta\zeta$, required to just balance a given time-averaged, depth-averaged, longitudinal density difference, $\Delta\rho$, is derived. The total pressure difference across the gate pictured in Figure 2-32 is

$$\Delta p = \frac{g\rho_s h_s^2}{2} - \frac{g\rho_f h_f^2}{2} \quad (15)$$

By substituting $h_f = h_s + \Delta\zeta$ into equation 15,

$$\Delta p = \frac{g\rho_s h_s^2}{2} - \frac{g\rho_f}{2} \left(h_s^2 + 2h_s\Delta\zeta + \Delta\zeta^2 \right). \quad (16)$$

If Δp is set to zero and rearranged, then

$$0 = \rho_s - \rho_f - \frac{2\rho_f \Delta\zeta}{h_s} - \frac{\rho_f \Delta\zeta^2}{h_s^2} \quad (17)$$

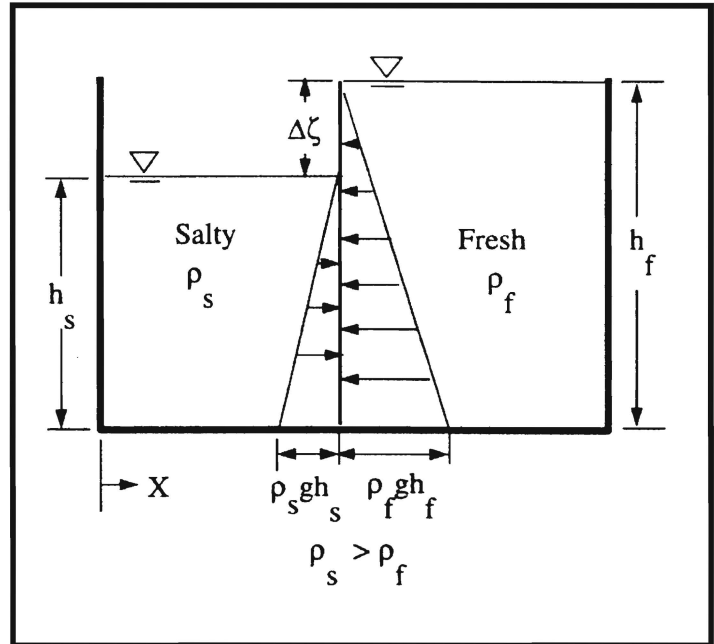


Figure 32
EXAMPLE OF THE NET PRESSURE DISTRIBUTIONS ON A GATE THAT SEPARATES TWO FLUIDS OF DIFFERENT DENSITIES AND DIFFERENT WATER LEVELS

where (ρ_s , ρ_f) are the densities, (h_s , h_f) are the water-surface heights of the salty and freshwater, respectively. H represents the undisturbed water surface height; g represents gravity; Δh represents the water level difference between the salty and freshwater; and M represents the moment created on the gate from the density difference across the gate.

if $\frac{\Delta\zeta}{h_s} \ll 1$ then to first order $\frac{\Delta\zeta^2}{h_s^2} \rightarrow 0$ and let $\Delta\rho = \rho_s - \rho_f$, then equation 17 becomes

$$\Delta\zeta = \frac{\Delta\rho h_s}{2\rho_f}. \quad (18)$$

By applying the Bousinesq approximation, then $\rho_f \sim \rho_0$ in the third term because $\frac{\Delta\rho}{\rho_0} \ll 1$,

$$\Delta\zeta \sim \frac{H\Delta\rho}{2\rho_0}, \quad (19)$$

an estimate of the net “tilt,” $\Delta\zeta$, to compensate for a time-averaged, depth-averaged density gradient, $\Delta\rho$.